ISSN: 1224-7626

ANALELE UNIVERSITĂŢII DIN ORADEA

Fascicula CHIMIE
XXIII
2016

EDITURA UNIVERSITĂŢII DIN ORADEA

- 2016-

Editor in chief: BADEA Gabriela Elena
gbadea@uoradea.ro

Editors
Gultekin Tarcan – Dokuz Eylul University, Turkey, gultekin.tarcan@deu.edu.tr
Arife Alev Karagozler - Adnan Menderes University, Aydin, Turkey, akaragozler@gmail.com
Cavit Uyanik - Kocaeli University, Kocaeli, Turkey
Prasath Deva Martin- TBML College, Porayar, Nagai, Tamilnadu, India, martinprasath@rediffmail.com
Hrefna Kristmannsdottir-Efla Engineering Company, Iceland
Jantschi Lorentz- Technical University of Cluj Napoca, România, lorentz.jantschi@gmail.com
Ioniţă Daniela- University Politehnica of Bucharest, România, md_ionita@yahoo.com
Cojocaru Anca- University Politehnica of Bucharest, România, a_cojocaru@chim.upb.ro
Maior Ioana- University Politehnica of Bucharest, România, i_maior@chim.upb.ro
Iovi Aurel - University Politehnica Timişoara, România
Gilău Ludovic – University of Oradea, România
Bungău Simona – University of Oradea, România, simonabungau@gmail.com
Badea Gabriela Elena- University of Oradea, România, gbadea@uoradea.ro
Fodor Alexandrina - University of Oradea, România, afodor@uoradea.ro
Cărăban Alina - University of Oradea, România, acaraban@uoradea.ro
Stănăşel Oana - University of Oradea, România, ostanasel@uoradea.ro
Gavriş Georgeta- University of Oradea, România, georgeta_gavris@uoradea.ro
Hodişan Sorin - University of Oradea, România, sorin.hodisan@yahoo.com
Sebeşan Mioara - University of Oradea, România, msebesan@uoradea.ro
Cozma Alina - University of Oradea, România, acozma@uoradea.ro
Bota Sanda - University of Oradea, România, sbota@yahoo.com
Petrehele Anda - University of Oradea, România, pcorinamara@yahoo.com
Morgovan Claudia - University of Oradea, România, cmorgovan@yahoo.com

Editorial Adress
University of Oradea, Chemistry Departament
Str. Armatei Române, nr.5, 410087, Oradea, Bihor, România
Tel (040)/0259/408132
e-mail: gbadea@uoradea.ro
General Information
ISSN: 1224-7626
Place of publishing: Oradea, Romania
Year of the first issue: 1995
Releasing frequency: 1 issue / year
Language: English
Abstracting/Indexing: **Chemical Abstracts Service-CAS Source Index (CASSI)**

TABLE OF CONTENTS

This volume contains articles presented at the:

INTERNATIONAL CONFERENCE ON SCIENCES 2016,

http://www.facultatea-stiinte-oradea.ro/evenimente/ics2016/international-conference-sciences-2016

University of Oradea, Faculty of Sciences
13-14 May 2016

MOLECULAR MODELING IN COMPOUNDS SERIES WITH DESCRIPTORS FAMILIES

Lorentz JÄNTSCHI[1] and Sorana D. BOLBOACĂ[2]
[1]Technical University of Cluj-Napoca, Department of Physics & Chemistry
[1]Babeş-Bolyai University of Cluj-Napoca, Department of Chemistry (associate)
[1]Oradea University, Department of Chemistry (associate)
[2]'Iuliu Haţieganu' University of Medicine and Pharmacy Cluj-Napoca, Department of Medical Education
[2]University of Agricultural Sciences and Veterinary Medicine Cluj-Napoca, Doctoral School of Veterinary Medicine (associate)
Lorentz.Jantschi@gmail.com, SBolboaca@gmail.com

Abstract: *A series of families of molecular descriptors were designed and used to relate the structural information with measured properties and activities for different series of chemical compounds. Here are revised the methodology for the calculation of the molecular descriptors with FPIF, MDF, MDFV, SAPF and SMPI families.*

Key words: Descriptors families; FPIF (fragmental property index family); MDF (molecular descriptors family); MDFV (molecular descriptors family - vertex); SAPF (structural atomic property family); SMPI (Szeged matrix property indices).

INTRODUCTION

First steps to the molecular models are recorded in 1861 (Loschmidt 1861[1]). Today molecular modelling involves theoretical methods and computational techniques for pushing further (see Rhinehardt et al. 2015[2]) the knowledge about the molecular structure.

When series of compounds are involved, then the expected result of a model is to provide a function or a relation between the structure and macroscopic observed behaviour of the molecules. Strategies like docking (Taha et al. 2015[3]), assaying (Peng et al. 2015[4]) and mapping (Radwan & Abdel-Mageed 2014[5]) are involved to better exploit the feature of the systematic experimental observation.

The strategies to develop families of descriptors began to attract concerns (see Kihl et al. 2015[6]).

Here a short survey of the families of molecular descriptors developed by the authors is given.

THE EXPERIMENTAL MEASUREMENTS

Modelling the molecular structure is the way of understanding of the microscopic level and its expression at the macroscopic one level. The accessing of the microscopic level is via measurements (see Fig. 1).

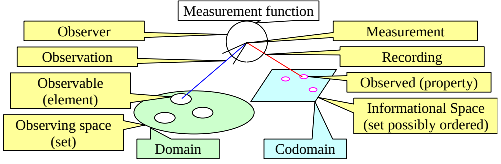

Fig. 1. Encoding the information from measurements

In regard of the measurements, there are many ways of expressing the encoded information, differing one from each other by the quality of the representation.

Thus, the primary measurement scale is binomial which encodes (in the informational space) logical values having as allowed operations equality ("=") and negation ("!") providing a structure of Boolean algebra (Boole 1854[7]). Mode and Fisher exact (Fisher 1922[8]) are the allowable statistics on, and examples of measurements associated with the encoded values are distinguishing between dead and alive, and looking for occurrences of the sides of a coin.

(Multi)nomi(n)al scale uses a finite and known series of unordered values to record the observations, being a discrete scale and having allowed the test for equality ("=") providing a structure of a standard set. One statistic have a clear meaning on the values measured on this scale - mode - and comparisons between series of measurements using this scale can be conducted with Chi-square test (Pearson 1900[9]). Examples of measurements expressed with this scale include 'ABO' blood group system, but also the classification of living organisms.

Ordinal scale is encoding discrete values and the allowed operations include the test for equality ("=") and (strict) inequality ("<") providing a structure of commutative algebra (Krull 1935[10]). The allowable statistic is the median and on the information collected with this scale is possible the ranking. An example of information collected using this scale is the number of atoms in molecules.

Interval scale provides continuous values implicitly falling into an interval or domain. As operations is possible to do comparisons using inequality operator ("≤") as well as to do subtractions. It provides a structure of one-dimensional affine space (Berwald 1918[11]), having allowed calculating of the mean, standard deviation, correlation, regression, and ANOVA. Examples include measurements of temperature, distance, time, and energy.

Ratio scale provides too continuous values on non-negative domain having as allowed operations inequality ("≤"), subtraction ("-") and multiplication ("*"). It provides a structure of a one-dimensional vector space (Bolzano 1804[12]) having allowed the most comprehensive list of statistics including geometric and harmonic means, coefficient of variation, doing of logarithms (Napier 1614[13]), and examples include chemical and biological measurements such as pH and sweetness relative to sucrose.

THE CHEMICAL STRUCTURE

Molecular modelling requires and is feed with measurements. If on one hand stays the measured values, on the other hand stays the chemical structure (see Fig. 2).

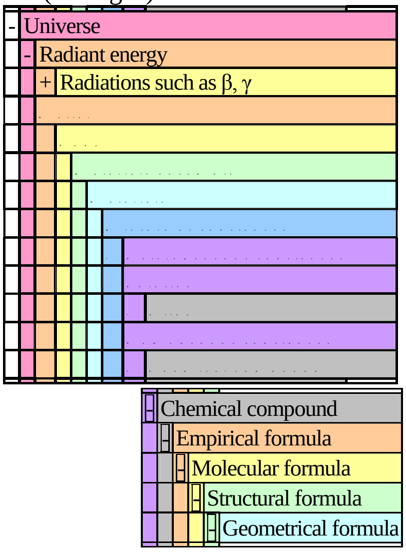

Fig. 2. To the layers of the chemical structure

If the Universe is seen as the whole observing space (see Fig. 2) then radiant energy differentiates as having a velocity comparable with light velocity (relativistic velocity) grouping radiations such as β, γ, being differentiated through properties. The other main group contains the matter seen as the whole non-relativistic observing space in which the body is seen as having the velocity much less than the velocity of light. It contains materials ensemble with possibly variable and discontinue (chemical) composition. Going deeper in the classification, on the next layer stays materials with variable and continue (chemical) composition which generally groups mixtures of substances possessing well defined chemical composition from which homogenous substances have constant (chemical) composition, to finally arrive at chemical compound concept with well defined and unique chemical composition. From this point on we may start to discuss about the chemical structure, and an empirical formula provides the ratio between the atoms in the compound, the molecular formula provides further the number of atoms from each type in the molecule, the structural formula

reveals the structural groups in the molecule and finally geometrical formula defines the relative arrangement of the atoms in the molecule. Although it is the last refinement level, sometimes (actually quite often) the geometrical formula may degenerate too being well known the geometrical isomerism (see Warder 1890[14]). Namely, knowing the distances between the atoms and the angles between them we still don't have enough knowledge to define a unique chemical structure, which in some cases may be problematic.

MOLECULAR MODELLING

Modelling the molecular structure is a prerequisite for structure-activity inference analysis. Building of a three-dimensional model (3D) is necessary when the calculated descriptors on the structure use the geometry of the molecule. Obtaining the 3D model can be achieved using a molecular modelling program (see Table 1 for a short list of).

Tab. 1. Molecular modelling software

Name	Provider website
Abalone	http://biomolecular-modeling.com
ADF	http://scm.com
ChemBioOffice	http://cambridgesoft.com
Gaussian	http://gaussian.com
HyperChem	http://hyper.com
Materials Studio	http://accelrys.com
Q-Chem	http://q-chem.com
Spartan	http://wavefun.com

When certain software (as given above) is used, sometimes conversions between different formats storing the chemical information are useful, as well as it helps some software for visualising (only) of the obtained models (see Table 2 for a short list of).

Tab. 2. Molecular modelling auxiliary software

Name	Intend
GLmol	Browser based visualization
Jmol	Java applet for visualization
MDL Chime	Browser plugin for visualization
Open Babel	conversions
PyMOL	Python application for visualization
RasMol	GNU GPL application for visualization
WebQC	conversions

Obtaining of the 3D model of the molecule involves a series of steps, as given below:

- Constructing of the topology, namely specification of the atoms by atom type and of the bonds by bond order;
- Building of a 3D arrangement, when typical routines possibly including molecular mechanics force fields, such as are CHARM (Brooks et al. 1983[15]), AMBER (Cornell et al., 1995[16]), MMFF94 (see Halgren 1996[17]), and OPLS (Jorgensen & Tirado-Rives 1998[18]);
- Refining of the 3D arrangement may involve semi-empirical methods, such as are AM1 (Dewar et al. 1985[19]), PM3 (Stewart 1989[20]), RM1 (Rocha et al. 2006[21]) and PM6 (Stewart 2007[22]).
- Further refining of the geometry with DFT (density functional theory) approaches including HF (Hartree-Fock, see Hartree 1928[23] & Fock 1930[24]), post-HF - such as are perturbation theory (Møller & Plesset 1934 [25]), coupled cluster (Purvis & Bartlett 1982[26]), configuration interaction (Maurice & Head-Gordon 1999[27]), and composite methods (Ohlinger et al. 2009[28]) and KS (Kohn-Sham, see Kohn & Sham 1965[29]) - such as are LDA (Parr & Yang 1994[30]), GGA (Perdew et al. 1992[31]) and PBE (Perdew et al. 1996[32]);

Special precautions at building and of refining of the 3D model should be given to the structures with geometrical isomers, because during the geometrical optimization the passing from one geometrical conformation to another is quite often encountered.

One of the outcomes of the molecular modelling is the charge distribution over the atoms in the molecule, or partial charges. Different approaches are available:

- Born (see Born & Goppert-Mayer 1931[33]);
- Callen (see Callen 1949[34]);
- Szigeti (see Szigeti 1949[35]);
- Mulliken (see Mulliken 1955[36] and thereafter);
- Coulson (see Coulson et al. 1962[37]);
- Politzer (see Politzer 1968[38])
- Löwdin (see Löwdin 1970[39]);
- Hirshfeld (see Hirshfeld 1977[40]);
- Cioslowski (see Cioslowski 1989[41]);
- Bader (see Bader 1990[42]);
- Optimization method based electrostatic potentials (see for instance Wang & Ford 1994[43]).

Along with the partial charges, the outcome of the molecular modelling includes the (relative) coordinates of the atoms (usually given in Å), the bonds and their types (see Tab. 3).

Tab. 3. Typical information from modelling

The list of the atoms			
Label	Type	Coordinates (x, y, z)	Partial charge
The list of the bonds			
Atom Label	Atom Label	Bond type or order	

Usually the methodology for relating the structure with the experimental measurements in series of compounds uses the molecular structure in which the hydrogen atoms are neglected (deleted). Some of the reasons are given in the next:

- biological activities determined in vivo have as environment (medium) aqueous solutions in which processes of (partial) dissociation in which the hydrogen atoms pass in the form of protons in solution, leaving the place occupied in the molecular structure;
- hydrogen atoms can form a single bond; if they are deleted, excepting their geometrical position information can always be rebuilt;
- because form a single bond, the hydrogen atoms do not contribute to the complexity of molecular (not create chains and branches are just terminals for the structure);
- deleting of the hydrogen atoms reduces the amount of calculations for a certain structure; considering only an alkane of the general formula C_nH_{2n+2}, removing the hydrogen atoms reduces the complexity of the topology to $^1/_9$ (a topological matrix records values for each pair of atoms and the atoms are about one third less).

MOLECULAR DESCRIPTORS FAMILIES

FPIF (from Fragmental Property Index Family; Jäntschi & Diudea, 2000[44]; see Tab. 4) is a matrix-based method, in which the matrices collects properties derived from structure for fragments obtained for each pair of atoms.

Tab. 4. Code of FPIF descriptors

Gene	I_M	D_M	A_P	P_D	F_C	S_M	M_I	L_O
Genome	R	T	M	__p__	si	S	P_	I
	D	G	E	__d__	se	P	P2	R
			C	_1/p_	ji	A	E_	L
			Q	_1/d_	je	G	E2	
				_p*d_	fi	H		
				_p/d_	fe			
				_p/d2				
				p2/d2				

FPIF = $I_M \times D_M \times A_P \times P_D \times F_C \times S_M \times M_I \times L_O$

Ex.: RGseCp2/d2SE2, DGjeP_p/d2GP_

It uses $d_M(a,b)$ - the topological distance in structure *M* from atom *a* to atom *b*; $\delta_M(a,b)$ - the topological detour - i.e. longest path - in structure *M* from atom *a* to atom *b*; $W_M(a,b)$ - set of walks; $P_M(a,b)$ - set of paths; $D_M(a,b)$ - set of distances - i.e. shortest paths; $\Delta_M(a,b)$ - set of detours - i.e.

longest paths; M\p - substructure derived from structure M when the atoms inside the path p are removed from *M* together with their connections. Sets (one or more) of atoms of a molecule M for every pair of atoms (a,b) are calculated for every of the following (six) set collecting criteria (called F_C - fragmentation criteria):

÷ F_C = si: $SzDi_{a,b} = \{c \in M \mid d_M(c,a) < d_M(c,b)\}$;

÷ F_C = se: $SzDe_{a,b} = \{ c \in M \mid \delta_M(c,a) < \delta_M(c,b)\}$;

÷ F_C = ji: $Cj_{a,b,p}$ when $p \in D_M(a,b)$;

÷ F_C = je: $Cj_{a,b,p}$ when $p \in \Delta_M(a,b)$;

÷ Cf: $Cf_{a,b,p} = \{ c \in M \mid d_{G\backslash p}(c,a) < d_{G\backslash p}(c,b)\}$

÷ F_C = fi: $CfDi_{a,b} = Cf_{a,b,p}$ when $p \in D_M(a,b)$;

÷ F_C = fe: $CfDe_{a,b} = Cf_{a,b,p}$ when $p \in \Delta_M(a,b)$,

where $CJ_{a,b,p} = \{c \in M \mid d_M(c,a) < d_M(c,b)$ and $\exists w \in W_M(c,a) \mid \{a\}=w \cap p\}$.

Four atomic properties (A_P an atomic property) are taken into calculation: M (A_P = M) - as relative atomic mass; E (A_P = E) as electronegativity (Sanderson scale [45]); C (A_P = C) as (set) cardinality; P (A_P = P) as partial charge (class I, [46], from Mulliken population analysis [47]). Eight property descriptor (P_D a property descriptor) expressions account atomic properties: p (P_D = p) - atomic property; d (P_D = d) - distance; $P_D = 1/p$; $P_D = 1/d$; $P_D = pd$; $P_D = p/d$; $P_D = p/d^2$; $P_D = p^2/d^2$. Five overlapping methods (S_M - superposing method) overlap atomic properties to provide the fragmental property: S (S_M = S) - sum; P (S_M = P) - multiplication; A (S_M = A) - arithmetic mean; G (S_M = G) - geometric mean; H (S_M = H) - harmonic mean. Two models of interaction give transform in a vector a descriptor (I_M - interaction model): R (I_M = R) - rare (uses the assumption that the property of all atoms are approximately located in the fragment centre of property - of which position is consequently obtained and used to express the descriptor vector); D (I_M = D) - dense (the effect of each atom are superposed using vector summation). Two distance metrics (D_M - metric of distance) provides the distance for expressing the descriptor values: T (D_M = T) - topological (from connectivity) and D (D_M = D) - topographical (from 3D model of the molecule obtained from different levels of theory [48]). Four square-matrix based indices (M_I - matrix index) collects overall molecular property: P_ (M_I = P_) - half-sum of matrix elements; P2 (M_I = P2) - half-sum of squared matrix elements; E_ (M_I = E_) - half-sum of Hadamard product of matrix with adjacency matrix; E2 (M_I = E2) - half-sum of squared Hadamard product of matrix with adjacency matrix. Finally, a molecular descriptor is obtained via a linearization operator (L_O - linearization operator) meant to transform nonlinearities to linearity at relationships: I (L_O = I) - identity function; R (L_O = R) - reciprocal function (f(x)=1/x); L (L_O = L) - logarithm function (f(x)=ln(x)). Thus, FPIF family of molecular descriptors puts together a total number of individuals equal with the number of all multiplications described above (2·2·4·8·6·5·4·3 - 46080) - see Tab. 4.

MDF (from Molecular Descriptors Family; Jäntschi 2004[49]; Jäntschi 2005[50]; see Tab. 5) is a method based on molecular fragments obtained for pairs of atoms.

Tab. 5. Code of MDF descriptors

Gene	D_M	A_P	I_D				I_M	F_C	S_M				L_O
Genome	t	C	D	Q	L	F	r	m	m	A	G	H	I
	g	H	d	q	l	f	R	M	M	a	g	h	i
		M	O	J	V	S	m	D	n	B	F	I	A
		E	o	j	E	s	M	P	N	b	f	i	a
		G	P	K	W	T	d		S	P	s		L
		Q	p	k	w	t	D						l

$MDF = D_M \times A_P \times P_D \times I_M \times F_C \times S_F \times L_O$

Ex: lsPRLGg, IhDDDCt

Similarly with FPIF, MDF it uses two distance operators (D_O): topological (t) and geometrical (g), six atomic properties (A_P): cardinality (C), number of directly connected hydrogen atoms (H), relative atomic mass (M), electronegativity (E - Sanderson scale, group electronegativity (G - Diudea & Silaghi 1989[51]), partial atomic charge (Q - Mulliken, and twenty-four interaction descriptors (I_D) as follows: D(d), d(1/d), O(p_1), o($1/p_1$), P(p_1p_2), p($1/p_1p_2$), Q($\sqrt{p_1p_2}$), q($1/\sqrt{p_1p_2}$), J(p_1d), j($1/p_1d$), K(p_1p_2d), k($1/p_1p_2d$), L($d\sqrt{p_1p_2}$), l($1/d\sqrt{p_1p_2}$), V(p_1/d), E(p_1/d_2), W(p_1^2/d), w(p_1p_2/d), F(p_1^2/d^2), f(p_1p_2/d^2), S(p_1^2/d^3), s(p_1p_2/d^3), T(p_1^2/d^4), t(p_1p_2/d^4). Interaction were modelled (I_M) using six functions: R and r - being rare, M and m - being medium, and D and d being dense - the upper letter encoded one having as reference the first atom of the fragment (*a* in the notation given at defining of FPIF) and lower letter nominating the reference on the probe atom (*b* in the notation given at defining of FPIF). Fragmentation is driven by one fragmentation criterion (F_C): m (F_C = m) - defines smallest fragment containing atom *a*; M (F_C = M) - defines largest fragment not containing atom *b*; D (F_C = D) - defines so called Szeged fragments (closer to atom *a* than to atom *b*), P (F_C = P) - Cluj path based fragments (see FPIF definition for the definition of Cluj path based fragments - $CF_{a,b,p}$, $p \in D_M(a,b)$), nineteen overlapping strategies for fragments interaction (S_F - superposing formula): m (S_F = m) - smallest value; M (S_F = M) - biggest value; n (S_F = n) - smallest absolute value; N (S_F = n) - biggest absolute value; S (S_F = S) - sum of; A (S_F = A) - S divided to number of fragments possessing real value of descriptor; a (S_F = a) - S divided to total number of fragments; B (S_F = B) - S divided to number of atoms; b (S_F = b) - S divided to number of bonds; P (S_F = P) - product of; G geometric mean rooted P as S is divided for A (S_F = A); g (S_F = g) - rooted P as S divided for a (S_F = a); F (S_F = F) - rooted P as S divided for B (S_F = B); f (S_F = f) - rooted P as S divided for b (S_F = b); s (S_F = s) - harmonic sum; H (S_F = H), h (S_F = h), I (S_F = I), i (S_F = i) harmonic means following same procedure from s as G (S_F = G), g (S_F = g), F (S_F = F), f (S_F = f) were derived as geometric means from P and same procedure as for A (S_F = A), a (S_F = a), B (S_F = B), b (S_F = b) derived as arithmetic means from S. Six linearization operators (L_O) being: I (L_O = I) - identity($f(x)=x$); i (L_O = i) - inverse ($f(x)=1/x$), A (L_O = A) - absolute of ($f(x)=|x|$), a (L_O = a) inverse of absolute of ($f(x)=1/|x|$), L (L_O = L) - logarithm of ($f(x)=\ln(x)$) and l (L_O = l) - logarithm of absolute of ($f(x)=\ln(|x|)$). Thus, MDF puts together a total number of individuals equal with the number of all multiplications ($2 \cdot 6 \cdot 6 \cdot 24 \cdot 4 \cdot 19 \cdot 6 = 787968$) - see Tab. 5.

MDFV (from Molecular Descriptors Family - Vertex; Bolboacă & Jäntschi 2009[52]; see Tab. 6) uses atoms in place of pairs of atoms (as FPIF and MDF uses). It implements two distance metrics (D_O): t (topological) and g(geometrical), seven atomic properties (A_P): C (cardinality), H (hydrogen's), M (mass), E (electronegativity, Sanderson scale), Q (partial charge, Mulliken population analysis), L (melting point under normal temperature and pressure conditions), A (electronic affinity), fifty-eight interaction descriptors (I_D, see Tab. 6).

Tab. 6. Code of MDFV descriptors

Gene	D_O	A_P	I_D							S_F	S_M	I_T	E_U	L_O
Genome	T	C	J	R	N	Z	V	I	D	A	A	f	D	I
	G	H	j	r	n	z	v	i	d	a	a	F	d	R
		M	O	K	W	S	F	A	0	I	I	c		L
		E	o	k	w	s	f	a	1	i	i	C		
		Q	P	L	X	T	G	B	2	F	F	p		
		L	p	l	x	t	g	b	3	P	P	P		
		A	Q	M	Y	U	H	C	4	C	C	a		
			q	m	y	u	h	c	5			A		
									6			i		
									7			I		

MDFV = $D_O \times A_P \times I_D \times S_F \times S_M \times I_T \times E_U \times L_O$

Ex.: TEuIFFDL and GLbIAcDR

Atoms (or vertices in graph theory naming) are cut and fragments (connected atoms) are collected. It is calculated first the fragmental property using one out of ten strategies (I_T - interaction type):

- I_T = f - fragment's field - superposes (adds) axial projections of I_D for all pairs of atoms (b,c) from fragment ((b,c) $\in$Fr(a)) taken once - giving interactions in the fragment independent of atom cut);
- I_T = F - field of the fragment in the cut - superposes (adds) axial projections of I_D for all pairs of atoms (a,b) with one atom in the fragment (b$\in$Fr(a)) - giving interaction of the fragment in the cut;
- I_T = c - fragment's descriptor centre - computes coordinates of the centre of the descriptor using once every pair of atoms of the fragment (b,c)$\in$Fr(a);
- I_T = C - fragmentation descriptor centre - computes coordinates of the centre of the descriptor using all pairs of atoms (a,b) with one atom in the fragment (b$\in$Fr(a)) - giving the weight of the fragment in the cut;
- I_T = p - fragment's potential - uses all pairs (b,c)$\in$Fr(a) to obtain the average direction (average of the directions) of the field; uses all pairs (b,c)$\in$Fr(a) to obtain the cumulated value (sums of the effects); gives the intrinsic potential of the fragment;
- I_T = P - potential of the fragment relative to the cut - uses all pairs of atoms (a,b) with one atom in the fragment (b$\in$Fr(a)) for giving the extrinsic potential of the fragment at the cut;
- I_T = a - select highest descriptor present in the fragment (from all pairs (b,c)$\in$Fr(a) of atoms present in the fragment); give strongest interaction in the fragment;
- I_T = A - select highest descriptor of the fragment with the cut (from all pairs (a,b) with b$\in$Fr(a)); give strongest interaction in the cut;
- I_T = m - select lowest descriptor present in the fragment (from all pairs (b,c)$\in$Fr(a) of atoms present in the fragment); give weakest interaction in the fragment;
- I_T = M - select highest descriptor of the fragment with the cut (from all pairs (a,b) with b$\in$Fr(a)); give weakest interaction in the cut.

In general, for a vertex cut more than one fragment may occur. Thus, this fact are accounted using superposing of the descriptors interaction at fragments (between fragments of same cut) level by the superposing at fragment (S_F) formula. When operates in the Minkowski space (using absolute values) two superposing derives: a (S_F = a) - standing for $\max(|\cdot_x|+|\cdot_y|+|\cdot_z|)$ and i (S_F = i) - standing for $\min(|\cdot_x|+|\cdot_y|+|\cdot_z|)$. When operates in the Euclidian space (using square values and after squared root of) other two superposing derives: A (S_F = A) - standing for $\max(\sqrt{(\cdot_x^2+\cdot_y^2+\cdot_z^2)})$ and I (S_F = I) - standing for $\min(\sqrt{(\cdot_x^2+\cdot_y^2+\cdot_z^2)})$. When the effects of two or more fragments are superposed, we can superpose it as vectors, and then S_F takes value of F (S_F = F), we can superpose only their directions (and add their values), and then S_F takes the value of P (S_F = P) or weighting their effect, and then S_F takes the value of C (S_F = C). Finally, superposing is conducted at molecular level from all cuts using same procedure described above at superposing at fragments of a cut. Thus, S_M superposes as minimum absolute (when S_M = i), as maximum absolute (when S_M = a), as minimum in Euclidean space (when S_M = I), as maximum in Euclidean space (when S_M = A), weighting effects (when S_M = C), superposing directions (when S_M = P) or vectorial superposing (when S_M = F). All values of the descriptors at molecular level obtained using the procedure described above possess two things: a value and a reference (a coordinate of its position). Thus, we can express as molecular descriptor the value of it (and then E_U = D) or a reference of it (a distance, and then E_U = d) where E_U is the expressing unit). A linearization operator (L_O) serves for linear regression designing of the analysis with MDFV family of descriptors and it takes three values: I (standing for identity with), R (standing for reciprocal or inverse of) and L (standing for logarithm of). Thus, MDFV family of molecular descriptors puts together a total number of individuals equal with the number of all multiplications described above ($2·7·58·7·7·10·2·3 = 2387280$) - see Tab. 6.

Transforming of MDF to a more complex and large family (as MDFV is) does not provided expected significant improvement of QSAR (quantitative structure-activity relationships) models (with MDFV) as were obtained (with MDF), another approach were developed: SAPF (see Tab. 7).

Tab. 7. Code of SAPF descriptors

Gene	C_F	D_O	A_P	D_P	P_P	O_M	M_P	L_O
Genome	D	T	C	I	I	S	I	I
	P	G	H	E	E	M	E	A
	C		M	H	H		H	S
			E	G	G		G	T
			A	A	A		A	Q
				Q	Q		Q	R
				S	S		S	L

SAPF = L_O×G_M×O_M×P_P×D_P×A_P×M_D×C_F

Ex.: SISHQEGC and TESHIMGP

SAPF (from Structural Atomic Property Family; Sestraş et al., 2012[53]; see Tab. 8; calculation details given in Jäntschi 2012[54]) cumulates atomic properties at molecular level. It locates the molecular centre using one (out of three methods, C_F) for this task involving a metric (out of two, M_D) for the distance, a atomic property (out of eight defined till date, A_P), a rising power for the distance (D_P, seven cases), a rising power for the property (P_P, same seven cases). At molecular level one of two sorts of operators (O_M, mean type or sum type) build the molecular property as generalized mean or sum (see O_M) of descriptor's values rising it at a power (G_M, again one out of same seven cases) and the result are subject to linearization (L_O, one out of seven cases). Thus, SAPF family of molecular descriptors puts together a total number of individuals equal with the number of all multiplications described above ($7·7·2·7·7·9(5)·2·3 = 259308$ - with 9 atomic properties; 144060 with 5 atomic properties, see Tab. 8).

SMPI (Szeged Matrix Property Indices; Bolboacă & Jäntschi 2016[55] see Tab. 9) it have a online interface free to be used (Jäntschi 2014[56]).

Tab. 8. Code of SMPI descriptors

Gene	A_P	D_M	I_D	M_O	L_O
Genome	A	T	E	m	I
	B	G	U	M	R
	C	U	D	I	L
	D		P	J	
	E			E	
	F			F	
	G				

SMPI = L_O×M_O×I_D×D_M×A_P

Ex.: ImETA (first), LFPUG (last)

For SMPI distance matrix are calculated, and then for each pair of (distinct) atoms the atoms closer to the first than to the second atom of the pair are collected into (these are fragments; are exactly one fragment associated to a pair of atoms by this way) a matrix (similarly to the unsymmetrical Szeged matrix on paths, but containing sets of atoms in place of their number; for [USzp] matrix definition see Diudea et al. 2001[57]). To each fragment it is assigned an atomic property A_P=A: Atomic mass (a.u.), as sum of; A_P=B: Atomic number (Z), as harmonic sum of; A_P=C: Cardinality (=1), as sum of; A_P=D: Solid state density (kg/m^3), as harmonic mean of; A_P=E: Electronegativity (revised Pauling; for Pauling see Pauling 1932[58]; for revised see Allred 1961[59]), as geometrical mean of; A_P=F: First ionization energy (kJ/mol), as average of; A_P=G: Melting point temperature (K), as Euler (PM(p), p=2) mean of. A distance matrix is calculated using three alternatives - D_M=T: Topological distance (bonds); D_M=G: Geometrical distance (Å); D_M=U: Weighted topological distance (as reversed bond order). An interaction descriptor produces the interaction effects matrix operating on the properties and on the distances matrices - I_D=E: $E_{i,j}=P_{i,j}*D_{i,j}$; I_D=U: $U_{i,j}=P_{i,j}/D_{i,j}$; I_D=D: $D_{i,j}=1*D_{i,j}$; I_D=P: $P_{i,j}=P_{i,j}*1$. On the resulted interaction effects matrix a molecular level operator calculates a value - M_O=m: min; M_O=M: max; M_O=I: half-sum($M_{i,j}$); M_O=J: half-sum($M_{i,j}*M_{j,i}$); M_O=E: half-sum($M_{i,j}*Ad_{i,j}$); M_O=F: half-sum($M_{i,j}*M_{j,i}*Ad_{i,j}$). Finally the calculated value is subject to a linearization - L_O=I: I(x)=x; L_O=R: R(x)=1/x; L_O=L: L(x)=Ln(x). A total number of 1512 ($7·3·4·6·3$) descriptors reflects the molecular structure of a molecule from (slightly) different (from one to another) perspectives.

An improvement were made to SMPI, by extending the principle applied for Szeged fragments (assigned letter: S) to other two matrices collecting fragments from molecule for pairs of atoms, namely to maximal fragments (assigned letter: M) - the largest set containing the first atom of the pair along with all it's connected atoms after removal of the second atom of the pair from molecule and to complements of the maximal fragments (assigned letter: N) - the set containing the second atom of the pair along with the rest of the atoms lost from the molecule when maximal fragments were extracted. Therefore, the gene sequence of FMPI is increased from SMPI with one gene (see Tab. 9) and the number of descriptors is multiplied with 3 (arriving at 4536).

Tab. 8. Code of FMPI descriptors

Gene	F_C	A_P	D_M	I_D	M_O	L_O
Genome	S	A	T	E	m	I
	M	B	G	U	M	R
	N	C	U	D	I	L
		D		P	J	
		E			E	
		F			F	
		G				

FMPI = $L_O \times M_O \times I_D \times D_M \times A_P \times F_C$

Ex.: ImETAS (first), LFPUGN (last)

SOFTWARE & DATA ANALYSIS

FPIF software to generate the family was build as a stand-alone executable (working on Win16 platform) being implemented the calculations by using Pascal programming language. Excepting SAPF, which also were implemented in Pascal (FreePascal version of it) the rest of the families were implemented using PHP language.

If initially were designed to work with a database (a MySQL one) and to save the descriptors as well as the later conducted regression analysis on a database, recently the software applications were revised to produce text-based human readable files. Based on this revised version following working plan is to be used for an analysis conducted with families of molecular descriptors described above.

Stage 0. Preliminary requirements

This stage is to be applied after a procedure which assumes that the geometry of the molecules is obtained and is saved in '*.hin' - HyperChem format and the partial charges are calculated.

Much convenient is to optimize the structures with software which have possibility to parallelize the calculation, such as is Spartan. If it is the case, then conversions from Spartan ('input' and 'output' files) to HyperChem are required. Program spartan_hin_convert_qsar.php was designed to do this, and it requires '*.spinput' files to be placed in a directory, '*.txt' Spartan output files to be placed in other one, as well as it requires that the Spartan calculations to be conducted with 'verbose log' in order to contain the partial charges too. Then, in a new directory the HyperChem files are generated.

Stage 1. Generation of the descriptors

A folder containing the structure files is the input data for all programs providing the descriptors in a single file, as in the following example:

mdf2004_a_generate.php → mdf2004.txt

It applies also for mdf2015_a_generate.php, mdfv2008_a_generate.php, sapf2011.exe, smpi2014.php, and fmpi2015.php.

The output files contain matrix-based data, with molecules in columns and descriptors in lines. The values are expressed with 4 significant digits as numbers in general form (in which are expressed with smallest number of characters).

Stage 2. Filtering of the descriptors

This step is intended (in the revised version) only to remove the duplicates - it is possible for simple molecules to have two different descriptors with exactly the same series of values for all molecules in the dataset.

Also it is possible that at given precision that the values to be different only in a order of magnitude; thus, the values of the descriptors should (and are) expressed relatively to the order of magnitude of the highest (absolute value).

The v2_mdf_x_compactize.php program compact the outputs of 'mdf*' families and v2_others_compactize.php do the same for the rest, when the output files are created as following: mdf2004.txt → mdf2004_r.asc

The 1_sort_all.php program is feed with '*_r.asc' files to produce sorted and distinct series of values (for the descriptors & for the molecules) as '*_t.asc' files as following:

mdf2004_r.asc → mdf2004_t.asc

Stage 3. Building of structure - property files

The properties and/or activities are collected in 'properties.asc' file, keeping the association with the structure (from '*.hin' files) with the first line having the names of the files containing the structures of the molecules for which the property (or properties) have that value(s). The first column contains the name of the property/activity.

The generate_property_files_v2.php program generates files for each property:

family_name+"_"+property_name+".txt"

Stage 4. Regression analysis

From this point on any software may be feed with the data to conduct the regression analysis.

A program (_r1v_all.exe) was designed to provide ("r1_"+input_filename) simple linear regressions and other (r2f_all_v2.exe) to account for additive and multiplicative effects with two descriptors.

REFERENCES

---

[1] Loschmidt, J. (1861). Konstitutions - formeln der organischen chemie in graphischer derstellung. As: Ostwalds Klassiker der exacten wissenschaften Nr. 190. Leipzig: Richard Anschütz. 384 p.

[2] Rhinehardt, K.L., Mohan, R.V., Srinivas, G. (2015). Computational modeling of peptide-aptamer binding. Methods in Molecular Biology 1268: 313-333.

[3] Taha, M., Ismail, N.H., Imran, S., Selvaraj, M., Rahim, A., Ali, M., Siddiqui, S., Rahim, F., Khan, K.M. (2015). Synthesis of novel benzohydrazone-oxadiazole hybrids as β-glucuronidase inhibitors and molecular modeling studies. Bioorganic and Medicinal Chemistry 23(23): 7394-7404.

[4] Peng, X., Wang, Q., Mishra, Y., Xu, J., Reichert, D.E., Malik, M., Taylor, M., Luedtke, R.R., Mach, R.H. (2015). Synthesis, pharmacological evaluation and molecular modeling studies of triazole containing dopamine D3 receptor ligands. Bioorganic and Medicinal Chemistry Letters 25(3): 519-523.

[5] Radwan, A. A., Abdel-Mageed, W. M. (2014). In Silico Studies of Quinoxaline-2-Carboxamide 1,4-di-N-Oxide Derivatives as Antimycobacterial Agents. Molecules 19(2): 2247-2260.

[6] Kihl, O., Picard, D., Gosselin, P.-H. (2015). A unified framework for local visual descriptors evaluation. Pattern Recognition 48(4): 1170-1180.

[7] Boole, G. (1854). An Investigation of the Laws of Thought. (Reprinted 2003 as Laws of Thought. New York: Prometheus Books), 430 p.

[8] Fisher, R.A. (1922). On the interpretation of $\chi 2$ from contingency tables, and the calculation of P. Journal of the Royal Statistical Society 85(1):87-94. doi:10.2307/2340521

[9] Pearson, K. (1900). On the criterion that a given system of deviations from the probable in the case of a correlated system of variables is such that it can be reasonably supposed to have arisen from random sampling. Philosophical Magazine Series 5 50(302): 157-175. doi:10.1080/14786440009463897

[10] Krull, Wolfgang (1935). Idealtheorie. As: Ergebnisse der Mathematik, und ihrer Grenzgebiete 4(3). Berlin: Julius Springer. 152 p.

[11] Berwald, L. (1918). Über affine Geometrie XXVII. Liesche F2, Affinnormale und mittlere Affinkrümmung. Mathematische Zeitschrift 1(1): 63-78.

[12] Bolzano, B. (1804). Betrachtungen über einige Gegenstände der Elementargeometrie. Prague: Karl Barth. 65 p.

[13] Napier, J. (1614). Mirifici Logarithmorum Canonis Descriptio. Edinburgh: Andrew Hart. 155 p.

[14] Warder, R. B. (1890). Recent theories of geometrical isomerism. Science 16(400): 188-188.

[15] Brooks, B. R., Bruccoleri, R. E., Olafson, B. D., States, D. J., Swaminathan, S., Karplus, M. (1983). CHARMM: A program for macromolecular energy, minimization, and dynamics calculations. J Comp Chem 4(2): 187-217.

[16] Cornell, W. D., Cieplak, P., Bayly, C. I., Gould, I. R., Merz, K. M. Jr, Ferguson, D. M., Spellmeyer, D. C., Fox, T., Caldwell, J. W., Kollman, P. A. (1995). A Second Generation Force Field for the Simulation of Proteins, Nucleic Acids, and Organic Molecules. J. Am. Chem. Soc. 117: 5179-5197.

[17] Halgren, T. A. (1996). Merck molecular force field. I. Basis, form, scope, parameterization, and performance of MMFF94. J. Comp. Chem. 17(5-6): 490-519.

[18] Jorgensen, W. L., Tirado-Rives, J. (1988). The OPLS Force Field for Proteins. Energy Minimizations for Crystals of Cyclic Peptides and Crambin. J. Am. Chem. Soc. 110(6): 1657-1666.

[19] Dewar, M. J. S., Zoebisch, E. G., Healy, E. F., Stewart, J. J. P. (1985). Development and use of quantum molecular models. 75. Comparative tests of theoretical procedures for studying chemical reactions. The Journal of the American Chemical Society 107(13): 3902-3909.

[20] Stewart J. J. P. (1989). Optimization of parameters for semiempirical methods I. Method. The Journal of Computational Chemistry 10(2): 209-220.

[21] Rocha, R. B., Freire, R. O., Simas, A. M., Stewart J. J. P. (2006). RM1: A reparameterization of AM1 for H, C, N, O, P, S, F, Cl, Br, and I. The Journal of Computational Chemistry 27(10): 1101-1111.

---

[22] Stewart, J. J. P. (2007). Optimization of Parameters for Semiempirical Methods V: Modification of NDDO Approximations and Application to 70 Elements". The Journal of Molecular Modeling 13(12): 1173-1213.

[23] Hartree, D. R. (1928). The Wave Mechanics of an Atom with a Non-Coulomb Central Field. Part I. Theory and Methods. Math. Proc. Cambridge 24(1):89-110. & Hartree, D. R. (1928). The Wave Mechanics of an Atom with a Non-Coulomb Central Field. Part II. Some Results and Discussion. Math. Proc. Cambridge 24(1):111-132.

[24] Fock, V. A. (1930). Approximation method for solving the quantum mechanical many-body problem (In German). Zeitschrift für Physik 61(1-2):126-148. & Fock, V. A. (1930). "Self consistent field" with exchange for sodium (In German). Zeitschrift für Physik 62(11-12):795-805.

[25] Møller, C., Plesset, M. S. (1934). Note on an Approximation Treatment form Many-Electron Systems. Physical Review 46(7): 618-622.

[26] Purvis, D. G., Bartlett, R. J. (1982). A full coupled-cluster singles and doubles model: The inclusion of disconnected triples. The Journal of Chemical Physics 76 (4): 1910-1919.

[27] Maurice, D., Head-Gordon, M. (1999). Analytical second derivatives for excited electronic states using the single excitation configuration interaction method: theory and application to benzo[a]pyrene and chalcone. Molecular Physics 96 (10): 1533-1541.

[28] Ohlinger, W. S., Klunzinger, P. E., Deppmeier, B. J., Hehre W. J. (2009). Efficient Calculation of Heats of Formation. The Journal of Physical Chemistry A 113(10): 2165-2175.

[29] Kohn, W.; Sham, L. J. (1965). Self-Consistent Equations Including Exchange and Correlation Effects. Physical Review 140(4A): A1133-A1138.

[30] Parr, R.G., Yang, W. (1994). Density-Functional Theory of Atoms and Molecules. Oxford: Oxford University Press. 333 p.

[31] Perdew, J. P., Chevary, J. A., Vosko, S. H., Jackson, K. A., Pederson, M. R., Singh, D. J., Fiolhais, C. (1992). Atoms, molecules, solids, and surfaces: Applications of the generalized gradient approximation for exchange and correlation. Physical Review B 46 (11): 6671-6687.

[32] Perdew, J. P., Burke, K., Ernzerhof, M. (1996). Generalized Gradient Approximation Made Simple. Phys. Rev. Lett. 77(18): 3865-3868.

[33] Born, M., Goppert-Mayer, M. (1931). Dynamische Gittertheorie der Kristalle. Handbuch der Physik 24(2): 623-794.

[34] Callen, H. B. (1949). Electric Breakdown in Ionic Crystals. Phys. Rev. 76: 1394-1402.

[35] Szigeti, B. (1949). Polarisability and dielectric constant of ionic crystals. Trans. Faraday Soc. 45: 155-166.

[36] Mulliken, R. S. (1955). Electronic Population Analysis on LCAO–MO Molecular Wave Functions. I. J. Chem. Phys. 23: 1833-1840.

[37] Coulson, C. A., Redei, L. B., Stocker, D. (1962). The Electronic Properties of Tetrahedral Intermetallic Compounds. I. Charge Distribution. Proceedings of the Royal Society of London. Series A, Mathematical and Physical Sciences 270(1342): 357-372.

[38] Politzer, P. (1968). Electron affinities of atoms. Transactions of the Faraday Society 64: 2241-2246.

[39] Löwdin, P. O. (1970). On the Nonorthogonality Problem. Advances in Quantum Chemistry 5: 185-199.

[40] Hirshfeld, F. L. (1977). Bonded-Atom Fragments for Describing Molecular Charge Densities. Theoret. Chim. Acta 44: 129-138.

[41] Cioslowski, J. (1989). General and unique partitioning of molecular electronic properties into atomic contributions. Phys. Rev. Lett. 62(13): 1469-1471.

[42] Bader, R. F. W. (1990). Atoms in Molecules: A Quantum Theory. Oxford: Oxford University Press. 438 p.

[43] Wang, B., Ford, G. P. (1994). Atomic charges derived from a fast and accurate method for electrostatic potentials based on modified AM1 calculations. J. Comput. Chem. 15: 200-207.

[44] Jäntschi L, 2000. Predicţia proprietăţilor fizico-chimice şi biologice cu ajutorul descriptorilor

---

matematici. Teză de doctorat (Chimie) - coordonator Prof. Diudea MV. Universitatea "Babeş-Bolyai" din Cluj-Napoca, Cluj-Napoca, Ian. 2000.

[45] Sanderson, R. T. (1983). Electronegativity and bond energy. Journal of the American Chemical Society 105(8): 2259-2261.

[46] Cramer, C. J. (2002). Essentials of Computational Chemistry: Theories and Models. New York: J. Wiley. 542 p.

[47] Mulliken, R.S. (1955). Electronic Population Analysis on LCAO-MO Molecular Wave Functions. I. The Journal of Chemical Physics 23(10): 1833-1831.

[48] Clark, T. (1985). A Handbook of Computational Chemistry. New York: Wiley. 332 p.

[49] Jäntschi, L. (2004). MDF - A New QSAR/QSPR Molecular Descriptors Family. Leonardo Journal of Sciences 3(4): 68-85.

[50] Jäntschi, L. (2005). Molecular Descriptors Family on Structure Activity Relationships 1. Review of the Methodology. Leonardo Electronic Journal of Practices and Technologies 4(6): 76-98.

[51] Diudea, M. V., Silaghi-Dumitrescu, I. (1989). Valence group electronegativity as a vertex discriminator. Revue Roumaine de Chimie 34(5): 1175-1182.

[52] Bolboacă, S. D., Jäntschi, L. (2009). Comparison of QSAR performances on carboquinone derivatives. TheScientificWorldJOURNAL 9(10): 1148-1166.

[53] Sestraş, R. E., Jäntschi, L., Bolboacă, S. D. (2012). Quantum mechanics study on a series of steroids relating separation with structure. JPC - Journal of Planar Chromatography - Modern TLC 25(6): 528-533.

[54] Jäntschi, L. (2012). Structure vs. Properties: Algorithms and Models. Habilitation thesis in Chemistry. Bucharest: CNATDCU (defended in 2013 in Cluj-Napoca: Babeş-Bolyai University). 175 p.

[55] Bolboacă, S. D., Jäntschi, L. (2016). Nano-quantitative structure-property relationship modeling on C_{42} fullerene isomers. Journal of Chemistry. Article in press.

[56] Jäntschi, L. (2014). Szeged Matrix Property Indices. Online calculation software (release version). URL: http://l.academicdirect.org/Chemistry/SARs/SMPI/

[57] Diudea, M.V.; Gutman, I.; Jäntschi, L.; 2001. Molecular Topology. New York: Nova Science. 335 p.

[58] Pauling, L. (1932). The Nature of the Chemical Bond. IV. The Energy of Single Bonds and the Relative Electronegativity of Atoms. Journal of the American Chemical Society 54(9): 3570-3582.

[59] Allred, A. L. (1961). Electronegativity Values from Thermochemical Data. Journal of Inorganic and Nuclear Chemistry 17(3-4): 215-221.

Analele Universităţii din Oradea-Fascicula Chimie, Vol. XXIII, 2016

β-CYCLODEXTRIN MODIFIED GRAPHENE/TYROSINASE BASED BIOSENSOR FOR DOPAMINE DETERMINATION

Luminiţa FRITEA[1, 2, 3], Mihaela TERTIŞ[2], Cecilia CRISTEA[2], Serge COSNIER[3], Robert SĂNDULESCU[2]
[1]Department of Preclinical Disciplines, Faculty of Medicine and Pharmacy, University of Oradea,
1 Decembrie Street, Oradea, Romania, fritea_luminita@yahoo.com
[2]Analytical Chemistry Department, Faculty of Pharmacy, "Iuliu Haţieganu" University of Medicine and Pharmacy, 4 Pasteur Street, 400349, Cluj-Napoca, Romania
[3]University Grenoble Alpes, DCM UMR 5250, F-38000 Grenoble, France

Abstract: *A cyclodextrin-modified graphene composite was obtained by noncovalent functionalization of graphene with β-cyclodextrin leading to an effective aqueous dispersion of the exfoliated graphene sheets. This nanocomposite was characterized by using spectral, microscopic and electrochemical techniques. The reduced graphene oxide modified with β-cyclodextrin was used in combination with tyrosinase entrapped in polyethylenimine film for the elaboration of a biosensor which was successfully applied for dopamine determination in biological samples by amperometry.*

Key words: *biosensor, reduced graphene oxide, β-cyclodextrin, tyrosinase, real samples*

INTRODUCTION

Graphene, a two dimensional carbon based nanomaterial, has been widely studied in the last ten years due to its unique physical and chemical properties such as: high surface area, excellent conductivity, facile production and versatile functionalization. Graphene and its derivatives are used in energy, electronics, catalysis, biosensing and drug delivery systems. A broad range of graphene-based configurations were elaborated for the development of electrochemical sensors for pharmaceutical, biomedical and environmental applications recording an improved sensitivity for a wide range of analytes.[1-5]

The graphene derivatives can be obtained by two methods: covalent functionalization (for instance by using diazonium salts, dienophile compounds, 1-ethyl-3-(3-dimethylaminopropyl) carbodiimide (EDC) or *N,N'*-dicyclohexylcarbodiimide (DCC) and *N*-hydroxysuccinimide (NHS), heteroatom doping (N_2, B)), and by non-covalent functionalization (π–π stacking, hydrophilic and hydrophobic interactions).[6-8] The platforms based on electrodes modified with graphene powder or graphene-composite are widely used for (bio)sensing applications.[9-14]

The graphene oxide (GO), derivative bearing functional groups containing oxygen, presents excellent hydrophilicity, but lower conductivity than the pristine graphene. Thus, the reduced graphene oxide (RGO) was obtained in order to overcome this limitation.[15,16] Despite of the advantageous properties of graphene, it presents also a major disadvantage: its poor dispersion in aqueous medium. Stable dispersions of graphene sheets have been achieved by using amphiphilic polymers and cyclodextrins, among others, as dispersing agents.[16,17]

Cyclodextrins (CDs) are non-reducing cyclic oligosaccharides consisting of six (*α*-cyclodextrin), seven (*β*-cyclodextrin), eight (*γ*-cyclodextrin) or more D(+)-glucopyranose units with a relatively hydrophobic cavity. The most notable characteristic of CDs is the inclusion complexes formation with various organic and inorganic molecules.[18] A various range of analytes was determined with high sensitivity and selectivity by using CD based electrochemical (bio)sensors due to their complexation ability.[18-21] Recently, the electrodes modified with graphene and cyclodextrins have been widely employed for the detection of many biological molecules such as dopamine (DA), among others, with higher performances.[15,16,18]

Herein, the improvement of the aqueous dispersion of RGO was successfully achieved by using a non-covalent functionalization with β-cyclodextrin (β-CD). The obtained graphene-composite was characterized by spectral, microscopic and electrochemical methods. The *β*-CD modified graphene platform was used for the elaboration of a tyrosinase based biosensor which was applied for DA detection with good analytical performances.

METHODS, TECHNIQUES, MATERIALS

Reagents and solutions

All the reagents and the chemicals were purchased from Sigma Aldrich. The 0.1 M phosphate buffer at pH 7.2 was used.

The reduced graphene oxide modified with *β*-cyclodextrin (RGO-CD) was prepared by dispersing 30 mg GO in 60 mL water and were sonicated for 2 hours, after that a solution of *β*-CD (240 mg/60 mL) was added and stirred together for 30 minutes. As reducing agent was used 600 mg of ascorbic acid. The unmodified RGO was prepared with the same procedure mentioned above without the addition of *β*-CD. After 48 hours of stirring, the suspension was centrifuged and the powder was dried in oven.

The 1 mg/ml polyethyleneimine (PEI) solution was prepared in water:alcohol (1:1) mixture. The 1 mg/ml tyrosinase solution was obtained by dissolving the appropriate weight of enzyme in distilled water. The urine was collected from a healthy patient and it was filtered (paper filter FILTRAK 390) before analysis, then diluted 1:100 with phosphate buffer (0.1 M, pH 7.2). The human serum was prepared by dissolving the lyophilized powder in 2 ml of distilled water and then diluted 1:100 with phosphate buffer (0.1 M, pH 7.2).

Experimental procedures

Electrochemical measurements were carried out by using a three-electrode cell with GCE or Pt as working electrode, Ag/AgCl as reference electrode and a platinum wire as the counter electrode and were recorded with an Autolab PGSTAT100 (Metrohm/EcoChemie, The Netherlands) controlled by Nova 1.10.4 software. Glassy carbon electrodes (GCEs) purchased from BASi. (3 mm diameter) were first polished using 2 μm diamond paste and then washed with plenty of water and ethanol. The electrode modification included some steps consisting in layer by layer (LBL) deposition of 5 µL of modifiers and then dried in the oven at 40°C for 10-15 minutes.

For the experiments with glucose oxidase (GOx) and glucose oxidase tagged with adamantane (GOx-Ad), Pt was used as working electrode (5 mm). 20 µL of a mixture of graphene (RGO, RGO-CD) and enzyme were casted onto the Pt electrodes, after that the electrodes were dried in vacuum for 30 minutes. The biosensor was tested towards glucose oxidation by using amperometry at 0.6 V vs. SCE. For the experiments with $[Ru(NH_3)_6]Cl_3$, 0.1 M $LiClO_4/H_2O$ was used as electrolyte and the cyclic voltammograms (CVs) were recorded with a scan rate of 50 mV/s.

The parameters for square wave voltammetry (SWV) were: frequency 25 Hz, amplitude 25 mV, initial potential -0.3 V, end potential 1 V. The amperometric determinations were made under stirring with 200 rpm at -0.2 V.

Electrochemical impedance spectroscopy (EIS) measurements were carried out in the presence of 10 mM $[Fe(CN)_6]^{3-/4-}$ solution in PBS (10 mM, pH 7.4). The impedance of the experimental system was measured in a frequency range from 100 mHz to 100 KHz using the open circuit potential (OCP).

The FTIR spectra were obtained by using a Thermo Scientific Nico-let iS10 in the wave number range from 650 to 4000 cm^{-1}. An Alpha 300R (WiTec) confocal Raman microscope was used for the microscopic optical images capture. The TEM images were obtained by using a Philips CM200 microscope operating at an accelerating voltage of 200 kV with F216 TVIPS camera.

RESULTS AND DISCUSSIONS

Spectral and microscopic characterization of the composite materials

The three types of graphene: GO, RGO, and RGO-CD, were characterized by spectral and microscopic techniques.

Some specific signals corresponding to different functional groups can be observed in the FTIR spectrum of GO. These signals are attributed to the: OH stretching vibration (a broad absorption band at 3232 cm^{-1}), stretching of C=O from carboxyl groups (a band at about 1720 cm^{-1}), stretching of C=O and C=C from aromatics (an absorption band at 1618 cm^{-1}), deformation vibration of OH (a band at 1346 cm^{-1}), C-O stretching vibration (two absorption bands at 1096 cm^{-1} and 1040 cm^{-1}) and bending of the aromatic sp^2 C-H at 878 cm^{-1}. [22-25]

All the characteristic bands for oxygen containing groups from the GO spectrum are significantly decreased in the RGO spectrum, indicating that those groups were partially eliminated by reduction process. The “shoulder” from 2790 cm^{-1} υ(C-H) presents weaker intensity due to the disappearance of C-H bonds during the aromatization of the graphene core.[26,27]

All the modifications observed in the FTIR spectra reveal that the GO sheets were successfully reduced (Figure 1).

In the case of the RGO-CD spectrum the band for hydroxyl groups (3313 cm^{-1}) and for carboxylic groups (1633 cm^{-1}) are diminished due to the reduction process of the GO. In addition, there appear some new bands at: 2928 cm^{-1} (C-H stretch in alkanes), 1201 cm^{-1}, 1148 cm^{-1}, 1075 cm^{-1}, 1020 cm^{-1} (C-O stretch in alcohols and ethers) attributed to β-CD molecule providing the evidence that the RGO was successfully functionalized with β-CD (Figure 1).

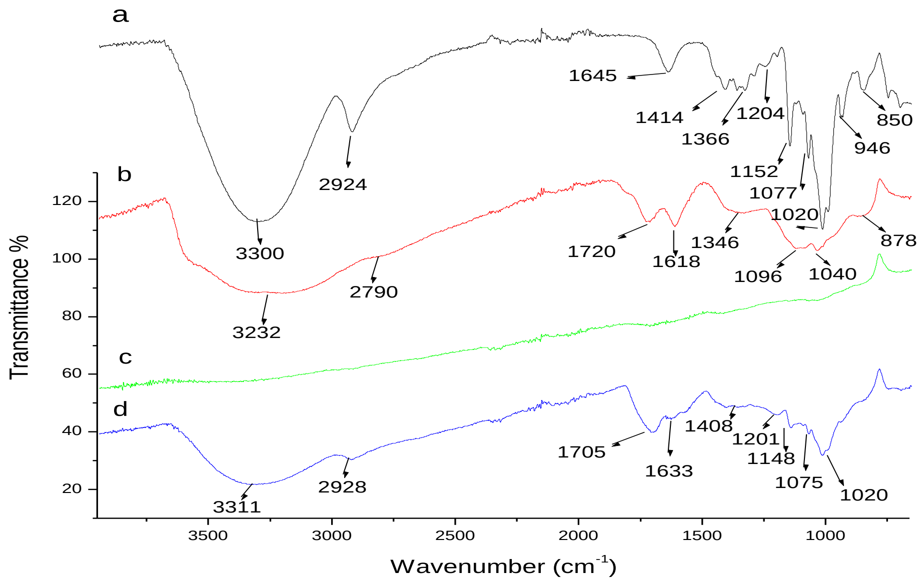

Figure 1. FTIR spectra registered for: (a) β-CD, (b) GO, (c) RGO, and (d) RGO-CD

In the images obtained by using TEM and optical microscopy, presented in Figure 2 (A - F), it can be observed that the RGO sheets are more aggregated in “black flakes” in comparison with the RGO-CD. Meanwhile, the RGO-CD sheets are more exfoliated probably due to the presence of β-CD with its good dispersing properties acting as a surfactant of graphene in water (Figure 2 A-F).[16,23]

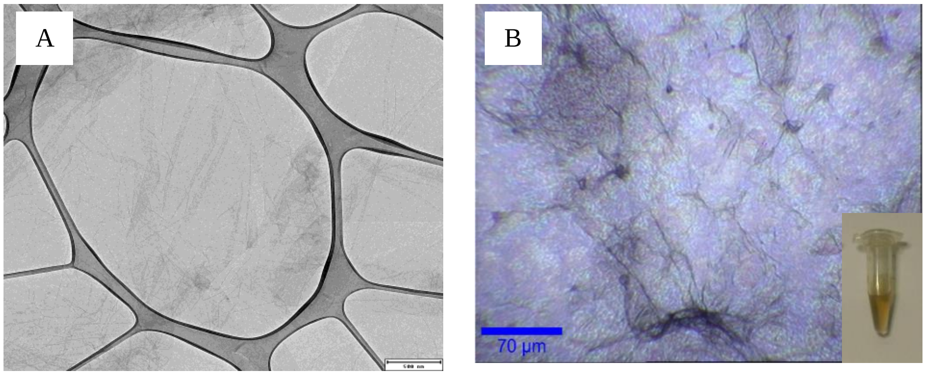

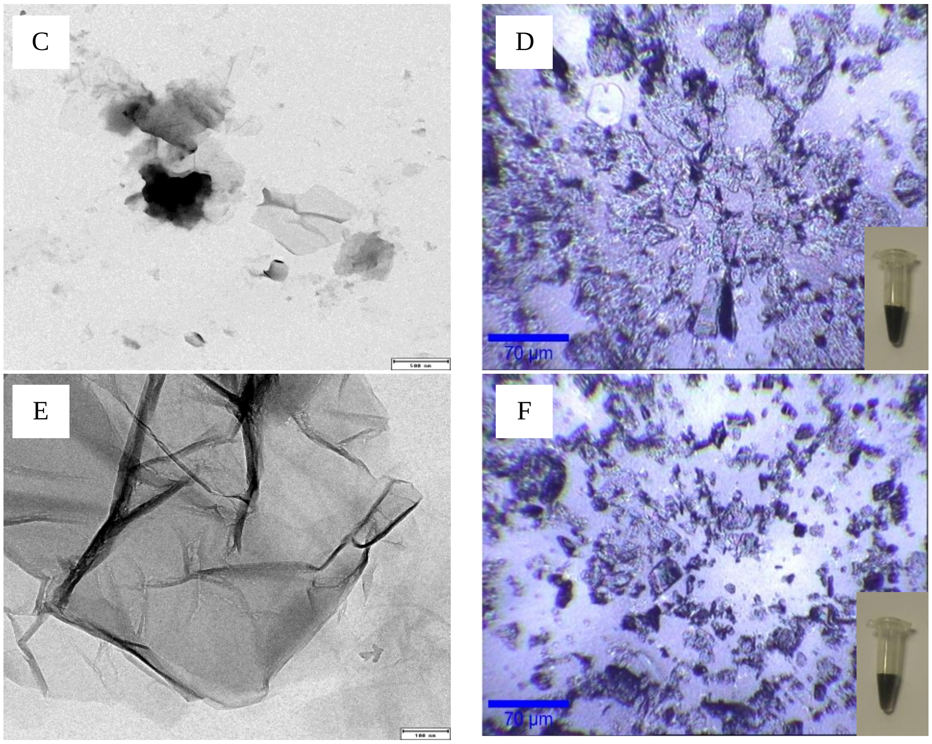

Figure 2. TEM (left) and microscopic images (right) for: GO (A and B), RGO (C and D) and RGO-CD (E and F)

Electrochemical characterization of the composite materials

The presence of CD in the carbon based nanocomposite was verified by means of the CD possibility to form inclusion complexes with adamantane. Thus, molecules of glucose oxidase (GOx) and glucose oxidase tagged with adamantane (GOx-Ad) were immobilized to the electrode surface and then, the obtained biosensors were tested towards glucose oxidation by using amperometry.

It can be observed that the value of the current intensity obtained for the biosensors containing RGO-CD and GOx-Ad is two times higher than the one obtained with unmodified GOx. This indicates the complexation between adamantane and CD cavity leading to a better immobilization of the biomolecules (Figure 3). Concerning the unmodified RGO, no significant difference of the analytical performances between the two types of enzymes used was observed.

The advantages of RGO-CD were also highlighted by the electrochemical behavior of Ru(III) containing solution (Figure 4). It can be observed that in the case of Pt electrode modified with RGO (RGO/Pt), there are two pairs of peaks corresponding to Ru(III)/Ru(II) redox couple (E_{pa1} = -0.28V/ E_{pc1} = -0.38V and E_{pa2} = -0.12V/ E_{pc2} = -0.21V). But in the case of Pt electrode modified with RGO-CD (RGO-CD/Pt) only one high peak is noticed for Ru oxidation and reduction respectively (E_{pa} = -0.28V, E_{pc} = -0.38V).

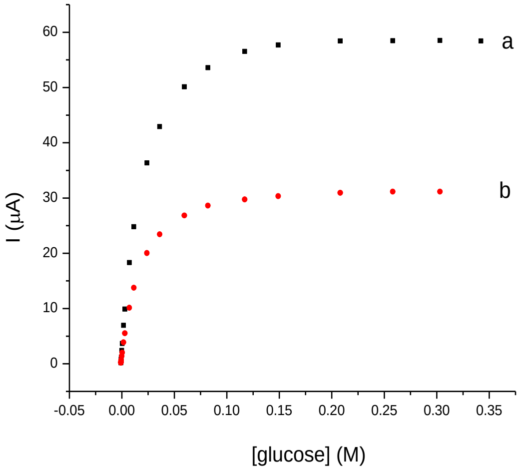

Figure 3. Calibration curves for glucose oxidation obtained at the Pt electrodes modified with 0.5 mg/mL RGO-CD and: (a) 0.25 mg/mL GOx-Ad and (b) 0.25 mg/mL GOx

These differences indicate that the electrode surface is homogenously covered by RGO-CD, meanwhile the RGO deposition onto the electrode leaves some uncovered places where the behavior is the same with the bare electrode. This assumption was sustained by the fact that the E_{pa2}, E_{pc2} present the same values as for the bare electrode. This result indicates once again the excellent dispersion of the graphene sheets assured by the CD, which confirm the microscopic observations. The value of the current peak intensity registered for Ru as redox probe was increased by the graphene deposition especially in the case of RGO-CD proving an improvement of the electroactive area of the electrode probably due to the homogenously covering with the graphene suspension.

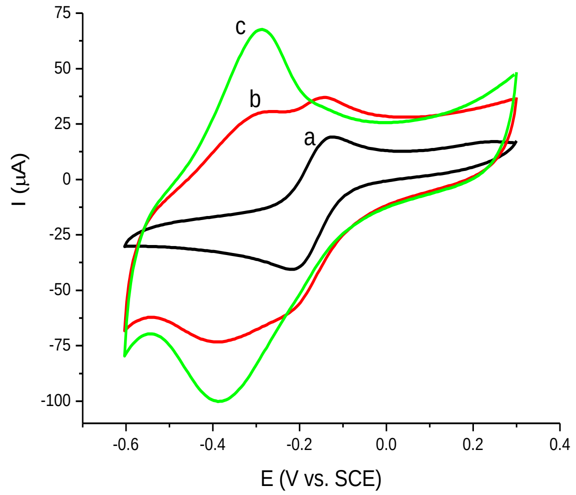

Figure 4. CVs *of 1 mM [Ru(NH*$_3$*)*$_6$*]Cl*$_3$ *obtained at: (a) Pt electrode, (b) RGO/Pt and (c) RGO-CD/Pt*

Square wave voltammetry (SWV) was also used to test the graphene functionalization with CD. Thus, the CD functionalized graphene was furthermore used for dopamine (DA) electrochemical determination. Comparing the RGO modified with CD and the bare GCE, it can be observed that the oxidation potential is shifted towards cathodic values with 49 mV due to the presence of the CD molecules cavities which facilitate the DA oxidation. The values of the peak intensity and the peak area obtained by using the electrode modified with the CD based nanocomposite are 2.4 times higher than those obtained on bare GCE. All these results highlighted that the CD and graphene improved the electrochemical properties of the sensor applied for DA detection (Table 1).

Table 1. The comparison between the data obtained from the SWVs of 10^{-3} *M DA at bare GCE, PEI modified GCE (PEI/GCE) and RGO-CD/PEI modified GCE(RGO-CD/PEI/GCE)*

Electrode type	**GCE**	**PEI/GCE**	**RGO-CD/ PEI/GCE**
E (V)	0.233	0.233	0.184
I (µA)	92.70	57.80	218.00
Peak area (µA)	18.60	13.80	44.30

The number of the RGO layers deposited onto the electrode surface was also optimized and the one layer of RGO configuration was chosen. By increasing the number of RGO layers, the decreasing of the peak intensity and area was observed and the potential was slightly shifted towards anodic values (Figure 5).

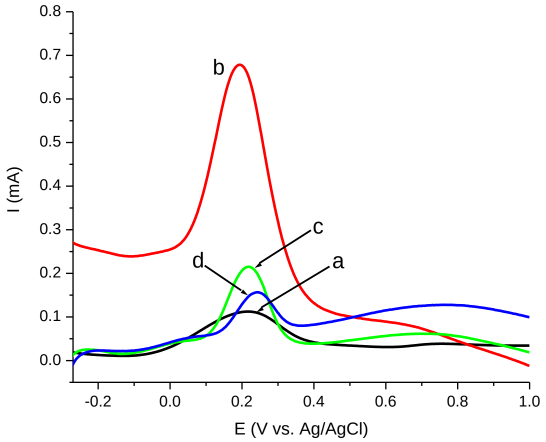

Figure 5. SWVs of 10^{-3} *M DA solution obtained at: (a) bare GCE and GCEs modified with:(b) one layer of RGO-CD and PEI;(c) three layers of RGO-CD and one layer of PEI;(d) five layers of RGO-CD and one layer of PEI*

This behavior can be explained by the compaction of the graphene structure harming the electron transfers. For one layer of RGO no preconcentration step is required. The oxidation response is highest only after 1 minute accumulation, indicating that the penetration of DA through the three and five graphene layers is required.

The deposition technique was also investigated comparing layer by layer method (LBL) and spin coating method. For the biosensor elaboration LBL method was chosen because the peak current intensity was 4.5 times higher in comparison with the spin coating method.

Electrochemical impedance spectroscopy (EIS) was used during the biosensor elaboration, following each step of the electrode modification through the variation of the charge transfer resistance (R_{ct}) represented in the Nyquist plots of EIS (Figure 6). It can be observed that the RGO-CD reduced the R_{ct} value from 264.87 Ω (in the case of bare GCE) to 217.25 Ω incresing the sensor conductivity due to its characteristic properties. The R_{ct} value was slightly incresed to 224.94 Ω by the addition of the tyrosinase probably due to its macromolecular structure.

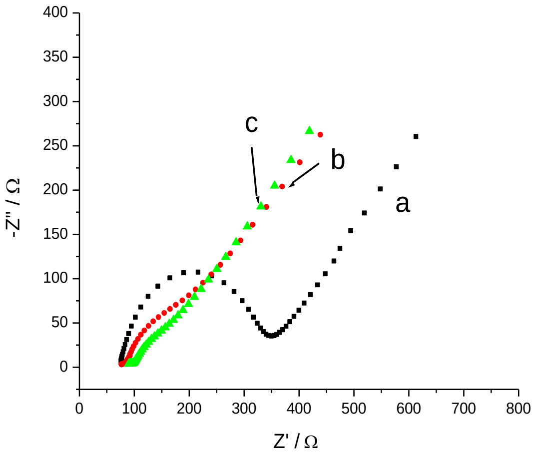

Figure 6. Nyquist plots of 10 mM $[Fe(CN)_6]^{3-/4-}$ in PBS (0.02 M; pH 7.4) at (a) bare GCE; (b) RGO-CD/GCE and (c) TYR/PEI/RGO-CD/GCE

Optimization and testing of the biosensor for dopamine

After the characterization of the RGO-CD composite material and the study of the electrochemical behavior of the electrodes modified with this material in the presence of different redox species, a biosensor was elaborated for dopamine detection.

The elaborated biosensor had the configuration consisting in one layer of RGO-CD and 50 µg of tyrosinase (TYR) entrapped in polymeric film (PEI). The biosensor elaboration process is schematically represented in Figure 7.

This biosensor presented a LOD of 4 µM (S/N=3) calculated with the equation: I (µA) = 0.0121 · C_{DA} (µM) + 0.0059; R^2= 0.9993; exhibiting a linear domain ranging from 4 to 140 µM.

Some interference tests were performed by using the elaborated biosensor and no significant interferences were observed for DA amperometric determination in the presence of equal concentrations of uric acid (UA), ascorbic acid (AA) and glucose (Figure 8).

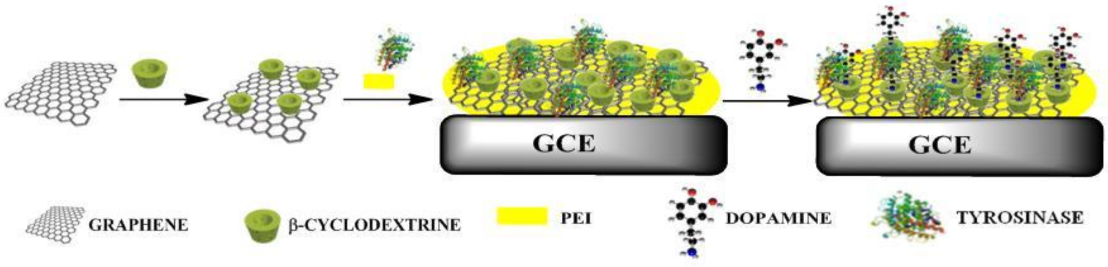

Figure 7. Schematic representation of the biosensor elaboration (adapted from 15)

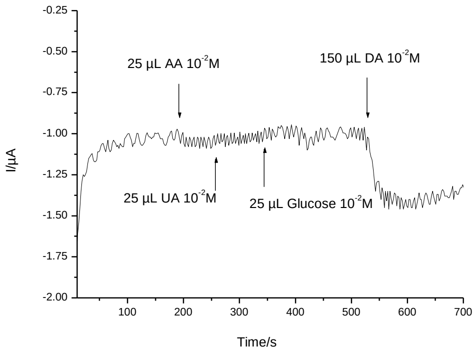

Figure 8. The current intensity variation in time obtained at TYR/PEI/RGO-CD/GCE after the addition of equal volumes (25 µL) of 10^{-2} M of DA, AA, UA and glucose solutions in PBS (pH 7.2; 0.1 M)

The performance of this biosensor for the detection of DA in biological samples was tested by using amperometry and by maintaining the modified electrode at -0.2 V for a stated time. The biologic samples (urine and human serum) were diluted 100 times before the analyses and then different volumes of 10^{-2} M standard DA solution were spiked obtaining good recovery rates (Table 2).

Table 2. The amperometric detection of DA from urine and serum samples

Samples	Volume of 10^{-2} M DA spiked (µL)	Recovery (%)	RSD (%)
PBS	5 10 25	- - -	-
Urine	5 10 25	99.13 99.56 98.28	1.1
Serum	5 10 25	97.65 97.73 100.34	2.1

CONCLUSIONS

The functionalization of graphene with *β*-cyclodextrin has improved the dispersion of this carbon based nanomaterial in aqueous media due to the presence of *β*-CD. The RGO-CD was characterized by using spectral, microscopic and electrochemical methods. The combination of the reduced graphene oxide modified with CD and tyrosinase entrapped in PEI film enhanced the electroanalytical performances of the biosensor allowing a selective and sensitive detection of dopamine in real samples.

ACKNOWLEDGMENTS:

The authors express their gratitude to PhD Alan Le Goff for his cooperation and revision and to PhD Jean-Luc Putaux for the transmission electron microscopy characterization. The authors are grateful for the financial support from PHC Brancusi 2015, no. 32602 QD and Romanian National Authority for Scientific Research for projects no. PN-II-RU-TE-2014-4-0460.

REFERENCES

[1] Lawal, A.T. (2015). Review: Synthesis and utilization of graphene for fabrication of electrochemical sensors. Talanta; Vol 131, pp. 424-443.

[2] Chen, D., Zhang, H., Liu, Y., and Li, J. (2013). Graphene and its derivatives for the development of solar cells, photoelectrochemical, and photocatalytic applications. Energy Environ Sci; Vol 6, pp. 1362-1387.

[3] Chen, X.M., Wu, G.H., Jiang, Y.Q., Wang, Y.R., and Chen, X. (2011). Graphene and graphene-based nanomaterials: the promising materials for bright future of electroanalytical chemistry. Analyst; Vol. 136, pp. 4631-4640.

[4] Chen, D., Tang, L., and Li, J. (2010). Graphene-based materials in electrochemistry (Review). Chem Soc Rev; Vol. 39, pp. 3157-3180.

[5] Liu, Y., Dong, X., and Chen, P. (2012). Biological and chemical sensors based on graphene materials. Chem Soc Rev; Vol. 41, pp. 2283-2307.

[6] Tertiș, M., Hosu, O., Fritea, L., Farcău, C., Cernat, A., Săndulescu, R., and Cristea, C. (2015). A novel label-free immunosensor based on activated graphene oxide for acetaminophen detection. Electroanal; Vol. 27 (3), pp. 638-647.

[7] Cernat, A., Tertiș, M., Păpară, C.N., Bodoki, E., and Săndulescu, R. (2015). Nanostructured platform based on graphene-polypyrrole composite for immunosensor fabrication. Int J Electrochem Sci; Vol. 10, pp. 4718-4731.

[8] Săndulescu, R., Tertiş, M., Cristea, C., and Bodoki, E. (2015). New Materials for the Construction of Electrochemical Biosensors, In Biosensors - Micro and nanoscale applications. InTech Rijeka Croatia, pp. 1-36.

[9] Keeley, G.P., O'Neill, A., Holzinger, M., Cosnier, S., Coleman, J.N., and Duesberg, G.S. (2011). DMF-exfoliated graphene for electrochemical NADH detection. Phys Chem Chem Phys; Vol. 13, pp. 7747-7750.

[10] Keeley, G.P., McEvoy, N., Nolan, H., Holzinger, M., Cosnier, S., and Duesberg, G.S. (2014). Electroanalytical Sensing Properties of Pristine and Functionalized Multilayer Graphene. Chem Mater; Vol. 26 (5), pp 1807-1812.

[11] Le Goff, A., Reuillard, B., and Cosnier, S. (2013). A Pyrene-Substituted Tris(bipyridine)osmium(II) Complex as a Versatile Redox Probe for Characterizing and Functionalizing Carbon Nanotube- and Graphene-Based Electrodes. Langmuir; Vol. 29 (27), pp 8736-8742.

[12] Lalaoui, N., Le Goff, A., Holzinger, M., Mermoux, M., and Cosnier, S. (2015). Wiring Laccase on Covalently Modified Graphene: Carbon Nanotube Assemblies for the Direct Bio-electrocatalytic Reduction of Oxygen. Chem Eur J; Vol. 21 (8), pp. 3198-3201.

[13] Singh, M., Holzinger, M., Tabrizian, M., Winters, S., Berner, N.C., Cosnier, S., and Duesberg, G.S. (2015). Noncovalently Functionalized Monolayer Graphene for Sensitivity Enhancement of Surface Plasmon Resonance Immunosensors. J Am Chem Soc; Vol. 137 (8), pp. 2800-2803.

[14] Pumera, M. (2011). Graphene in biosensing. Mater Today; Vol. 14, pp. 308-315.

[15] Fritea, L., Tertiș, M., Cosnier, S., Cristea, C., and Săndulescu R. (2015). A novel reduced graphene oxide/β-cyclodextrin/tyrosinase biosensor for dopamine detection. Int J Electrochem Sci; Vol. 10, pp. 7292-7302.

[16] Fritea L., Le Goff, A., Putaux, J-L., Tertiş, M., Cristea, C., Săndulescu, R., and Cosnier, S. (2015). Design of a reduced-graphene-oxide composite electrode from an electropolymerizable graphene aqueous dispersion using a cyclodextrine-pyrrole monomer. Application to dopamine biosensing. Electrochim Acta; Vol. 178, pp. 108-112.

[17] Guo, Y., Guo, S., Ren, J., Zhai, Y., Dong, S., and Wang, E. (2010). Cyclodextrin Functionalized Graphene Nanosheets with High Supramolecular Recognition Capability: Synthesis and Host-Guest Inclusion for Enhanced Electrochemical Performance. ACS Nano; Vol.4, pp. 4001-4010.

[18] Fritea, L., Tertiş, M., and Săndulescu, R. (2015). Applications of Cyclodextrins in Biomedical Electrochemistry. in: Cyclodextrins: Synthesis, Chemical Applications and Role in Drug Delivery. Nova Science Publishers, Inc. USA. pp. 45-84.

[19] Fritea, L., Tertiş, M., Topală, T.L., and Săndulescu, R. (2013). Electrochemical and spectral study of cyclodextrins interactions with some pharmaceutical substances. Farmacia; Vol. 61 (6), pp.1054-1068.

[20] Fritea, L., Tertiş, M., Cristea, C., and Săndulescu, R. (2013). New β-Cyclodextrin entrapped in polyethyleneimine film-modified electrodes for pharmaceutical compounds determination. Sensors; Vol. 13, pp.16312-16329.

[21] Fritea L., Tertiş, M., Cristea, C., Cosnier, S., and Săndulescu, R. (2015). Simultaneous determination of ascorbic and uric acids in urine using an innovative electrochemical sensor based on β-Cyclodextrin. Anal Lett; Vol. 48 (1), pp. 89-99.

[22] Bustos-Ramírez, K., Martínez-Hernández, A.L., Martínez-Barrera, G., De Icaza, M., Castaño, V.M., and Velasco-Santos, C. (2013). Covalently Bonded Chitosan on Graphene Oxide via Redox Reaction. Materials; Vol. 6, pp. 911-926.

[23] Hu, X., Qi, R., Zhu, J., Lu, J., Luo, Y., Jin, J., and Jiang, P. (2014). Preparation and properties of dopamine reduced graphene oxide and its composites of epoxy. J Appl Polym Sci; Vol. 131, DOI: 10.1002/app.39754.

[24] Stankovich, S., Piner, R.D., Chen, X., Wu, N., Nguyen, S.B.T., and Ruoff, R.S. (2006). Stable aqueous dispersions of graphitic nanoplatelets via the reduction of exfoliated graphite oxide in the presence of poly(sodium 4-styrenesulfonate). J Mater Chem; Vol. 16, pp. 155-158.

[25] Xu, C., Wang, X., Wang, J., Hu, H., and Wan, L. (2010). Synthesis and photoelectrical properties of β-cyclodextrin functionalized graphene materials with high biorecognition capability. Chem Phys Lett; Vol. 498, pp. 162-167.

[26] Pei, S., and Cheng, H-M. (2010). The reduction of graphene oxide. Carbon; Vol. 50, pp. 3210-3228.

[27] Choi, E-Y., Han, T.H., Hong, J., Kim, J.E., Lee, S.H., Kim, H.W., and Kim, S.O. (2010). Noncovalent functionalisation of graphene with end-functional polymers. J Mater Chem; Vol. 20, pp. 1907-1912.

SYNTHESIS AND CHARACTERIZATION MESOPOROUS MAGNETITE IN THE PRESENCE OF L-LEUCINAMIDE

Ioana Lavinia ARDELEAN[1], Luric Bogdan NICULAE STOENCEA[1], Denisa FICAI[1], Anton FICAI[1], Gheorghe NECHIFOR[1]

[1]University Politehnica of Bucharest, Faculty of Applied Chemistry and Material Science; 1-7 Polizu St., Bucharest, Romania, (dy4_ioana@yahoo.com)

Abstract:

In this paper the synthesis of mesoporous magnetite nanoparticles using leucinamide as stabilizer agent is presented. Mesoporous magnetite nanoparticles were obtained through precipitation method. For this purpose, the precursors (Fe^{2+} and Fe^{3+}) solution was sprayed into a sodium hydroxide (for obtaining pure Fe_3O_4) and sodium hydroxide / L-leucinamide precipitation bath (for obtaining Fe_3O_4@LEU) issuing a black precipitate. In order to determinate the structure and morphology of the Fe_3O_4 and Fe_3O_4/leucinimide nanoparticles the following methods were used: Fourier transform infrared spectroscopy (IR), X-ray diffraction (XRD), Brunauer-Emmett-Teller (BET) and scanning electron microscopy (SEM). The Brunauer-Emmett-Teller (BET) analysis revealed a mesoporous structure for the samples with a specific surface area of about 156m^2/g (unstabilized Fe_3O_4 nanoparticles) and 147 m^2/g (for the stabilized Fe_3O_4 nanoparticles) which proves, along with FTIR, SEM and even XRD data, that the presence of the leucinamide leads to an increase of the hydrodynamic size. The average pore size of the MNPs is about 5-6 nm which means that mesoporous materials were obtained.

Keywords: magnetic nanoparticles; co-precipitation methods; stabilizing agent.

INTRODUCTION

In the last years a considerable attention has been paid to the preparation and characterization of the mesoporous magnetic nanoparticles due to the biomedical (bioseparation, catalysis, contrast agent for MRI, drug delivery), industrial (separation, magnetic inks, photocatalysis) and environmental applications (potential adsorbents for heavy metals: Cu, Pd, Co, Ni, Hg)[1-4].

The lately studies about on magnetic materials have shown the great importance of these particles in different areas. Magnetic properties due to very important nanoparticles mesoporous of magnetite of particular importance especially in the medical field such as: drug delivery system, hyperthermia, magnetic resonance imaging. The nanoparticle mesoporous of magnetite are also used industrially as biosensors, catalysis, ferrofluids, photocatalysts, pigments, etc. The nanoparticles mesoporous are used in different types in specified applications depending on size, shape, but also their surface area.[1-11]

In the last period for obtaining magnetic nanoparticles mesoporous used a variety of methods of synthesis of which is the most used is co-precipitation. The co-precipitation method is very used because the synthesis is very easy in obtained the magnetic nanoparticles, the low cost, the temperature of prepared the magnetic nanoparticles can be different. For obtaining magnetic nanoparticles also sol-gel, thermal decomposition, hydrolysis, solvothermal or hydrothermal method can be used [1-11].

Xu and all.[12] present the synthesis of nanoparticle magnetite in organic phase, using the iron (III) chloride as a precursor. Sohu Xuan and all.[13] prepared the nanoparticles of magnetite using ascorbic acid as stabilizer, by hydrothermal methods. Both methods are efficient and lead to nanoparticles with controlled size and dispersivity but require more expersive precursors and the synthesis rate is more laborious comparing with precipitation.

In this work, the co-precipitation method was used for obtaining magnetic nanoparticles. L-leucinamide hydrochloride was used as stabilizing agent of mesoporous magnetite nanoparticles, influence of the leucinamide being studied form the point of view of crystallinity, size and specific surface area.

EXPERIMENTAL DETAILS

MATERIAL AND METHODS

For preparing the mesoporous nanoparticles of magnetite were used these principal materials: iron (III) chloride – FeCl$_3$ (Sigma Aldrich), ammonium iron(II) sulfate hexahydrate – Fe(NH$_4$)(SO$_4$)$_2$ (Silal Trading), L-leucinamide hydrochloride (Mann Research Laboratories INC), sodium hydroxide – NaOH (Silal Trading), and distilled water. Mesoporous of magnetite nanoparticles were prepared by co-prcipitation methods, as presented in Figure 1 . The precipitation solution was prepaired by disolving 2.5 g leucinamide and 10 g NaOH in 250 ml distiled water under mechanical stirring, at room temperature. The pH was adjusted to 12 and was maintained above 10 during the precipitation of Fe$_3$O$_4$@Leu by adding supplementary NaOH solution. The stirring is maintained while the magnetite precursors are added (a solution containing 6.99 g FeCl$_3$ and 8.45 g Fe(NH$_4$)(SO$_4$)$_2$ in 100 ml distiled water by spraying. The spraying was set at about 3 ml/min. After precipitation and maturation (~2h), the mesoporous magnetic nanoparticles were filtered and washed, three times, with distilled water until neutral pH and chloride free filtrated is obtained and were dried by freeze drying to avoid supplementary oxidation of the magnetic nanoparticles. During the entire synthesis procedure, nitrogen was bubbled into the precipitation bath in order to avoid oxidation of magnetite to maghemite.

The mesoporous magnetic samples were characterized by: XRD, FT-IR, SEM and BET.

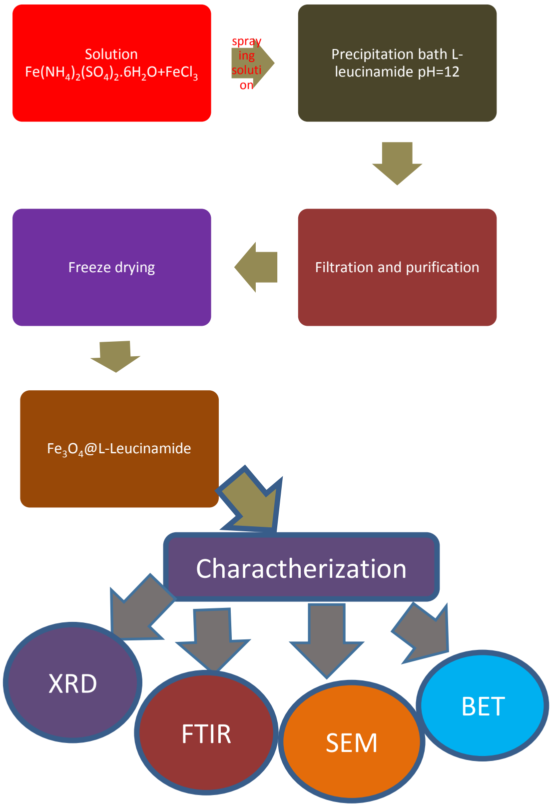

Figure 2. The synthetic steps of Fe$_3$O$_4$@L-leucinamide

X-ray diffraction analysis was carried out on a Panalytical X’Pert Pro MPD equipment, with CuK$_\alpha$ radiation. The samples were scanned in the Bragg angle, 2θ=10–90^0, with a sampling interval of 0.02^0.

IR spectroscopy was performed on a Nicolet iS 50 FT-IR spectrometer equipped with a broad range DTGS detector providing high-sensitivity infrared information from 4000 cm^{-1} to 100 cm^{-1} and an integral diamond ATR unit. The system is configured with the built-in iS50 ATR module and an iS50 ABX Automated Beamsplitter exchanger. The spectra were recorded in ATR mode over the wave number range of 400 - 4000cm^{-1}, with a resolution of 4 cm^{-1} co-adding 64 spectra for improving the spectral quality. For a better identification of the peaks, the obtained spectra were resolved using a Gaussian-Lorentzian peak resolve procedure assuming a linear baseline.

The Brunauer–Emmett–Teller (BET) analysis was performed on a Micrometrics Gemini V surface area and pore size analyzer.

Morphological data were obtained by scanning electron microscopy of the goldcoated specimens, using a QUANTA INSPECT F SEM device equipped with field emission gun (FEG) with a resolution of 1.2 nm and with X-ray energy dispersive spectrometer (EDS).

RESULTS AND DISCUSSION

➢ *X-ray diffraction*

X-ray diffraction can be used in order to characterize the crystallinity of nanoparticles, the average crystallite size and the purity of magnetite nanoparticles. Based on the literature data[14,15] as well as the ICDD database it can conclude that the synthesized mesoporous MNPs present only the characteristic peaks of a cubic spinel structure, proved by the strongest reflection of (311) plane (Fig. 1), characteristic of such a phase[16]. Also all the peaks indexed as planes (220), (311), (400), (422), (511) and (440) are characteristic for the magnetite [17,18,19](ICDD data base).

The XRD diffraction patterns of the magnetic materials highlight that the crystallinity and the crystallite size of the stabilized Fe_3O_4@LEU is modified comparing with the Fe_3O_4 material. The XRD diffraction patterns of Fe_3O_4@LEU exhibit the same peaks as pure Fe_3O_4 but, the peaks with low intensity are not clearly evidentiated especially because of the lower size/crystallinity. The lower crystallinity of the Fe_3O_4@LEU is especially evidentiated based on the peaks from 2Theta = ~54, 72 and 74° which are not well defined because the stabilizing agent act as a shielding layer.

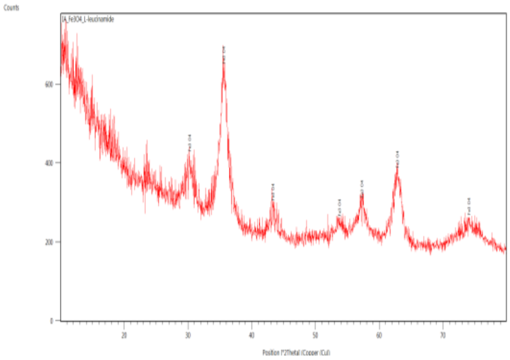

Figure 3. The XRD patterns of the synthesized Fe_3O_4@L-leucinamide

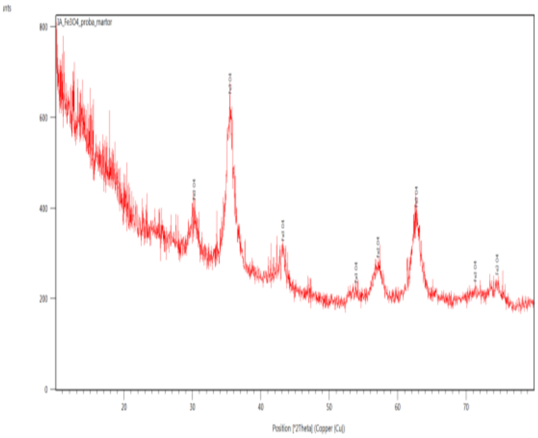

Figure 4. The XRD patterns of the synthesized Fe_3O_4

➢ ***BET analysis***

BET analysis was used for evaluate the the surface area and pore size of the magnetic materials.

The BET surface areas of the two samples (the Fe_3O_4 and Fe_3O_4@LEU samples) are summarized in Table 1. Based on the BET analysis of the pure magnetite, a specific surface area of 156m^2/g and an average pore size of 5.75nm were calculated. In comparison to another dispersion agent which lead to an important decrease of the specific surface area and an increase of the pore size[20] (trichloroacetic acid, salicylic acid and glutamic acid) in the case of Fe_3O_4@LEU, the specific surface area decreased from 156m^2/g to 147m^2/g while practically no changes of the pore size occurs. The different behavior is explained based on the differ ent chemical structure of the leucinamide comparing with the three stabilizing agents used in the previous paper (trichloroacetic acid, salicylic acid and glutamic acid). Once leucinamide is covering the surface of the magnetite core, is able to form additional H-bonds and so the hydrodynamic size is increase (specific surface area decrease) while in the case of the above mentioned acids, at the synthesis pH the surface is negatively charged and no additional association can occurs.

Table 1. BET data of the synthesized MNPs samples

Samples	**Specific surface area S_{BET} (m^2/g)**	**Average pore size D_{BET} (nm)**
Fe_3O_4@L-leucinamide	147.6920	5.7206
Fe_3O_4@sample	156.0278	5.7466

Based on these data we can conclude that the mechanism of the formation of the Fe_3O_4@stabilizing agent is strongly dependent on the nature of the stabilizing agent the concentration and pH.

➢ *Infrared spectroscopy*

The FTIR spectrum of Fe_3O_4 and Fe_3O_4@LEU (

Figure *5*) exhibit the main absorption bands of magnetite, especially the two intense peaks, from 529 and 533 cm^{-1}, that are due to the stretching vibration mode associated to the metal-oxygen absorption band (Fe – O bonds in the crystalline lattice of Fe_3O_4)[17,21].

The absorption band between 1000 and 1650cm^{-1} corresponds to H-O-H bending vibration, typical of the H_2O molecule, and bending vibration associated to the O – H bond between 900 and 1000cm^{-1}. The absorption bands from between 1507 cm^{-1} and 900 cm^{-1}, respectively is characteristic to O–H in plane and out of plane bonds[122]. The absorption bands between 900 and 1000cm^{-1} is characteristic to strong hydrogen bridges.

The presence of leucinamide can be clearly identified based on the spectrum of the region 1000 – 1650cm^{-1}. It can see that the amide bands intensity of the Fe_3O_4@LEU is much higher than that of the pure Fe_3O_4. This observation can be also correlated with the XRD data. The crystalline loss observed in XRD can be explained based on the leucinamide shell covering the magnetite core.

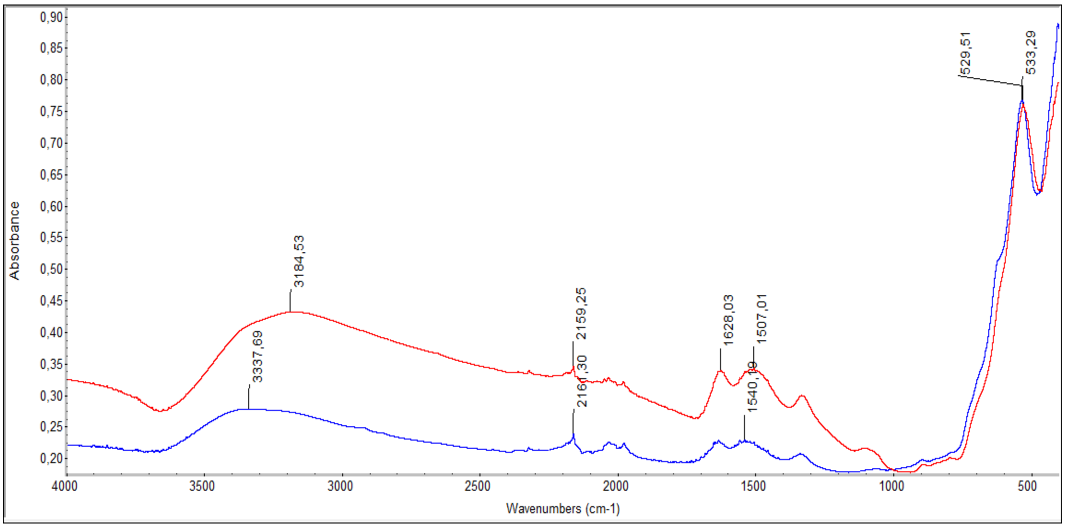

Figure 5. FTIR spectra of the magnetic samples: Fe_3O_4 (blue line) and Fe_3O_4@L-Leucinamide (red line)

➢ *SEM*

The most representative SEM images of the Fe_3O_4 and Fe_3O_4@L-leucinamide are presented in Figure 5. Based on these images, as expected, two different morphologies can be identified because of the presence of L-leucinamide. Based on its structure, L-leucinamide can interact with the magnetite nanoparticles via the carboxylate group but also with other L-Leucinamode molecules via the two amino groups. In the case of pure magnetite, individual nanoparticles can be clearly visualized at high magnification. The size of these nanoparticles is in the 4-10nm range. In the case of Fe_3O_4@LEUC, due to the presence of the organic stabilizing agent, large agglomerated (up to 500nm) can be identified consisting of a large number of magnetite nanoparticles joined together by the means of leucinamide molecules.

Fe_3O_3@LEU	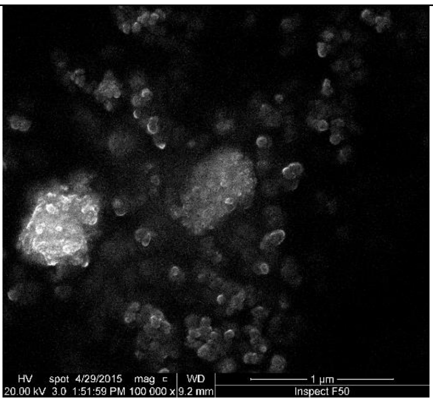	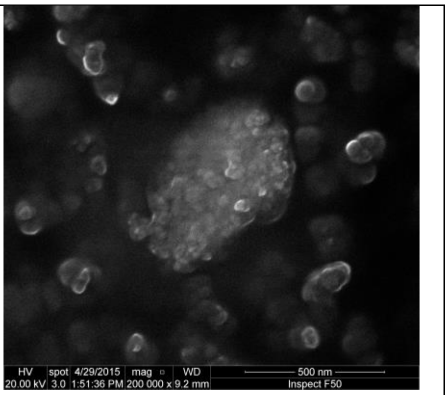
Fe_3O_4	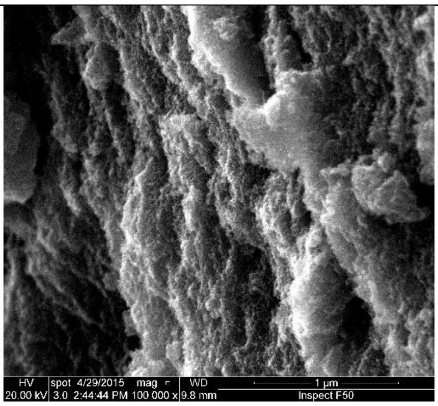	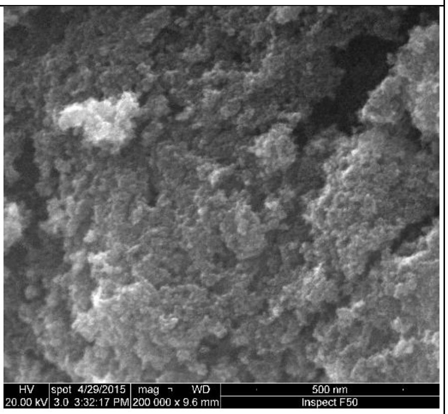

Figure 6. SEM images of the stabilized and non-stabilized magnetic nanoparticles

CONCLUSION

New magnetic nanoparticles were obtained by modified co-precipitation method starting from magnetite precursors and L-leucinamide as stabilizing agents, by spraying the solution of the magnetite precursors into the alkaline stabilizing agent solution. The obtained results reveal important difference between the bare Fe_3O_4 and Fe_3O_3@LEUC, the presence of the leucinamide can be identified based on the FTIR data while the XRD and SEM data confirm important changes of Fe_3O_3@LEUC comparing with Fe_3O_3, due to the core@shell structure formation. The mechanism of formation of these suprastructures is strongly correlated with the functional end groups of the stabilizing agent, namely amino groups which form strong hydrogen bonds and thus strong morphological changes occurs in the case of Fe_3O_3@LEU comparing with bare Fe_3O_4.

REFERENCES

1.D. Ficai, A. Ficai, M. Alexie, M. Maganu, C. Guran, E. Andronescu; (2011). Amino-functionalized Fe_3O_4/SiO_2/APTMS nanoparticles with core-shell structure as potential materials for heavy metals removal; Revista de Chimie,Vol. 62(6):622-625;

2.D. Ficai, A. Ficai, B.S. Vasile, M. Ficai, O. Oprea, C. Guran, E. Andronescu (2011). Synthesis of rod-like magnetite by using low magnetic field; Digest Journal of Nanomaterials and Biostructures; vol. 6(3): 943-951;

3.D. Ficai, E. Andronescu, A. FICAI, G. Voicu, B. Vasile, V. Ionita, C. Guran; (2012) Synthesis and characterization of mesoporous magnetite based nanoparticles; Current Nanoscience;vol. 8(6): 875-879;

4.Liu, S.H.; Xing, R.M.; Lu, F.; Rana, R.K.; Zhu, J.J. (2009) One-Pot Template-Free Fabrication of Hollow Magnetite Nanospheres and Their Application as Potential Drug Carriers. J. Phys. Chem. C., 113, 21042-21047

5.Chen, L.; Xu, Z.; Dai, H.; Zhang, S. (2010). Facile synthesis and magnetic propertiesof monodisperse Fe_3O_4/silica nanocomposite microspheres with embedded structures via a direct solution-based route. J. Alloy Compd.,497, 221- 227;
6.Zhou, J.; Wu, W.; Caruntu, D.; Yu, M.H.; Martin, A.; Chen, J.F.; O'Connor, C.J.; Zhou, W.L. (2007). Synthesis of porous magnetic hollow silica nanospheres for nanomedicine application. J. Phys. Chem. C., 111, 17473-17477.
7.M. Mahmoudi; S. Sant; B. Wang; S. Laurent; T. Sen; (2011) Superparamagnetic iron oxide nanoparticles (SPIONs): Development, surface modification and applications in chemotherapy; Advanced Drug Delivery Reviews 63, pp. 24-46.
8.J.C. Aphesteguy; G.V. Kurlyandskaya; J.P de Celis; A.P. Safronov; N.N. Schegoleva; (2015) Magnetite nanoparticles prepared by co-precipitation method in different conditions; Materials Chemistry and Physics 161,pp.243-249.
9.L. Shen; Y. Qiao; Y. Guo; S. Meng; G. Yang; M. Wu; J. Zhao; (2014) Facile co-precipitation synthesis of shape-controlled magnetite nanoparticles; Ceramics International 40 pp.1519-1524.
10.T. Neuberger; B. Schöpf; H. Hofmann; M. Hofmann; Brigitte von Rechenberg; (2005) Superparamagnetic nanoparticles for biomedical applications: Possibilities and limitations of a new drug delivery system; J. Magnetism and Magnetic Materials 293 483-496.
11.K. Petcharoen; A. Sirivat; (2012) Synthesis and Characterization of magnetite nanoparticles via the chemical co-precipitation method; Materials Science and Engineering B 177 421-427.
12.Mutasim I. Khalil; (2015) Co-precipitation in aqueous solution synthesis of magnetite nanoparticles using iron(III) salts as precursors; Arabian Journal of Chemistry vol. 8, 279–284
13.S. Xuan, L. Hao, W. Jiang, X. Gong, Y. Hu, Z. Chen; (2007) Preparation of water-soluble magnetite nanocrystals through hydrothermal approach; J. Magn. Magn. Mater., 308 pp. 210–213
14.Bragg W.L. Nature. 1915, 95: 561.
15.Ayala-Valenzuela O, Matutes-Aquino J, Betancourt-Galindo R, Garcia-Cerda L.A, Rodriíguez F. O, Fannin P.C, Giannitsis A.T. (2005) Journal of Magnetism and Magnetic Materials. 294: e37-e41.
16.Kim Y. Il, Kim D, Lee C.S. Physica B. 2003, 337: 42 – 51.
17.Javier A. Lopez; Ferney González; Flavio A. Bonilla; Gustavo Zambrano; Maria E. Gómez; (2010). Synthesis and characterization of Fe_3O_4 magnetic nanofluid; RevistaLatinoamericana de Metalurgia y Materiales; vol. 30 (1), pp.60-66.
18.Vaidyanathan G., Sendhilnathan S, Arulmurugan R. Journal of Magnetism and Magnetic Materials. 2007 313: 293 – 299.
19.Betancourt-Galindo R, Rodríguez -Fernández O. S. Superficies y Vacío 17 (1): 38 - 41.
20.I.L. Ardelean; L.B. Niculae Stoencea; M. Rădulescu; D. Ficai; A. Ficai; G. Voicu; R. Truşca; G. Nechifor; E. Andronescu (2016) Synthesis and characterization of a new mesoporous magnetite nanoparticles using
21.Ahn Y, Choi E.J, Kim E.H, Rev. Adv. Mater. Sci. 2003, 5: 477.
22.Ling Z; Rong He, Hong-Chen G. Applied Surface Science. 2006, 253(5): 2611-2617.

OZONE: THE OUTCOMES OF AN INTERDISCIPLINARY TEACHING APPROACH

Mirela-Lucia ARDELEAN, Eugen FÜRTÖS, Mirela BACIU, Maria COBILIȚA
Liceul Teoretic „Onisifor Ghibu", ORADEA, Aleea Onisifor Ghibu, nr. 3-5
mirelaardelean@yahoo.com

Abstract: *This paper presents a teaching research as a plea for interdisciplinary approach learning of the issues with scientific content suitable for this method. Thus, the lesson "Freons. The ozone layer depletion" was taught to an 11thgrade students, Mathematics-Informatics track, once by the Chemistry teacher, as an application to the unit "Halogenated compounds", and then by an interdisciplinary team of the Chemistry, Physics, Geography and Biology teachers of that class. The results, measured by statistical processing of the students' scores in the assessment items show the added value brought by the interdisciplinary method, pointed out by the increased percentage of solving all items, especially those in higher cognitive categories, by improving the studied indicators. Also remarkable is an increase in the students' motivation for the study of sciences in systemic approach.*

Key words**: **interdisciplinarity, assessment items, ozone layer, stratosphere, freons, radiations

INTRODUCTION

The ozone issue belongs to the 11th grade Chemistry syllabus, theoretical studies in sciences, Mathematics-Informatics and Natural Sciences, subsumed to the topics of "The Importance of Halogen Compounds" and "Freons. Destruction of the Ozone Layer".[13] These contents are correlated with the general skills of "Communicating understood concepts in problem solving, in formulating explanations, in the conduct of investigations and reporting outcomes" and "Assessing consequences of processes and the action of chemical products on oneself and the environment", superior skills, affiliated to mental processes of analysis, synthesis, assessment, with practical implications and leading to the knowledge of aspects related to pollution, ecosystem and to moral-eco-civic awareness.

Teaching experience in the classroom of the two topics made me search for solutions to optimize the teaching process, so that acquirement of the targetted skills be associated with efficiency, interdisciplinary synthesis, the most relevant information and, not the least, the joy of learning. I have, therefore, conducted an interdisciplinary approach to the topic "Freons. Destruction of the Ozone Layer", working together with fellow teachers of Geography, Physics and Biology who teach 11th grade, Mathematics-Informatics track.

Reading the curricula of "intersection" tracks, I noticed that there were favourable conditions for an interdisciplinary approach.[10, 11, 12]

TEACHING RESEARCH METHODOLOGY

The lesson "Freons. Destruction of the Ozone Layer" was initially taught as an application to substitution reactions of halogenated derivatives, in Chemistry class.[9] The topic of ozone layer destruction was secondary, an illustration of the negative effects of freons on the ozone layer surrounding the Earth. Although to explain the mechanisms of ozone layer destruction I resorted to students' acquisitions in the fields of Physics, Geography and – less – Biology, emphasis was placed on the chemical mechanism of freon action on stratospheric ozone.

The Chemistry lesson "Freons. Destruction of the Ozone Layer" complied with the following teaching plan:

LESSON TYPE: acquiring new knowledge

GENERAL SKILLS:

- ❖ Explanation of phenomena, processes, procedures
- ❖ Investigation of behavior of chemical substances or systems
- ❖ Communication of understood concepts in problem solving, formulation of explications and reporting outcomes
- ❖ Assessing consequences of processes and the action of chemical products on oneself and the environment

SPECIFIC SKILLS:

- ❖ Explaining the behavior of compounds in a given context
- ❖ Processing a large volume of information and telling the difference between relevant/irrelevant and subjective/objective information
- ❖ Critical interpretation of information from various sources
- ❖ Recognizing types of issues of general interest that can be met by Chemistry

OPERATIONAL OBIECTIVES:

- ❖ **O 1:** To correlate uses of freons with their physical and chemical properties (chemical inertia);
- ❖ **O 2:** To identify the causes of the thinning of the ozone layer, based on interpreting the reaction mechanism of ozone with freons;
- ❖ **O 3:** To deduce the beneficial effects of high altitude ozone on the Earth ecosystem by energetic interpretation of ozone formation reaction;
- ❖ **O 4:** To argument the phenomenon of

significant ozone layer destruction aat low temperatures and high altitudes, knowing the catalytic base of polar atmospheric clouds in the reaction of CFCs with the ozone and based on geographical knowledge about atmosphere;

TEACHING STRATEGIES:

❖ Teaching methods: heuristic conversation, questioning, guided discovery, explaining, modelling, brainstorming, assessment

❖ Teaching materials and aids: plate with oxygen-ozone transformations in stratosphere, video projector, information material – Powerpoint presentation, assessment sheet

❖ Forms of organizing the students’ activity: frontal and work groups

The correlation between the sequence of essential information provided by the teacher, the areas they belong to and the targetted operational objectives are given in the *Table 1*. The students are organized into groups of two and fill the assignments in their worksheets based on the Chemistry teacher’s explanations, then assess and correct themselves based on the correct worksheet, projected after each sequence corresponding to the targetted operational objective.

Table 1. Schematic plan for the deployment of “Freons. Depletion of the ozone layer” Chemistry lesson

No	Essential information	Subject area	Work task for students	Teaching method / means	Targetted objective
1	-Freons are fluorochlorinated derivatives of alkanes	Chemistry	-To write the molecular and structural formulas of freons and name them -To specify by what type of reactions can freons be obtained and exemplify	-conversation -modelling -algorithmization	
2	-Freons are gases with much lower density than air, colourless, odorless, non-toxic to humans, non-flammable, chemical inert at low altitudes, insoluble in water, Freon itself (CF_2Cl_2) has b.p. = -30°C, easily liquefying and vaporizable.[9] -Uses (with the students’ contribution from their general knowledge): cooling agents in refrigerators, air conditioners, in the composition of aerosols, sprays, fire foam, solvent for cleaning electronic circuits, etc.[9]	Chemistry Physics partially Biology	-To correlate the uses of freons with their properties	-conversation -explanation -work sheet -feed-back	**O 1**
3	-Freons attack the ozone layer (a natural constituent of the atmosphere, located between 15-40 km altitude), a process intensified (catalyzed) by ice crystals from the polar stratospheric clouds (PSC); Freon, stable, is not decomposed by low energy radiation in the troposphere, but by the high one, present at higher altitudes, in the stratosphere.[8,1] -Ozone is a very unstable bluish gas, with a characteristic odour. -The structure of the molecule shows three oxygen atoms in an angular configuration.[3] -It breaks down into molecular oxygen, releasing energy: $2O_3 \rightarrow 3O_2$ + Energy. The process is intensified by cooling. Below 100°C there can be ozone molecules, the breakdown reaction rate being very low.[7] -Each radical-Chlorine atom leads to the destruction of more than 100000 ozone molecules.[9]	Chemistry Geography	-To deduce the chemical reaction mechanism between freon and ozone <u>Clues:</u> the different chemical stability of C-F and C-Cl bonds -Based on the chemical mechanism of chain reactions between freons and ozone, to explain the degradation of stratospheric ozone layer	-guided discovery -explanation -plate -ppt -explanation -algorithmization -modelling -questioning -worksheet -feed-back	**O 2**
4	-Most of atmospheric ozone, over 90%, lies between 10 and 40 km altitude, in the stratosphere,	Chemistry Physics	-Based on the energetic mechanism of	-guided discovery	

	the highest concentration being at about 30 km altitude.[1] There, oxygen density is high enough to produce molecular dissociation.[7] The "ozone equations" are $UV/C + O_2 = O + O$ $O + O_2 = O_3$ $O_3 + UV/B = O_2 + O + IR$ $O_3 + O = O_2 + O_2$, where the wave length of λ is UV/C < 240 nm, $240 \text{ nm} < \lambda$ UV/B < 320 nm, λ IR > 500 nm.[1, 15]	Geography Biology	formation-decomposition ozone reactions, to infer possible effects of the ozone layer on life on Earth.	-explanation -plate -ppt -explanation -algorithmization -questioning -brainstorming -worksheet -feed-back	**O 3**
5	-In 1985, the British Antarctic Survey researchers found a hole in the ozone layer in the Antarctic, confirming the hypothesis of two researchers in 1974. Stratospheric ozone diminishes several times every year, especially in some seasons, the "ozone hole" being much bigger in the Antarctic.[8] -The most important pollutants attacking the ozone are CFCs (freons, chlorofluorocarbons) and halons, which contain bromine, eg. bromomethane). There are also other natural or anthropic pollutants, coming from cars, refineries, power plants, factories, volcanoes, etc. that contribute to the depletion of ozone.[8, 1, 16]	Chemistry Geography Physics	-To identify causes of ozone depletion at high altitude and explain what factors make possible their action. -Explain why the ozone hole is larger at low temperatures (-80°C) and high altitudes (the Antarctic), during winter-spring months, even if pollution activities are reduced? Clues: PSC, atmospheric movement, polar vortex	-conversation -questioning -worksheet -explication -brainstorming -ppt -feed-back	**O 4**

The assessment sheet proposed at the end of the lesson is designed to address the following assessment objectives, qualitatively correlated with the operational objectives and specific and overall skills of the topic:

- **E 1**: To explain the substrate of the use of freons in a particular field, in terms of their physical and chemical properties
- **E 2**: To identify and explain the link between the depletion of stratospheric ozone layer and pollutants, particularly freon
- **E 3**: To state and explain features related to location, chemical and energetic formation, roles and effects of stratospheric ozone layer on the Earth-space ecosystem
- **E 4**: To identify and explain the thinning mechanisms of the stratospheric ozone layer, as well as its effects on Earth

1. The following questions may have one or several correct answers. Correct the letter corresponding to the correct answer.

Stratospheric ozone:

A. Is formed at:
a) 10-15 km altitude;
b) 19-30 km altitude.

B. Its formation causes the absorbtion of mainly:
a) infrared radiations;
b) high / medium energy UV radiations;
c) low energy UV radiations.

C. It has beneficial effects on the Earth ecosystem because during the formation of the ozone molecule:
a) it absorbs the UV radiations that might harm the health of Earth's creatures;
b) it absorbs heat, reducing the greenhouse effect.

D. It has lately undergone significant thinning, due to:
a) pollution;
b) the planet's global warming

2. Fill the phrase with the expressions and words given in the list of contents below:

The Sun sends to Earth various .... carriers of consumed ...., among others, to: to ...., ... In turn, the Earth radiates .... into space, thus achieving .... The ozone layer diminishes .... because it converts the relatively high energy of the .... into .... energy, only a part of which reach the Earth. .... is disrupted by .... which produce: .... and by .... which destroy …………................ and contribute to the increase of ....

List of contents: *global warming*, *thermal balance, anthropic activities, pollutants, radiations, thermal energy, photosynthesis, energy, water evaporation, UV radiations, ozone layer, greenhouse effect, IF radiations*.

3. Briefly explain why:
A. Freons are used in sprays
B. A freon molecule can destroy several molecules of ozone
C. Deterioration of stratospheric ozone layer affects the

planet's life (bios)

D. The temperature in stratosphere increases with altitude

E. In the North Pole area the ozone layer depletion is less significant than at the South Pole, although in the northern hemisphere there are more polluting activities

F. Ozone production is highest in upper tropical stratosphere

G. Depletion of the ozone layer leads as well, through "plants" link, to the decrease of its concentration

Test assessment and scoring scale is given in *Table 2*.

Table 2. Test assessment and scoring scale

No. item	Correct answer (*italic*)	Score	
		partial	total
1 A	*b*	1	**4**
1 B	*b*	1	
1 C	*a*	1	
1 D	*a*	1	
2	*Radiations/ energy/ global warming/photosynthesis/ water evaporation/ thermic energy/ thermal balance/global warming/ UV radiations/ IF radiations/thermal balance/ anthropic activities/global warming/ pollutants/ ozone layer/ greenhouse effect*	16·1	**16**
3 A	*Freons are colourless, odourless, non-flammable, non-toxic to humans, chemically inert, easily liquefiable under pression and quickly evaporate when pressure decreases*	8	**70**
3 B	*The radical-chlorine atom combines with the oxygen atom and the formed CIO radical attacks reacts with a new oxygen atom; thus consuming the oxygen atoms which normally lead to ozone formation and releases chlorine that also destroys ozone*	8	
3 C	*When formed by the stratospheric oxygen, ozone captures high energy UV radiations which would damage the cellular DNA of living things on Earth*	8	
3 D	*At high altitudes, in the stratosphere, oxygen is decomposed by high energy radiations (UVC) and turned intoozone, a heat releasing process*	10	
3 E	*Temperatures are not so low at the North Pole as to allow the emergence of stratospheric polar clouds (PSC) – catalysts of freons degradation and, implicitly, of ozone layer depletion; in addition, the polar vortex is not so emphasized*	10	
3 F	*In the upper tropical stratosphere, the flux of solar radiations closer to the perpendicular to the Earth's surface in the area is maximum, so the endothermic process of ozone production intensifies*	13	
3 G	*Ozone destruction leads to plant destruction, thus, the photosynthesis is reduced, oxygen production decreases and, consequently, oxygen-formed ozone production decreases as well*	13	
Default points		**10**	
TOTAL SCORE		**100**	

The correspondence of items with assessment objectives is shown in *Table 3*:

Table 3. The correspondence between items and assessment objectives

Item	Targetted assessment objective			
	E 1	E 2	E 3	E 4
1 A			▲	
1 B			▲	
1 C			▲	
1 D				▲
2			▲	▲
3 A	▲			
3 B		▲		
3 C			▲	

3 D			▲	
3 E				▲
3 F			▲	
3 G				▲

One notices that Item 2 targets two assessment objectives, while only one goal corresponds to all the other items. The items' degree of "fulfilling" the objectives is shown in *Table 4*:

Table 4. Degree of "fulfilling" assessment objectives by items

Assessment objective	**E 1**	**E 2**	**E 3**	**E 4**
% items / objective	1/12 (8.33%)	1/12 (8.33%)	7/12 (58.33%)	4/12 (33.33%)

The items are distributed into four general classes of cognitive complexity, according to Blooms taxonomy: KNOWLEDGE (A), UNDERSTANDING (B), APPLICATION (C) and ANALYSIS (D), as shown in *Table 5*.[14]

Table 5. Classification of items according to cognitive level criterion

Item	**Score of items/cognitive level of items**			
	A – Knowledge	**B - Understanding**	**C - Application**	**D- Analysis**
1 A	▲ (1%)			
1 B	▲ (1%)			
1 C	▲ (1%)			
1 D	▲ (1%)			
2		▲ (16%)		
3 A		▲ (8%)		
3 B		▲ (8%)		
3 C		▲ (8%)		
3 D			▲ (10%)	
3 E			▲ (10%)	
3 F				▲ (13%)
3 G				▲ (13%)

Table 6 reflects the extent to which the items "cover" the four cognitive levels as percentage and scoring:

Table 6. The representativity, în the total score, of all cognitive type items

Item level	**A**	**B**	**C**	**D**
% items / type cognitive level	4/12 (33.33%)	4/12 (33.33%)	2/12 (16.66%)	2/12 (16.66%)
Maximum total score	4.00%	40.00%	20.00%	26.00%

Table 7 shows the types of items used in the assessment form, based on objective scoring:

Table 7. Classification of items by objectivity in scoring

Item no.	**Bloom level**	**Item type**
1 A	A	Objective – with double choice
1 B	A	Objective – with multiple choice
1 C	A	Objective – with double choice

1 D	A	Objective – with double choice
2	A	Semi-objective – gap filling
3 A	A	Subjective – problem solving
3 B	A	Subjective – problem solving
3 C	A	Subjective – problem solving
3 D	A	Subjective – problem solving
3 E	A	Subjective – problem solving
3 F	A	Subjective – problem solving
3 G	A	Subjective – problem solving

Table 5 reveals the equal percentage of items targeting knowledge and of those which target understanding cognitive acquisitions, as well as the fact that the total percentage of items targeting knowledge and understanding is double that of those targeting more complex conceptual operations – application and information analysis, as these are defining stages for the assimilation of cognitive skills and for the potential application of knowledge in the context of problem solving or transfer to other scientific topics, towards superior synthesis or holistic approaches.

However, grading grants a lower total score to items in A and B fields (knowledge and understanding) than to items in C and D fields (application and analysis), which shows the importance given, in the assessment test economy, to the acquired upper cognitive skills.

The quantitative results of the assessment are expressed by different mathematical processing of scores or grades into which they were converted. Thus, *Table 8* shows the scores for each item obtained by the students and their grades, *Table 9* shows the overall situation of item solving in different aspects, *Table 10* reflects the situation of overall item solving, relative to their cognitive level, and *Table 11* records the students' grades frequency.

Table 8. Obtained scores / items and students' grades

Paper no.	**Item no.**												**Total score (rounded +10 default points)**	**Grade**
	1A	**1B**	**1C**	**1D**	**2**	**3A**	**3B**	**3C**	**3D**	**3E**	**3F**	**3G**		
1	1	1	-	1	4	6	6	8	-	-	-	3	40	4
2	1	1	1	1	11	5	3	7	-	-	-	-	40	4
3	1	1	1	1	14	8	8	8	10	10	8	10	90	9
4	1	1	1	1	12	8	4	8	10	10	-	4	70	7
5	1	1	-	1	13	6	6	6	8	8	-	-	60	6
6	-	1	1	1	14	7	5	7	7	7	-	-	60	6
7	1	1	1	1	14	8	8	8	10	8	-	10	80	8
8	1	1	1	1	16	8	8	8	10	8	5	13	90	9
9	-	1	-	1	14	8	5	7	7	7	-	-	60	6
10	-	1	1	1	16	7	5	8	10	10	8	13	90	9
11	1	1	1	1	15	6	5	6	10	6	2	6	70	7
12	-	1	1	1	8	4	-	5	-	-	-	-	30	3
13	1	1	1	1	16	8	6	8	10	10	5	13	90	9
14	1	1	1	1	14	8	6	8	10	8	2	10	80	8
15	-	1	1	1	8	4	-	4	4	4	-	3	40	4
16	1	1	1	1	15	8	5	8	10	6	6	8	80	8
17	-	1	-	1	6	6	-	6	-	-	-	-	30	3
18	1	1	1	1	8	6	2	6	-	4	-	-	40	4
19	-	1	1	1	10	6	2	8	2	4	-	5	50	5

20	1	1	1	1	11	6	4	8	4	8	-	5	60	6
21	-	1	1	1	5	6	2	6	4	4	-	-	40	4
22	1	1	1	1	14	6	5	8	10	8	-	5	70	7
23	-	1	1	1	5	6	-	6	-	-	-	-	30	3
24	1	1	1	1	6	5	-	5	-	-	-	-	30	3
25	1	1	1	1	10	7	-	7	-	7	-	5	50	5

Table 9. Overall item solving situation

Item no.	**1A**	**1B**	**1C**	**1D**	**2**	**3A**	**3B**	**3C**	**3D**	**3E**	**3F**	**3G**
Item type (Bloom)	**A**	**A**	**A**	**A**	**B**	**B**	**B**	**B**	**C**	**C**	**D**	**D**
Score / item	1	1	1	1	16	8	8	8	10	10	13	13
Maximum score – all students	25	25	25	25	400	200	200	200	250	250	325	325
Achieved score	16	25	21	25	279	163	95	174	136	137	36	113
% of item solving	64%	100%	84%	100%	69%	81%	47%	87%	54%	54%	11%	34.77 %
No.of maximum score students	16	25	21	25	3	8	3	12	10	4	0	3
% maximum score students	64%	100%	84%	100%	12%	32%	12%	48%	40%	16%	0.00%	12%
No. of students with partial solution	-	0	0	0	22	17	16	13	7	15	7	12
% partial solution students	-	0	-	0	88%	68%	64%	52%	28%	60%	28%	48%
No. of students with no solution item	9	0	4	0	0	0	6	0	8	6	18	10

% students with no solution item	36%	0	16%	0	0.00%	0.00%	24%	0.00%	32%	24%	72%	40%

For a more plastic illustration, the data on item solving overall situation were plotted in *Figure 1*.

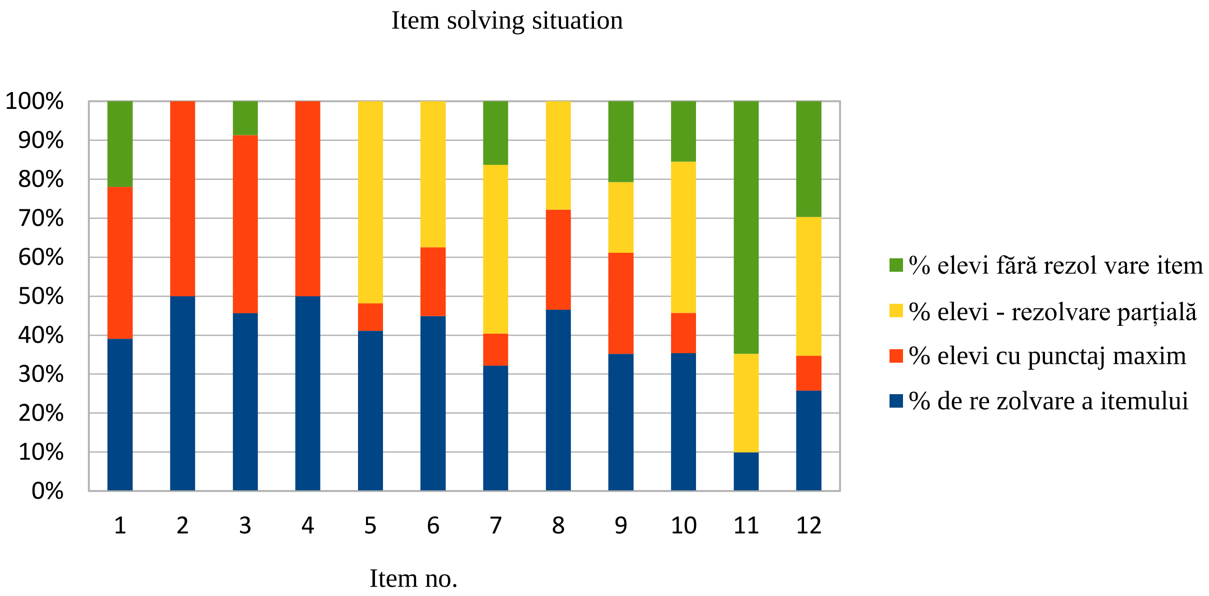

Figure 1. Analysis of item overall solving situation

Table 10. Item overall solving situation, relative to their cognitive level

Item level (bloom)	**A**	**B**	**C**	**D**
Maximum total score	100	1000	500	650
Total score achieved	87	711	273	149
% solution / item level	87.00%	71.10%	54.60%	22.92%

Figure 2 presents the degree of item solving on cognitive complexity classes.

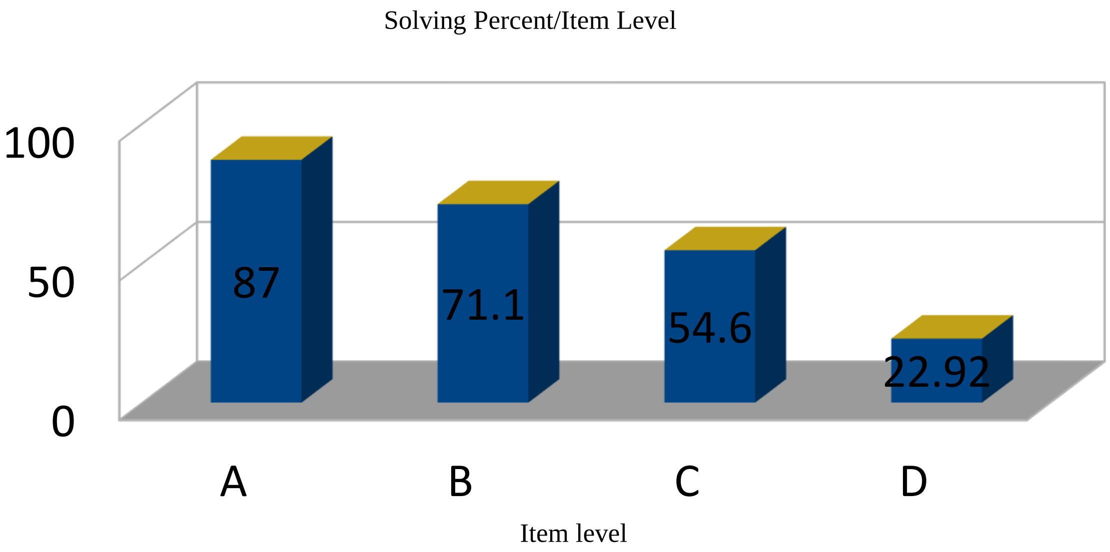

Figure 2. Item solving degree relative to their cognitive level

Table 11. Grade frequency

	GRADE FREQUENCY										CLASS AVERAGE
	1	**2**	**3**	**4**	**5**	**6**	**7**	**8**	**9**	**10**	
STUDENTS NO.	-	-	4	5	2	4	3	3	4	-	5.88
	9				6		6		4		
% students	36.00%				24.00%		24.00%		16.00%		

Figure 3 shows students' grades frequency in the assessment test

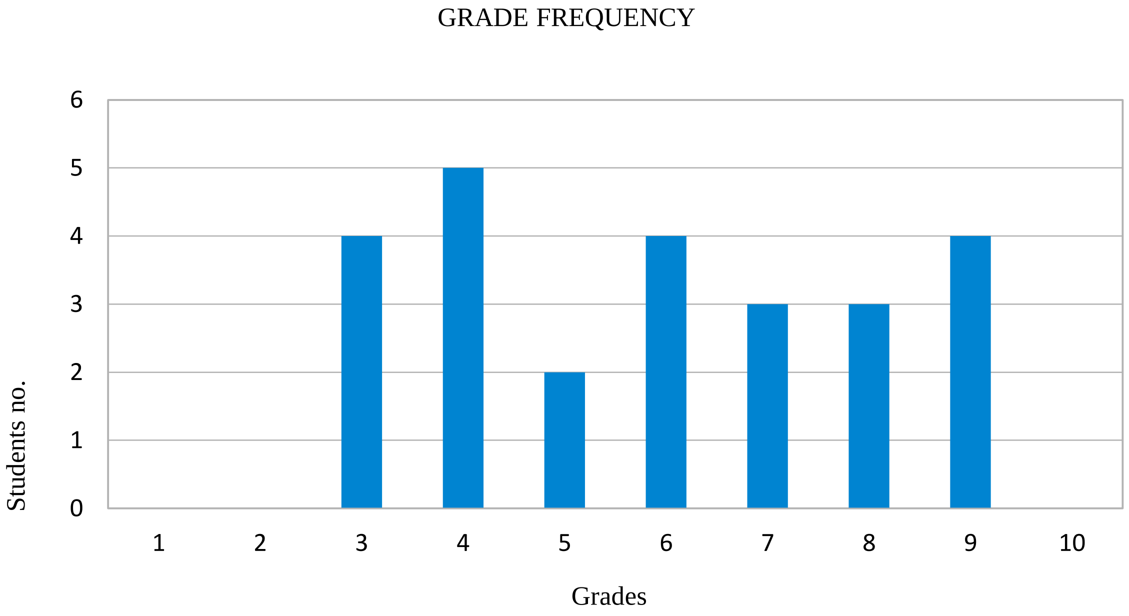

Figure 3. Students' grades frequency in the assessment test

By processing the results obtained by the students in the assessment for the monodisciplinary taught lesson, we have found out that

- ❖ All students answered correctly the questions for 1 A and 1 B items, thus having appropriately acquired the knowledge that during stratospheric ozone formation mainly ultraviolet radiation is absorbed and that the ozone layer depletion is caused by pollution;
- ❖ Most students gave relatively high weighting solutions of items aimed at basic knowledge (according to Bloom categories), a foundation to the notions necessary for knowledge understanding and application;
- ❖ There is a satisfactory proportion of student correlation between freons properties and their uses, they understand the biological effect of ozone layer depletion and have, in a rather high proportion, a correct vision on the role of ozone in the energetic relationship within the Sun-Earth ecosystem;
- ❖ The mechanism of the ozone decomposition by freons is poorly mastered;
- ❖ Application of knowledge in the explanation and analysis of issues implying work with geographical, physical and biological contents related to climate, latitude and altitude influence on the production or thinning of the ozone layer, related to the relationship between plants and stratospheric ozone concentration variation proves to be unsatisfactory;
- ❖ The percentage of overall solving of items decreases significantly from the items aiming "knowledge" cognitive type acquisitions to the "understanding", "application" and then "analysis" type ones;
- ❖ Seven of the items (58,33%) were not approached by some students, the percentage being overwhelming in "applicaton" and "analysis" type items, especially in the item aimed at the analysis of ozone production relative to latitude and altitude;
- ❖ Grade frequency shows 36% percentage of students with unsatisfactory grades, an equal percentage of of students with satisfactory and good grades (24%), and 16% of students with very good grades.

It should be noted that the class this lesson was taught to shows a polarization of skills and motivation for study, as well as a middle segment well represented, which is also reflected in the grade frequency specifying that the percentage of very good grades was almost half of the unsatisfactory grades percentage, and class average was 5.88, which shows a mendable result.

These assessment results, as well as the complexity of the ozone issue, which requires notional and conceptual constructs in Physics, Chemistry, Geography and Biology made me approach the issue of stratospheric ozone in an interdisciplinary team.

The interdisciplinary approach of the topic focused – except the first one (**O 1:** To correlate the uses of freons with their physical and chemical properties), regarded as satisfactorily fulfilled in the unidisciplinary Chemistry lesson – the same operational objectives, subsumed to the specific and general skills in the field of Physics, Chemistry, Biology and Geography, which are adequate to this topic.

The substantial difference between the two classes, the mono-, respectively the pluridisciplinary one, consisted in the increased intake of information provided by each teacher, as well as in the depth, relevance, originality and accuracy of scientific scientific information each subject brought to the lesson.[2, 4, 5, 6, 20, 17, 18, 19, 20] The teachers pass each other "the torch" from one learning sequence to another, depending on the stage of the targetted objectives, each applying the adequate teaching method and means. Moreover, the style of interactive methods was kept by all the teachers in the interdisciplinary approach, and the students' organization followed the same path as in the case of the first teaching.

The interdisciplinary lesson ended with the same assessment sheet, the same assessment objectives as for the mono-disciplinary lesson, in order to compare the efficiency of the two teaching approaches.

At the end of the lesson, the teachers asked the students for a comparative qualitative assessment of the two teaching methods, and the unanimous satisfaction responses for the interdisciplinary approach provided a gratifying feed-back for this kind of teaching approach.

Homework consisted of a project. Thus, the students were divided into three teams which, after research, were to draw a poster on "Life on Earth wouldn't be possible without ozone", a poster on "Ozone can be… bad!", and another one presenting protection measures for the stratospheric ozone layer, namely for minimizing tropospheric, photochemical ozone production. Each of the three teams was to present its poster, well argued, well documented, aesthetically designed and presented, for further assessment within a debate on the topic of "Good… Ozone versus Bad… Ozone".

The quantitative results of assessment through the items of the assessment sheet in the interdisciplinary lesson are presented in the tables below. Thus, *Table 12* shows the scores obtained by the students for each item and their grades, *Table 13* reveals the item solving overall situation in different aspects, *Table 14* reflects the situation of overall item solving, relative to their cognitive level, and *Table 15* records the students' grades frequency.

Table 12. Obtained scores / items and students' grades after the interdisciplinary approach

Paper no.	**Item no.**												**Total score (rounded + 10 default points)**	**Grade**
	1A	**1B**	**1C**	**1D**	**2**	**3A**	**3B**	**3C**	**3D**	**3E**	**3F**	**3G**		
1	1	1	1	1	8	7	6	8	6	4	3	4	60	6
2	1	1	1	1	14	8	4	8	4	2	-	6	60	6

3	1	1	1	1	16	8	8	8	10	10	9	11	80	8
4	1	1	1	1	16	8	6	8	10	10	6	10	90	9
5	1	1	1	1	14	8	6	8	8	8	-	5	70	7
6	1	1	1	1	15	7	6	7	10	8	4	3	70	7
7	1	1	1	1	16	8	8	8	10	8	3	9	80	8
8	1	1	1	1	16	8	8	8	10	9	10	13	100	10
9	1	1	-	1	14	8	6	7	8	8	2	5	70	7
10	1	1	1	1	16	8	8	8	10	10	13	13	100	10
11	1	1	1	1	15	7	6	8	10	7	3	7	80	8
12	-		1	1	9	5	1	5	2	-	-	-	30	3
13	1	1	1	1	16	8	8	8	10	10	13	13	100	10
14	1	1	1	1	15	8	7	8	10	8	4	10	80	8
15	1	1	1	1	13	8	6	8	10	7	4	4	70	7
16	1	1	1	1	16	8	6	8	10	8	8	10	90	9
17	-	1	-	1	7	6	-	7	2	2	-	-	40	4
18	1	1	1	1	11	7	6	8	6	4	-	8	60	6
19	1	1	1	1	11	8	4	8	6	5	2	6	60	6
20	1	1	1	1	14	8	4	8	6	9	4	6	70	7
21	1	1	-	1	6	8	4	7	7	2	2	4	50	5
22	1	1	1	1	16	7	8	8	10	8	5	10	90	9
23	-	1	1	1	8	8	-	7	4	-	-	-	40	4
24	1	1	1	1	9	7	4	8	4	4	-	4	50	5
25	1	1	1	1	12	7	4	8	6	7	-	6	60	6

Table 13. Overall situation of item solving after the interdisciplinary approach

Item no.	**1A**	**1B**	**1C**	**1D**	**2**	**3A**	**3B**	**3C**	**3D**	**3E**	**3F**	**3G**
Item type (Bloom)	**A**	**A**	**A**	**A**	**B**	**B**	**B**	**B**	**C**	**C**	**D**	**D**
Score / item	1	1	1	1	16	8	8	8	10	10	13	13
Maximum score – all students	25	25	25	25	400	200	200	200	250	250	325	325
Achieved score	22	24	22	25	323	188	134	192	189	158	95	167
% of item solving	88%	96%	88%	100%	80%	94%	67%	96.%	75.60 %	63.20 %	29.23 %	51.38 %

No. of maximum score students	22	24	22	25	8	16	6	19	12	4	2	3
% of maximum score students	88%	96%	88%	100%	32%	64%	24%	76%	48%	16%	8%	12%
No. of students with partial solution	3	1	3	0	17	9	17	6	13	19	15	19
% Students with partial solution	12%	4%	12%	0.00%	68%	36%	68%	24%	52%	76%	60%	76%
No. of students with no solution Item	3	1	3	0	0	0	2	0	0	2	8	3
% Item students with no solution	12%	4%	12%	0.00%	0.00%	0.00%	8%	0.00%	0.00%	8%	32%	12%

For a more plastic illustration, the data on the overall situation of item solving following the interdisciplinary approach were plotted in *Figure 4*.

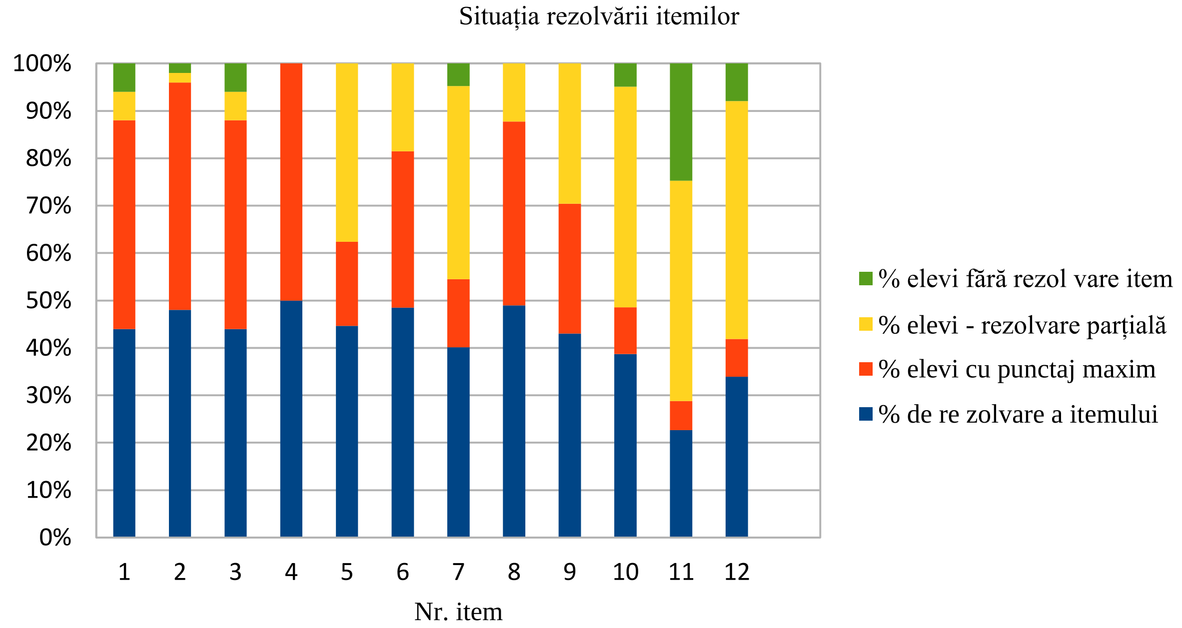

Figure 4. Analysis of the situation of overall item solving, following the interdisciplinary approach

Table 14. Overall item solving situation relative to their cognitive level, following the interdisciplinary teaching approach

Item level (bloom)	**A**	**B**	**C**	**D**

Maximum total score	100	1000	500	650
Total score achieved	93	837	347	262
% solving / item level	93.00%	83.70%	69.40%	40.30%

Figure 5 shows the degree of item solving by cognitive complexity classes.

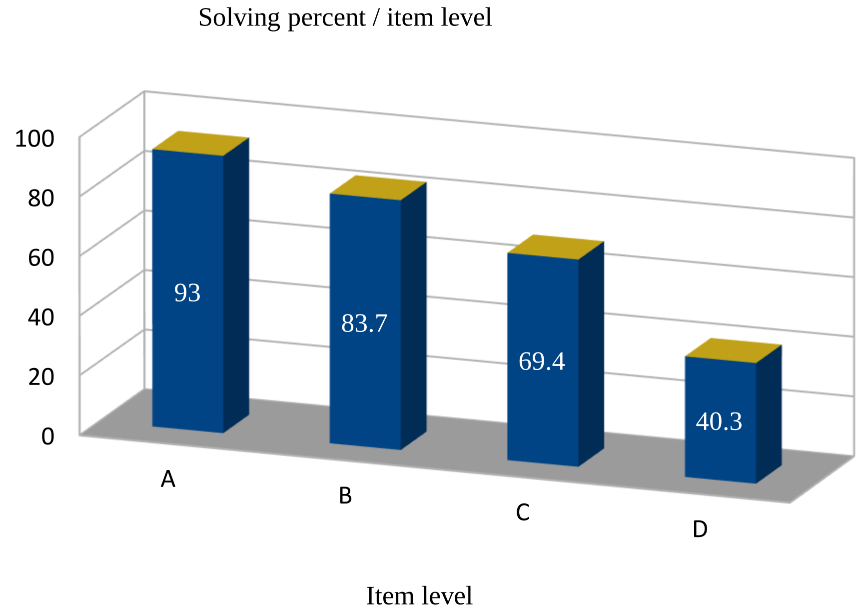

Figure 5. The degree of item solving relative to their cognitive level, following the interdisciplinary teaching approach

Table 15. Grade frequency after the interdisciplinary teaching approach

	Grade frequency										**Class average**
	1	**2**	**3**	**4**	**5**	**6**	**7**	**8**	**9**	**10**	
Students' number	-	-	1	2	2	5	5	4	3	3	**7.04**
	3				7		9		6		
% students	12.00%				28.00%		36.00%		24.00%		

Figure 6 illustrates students' grades frequency in the assessment test following the interdisciplinary teaching approach

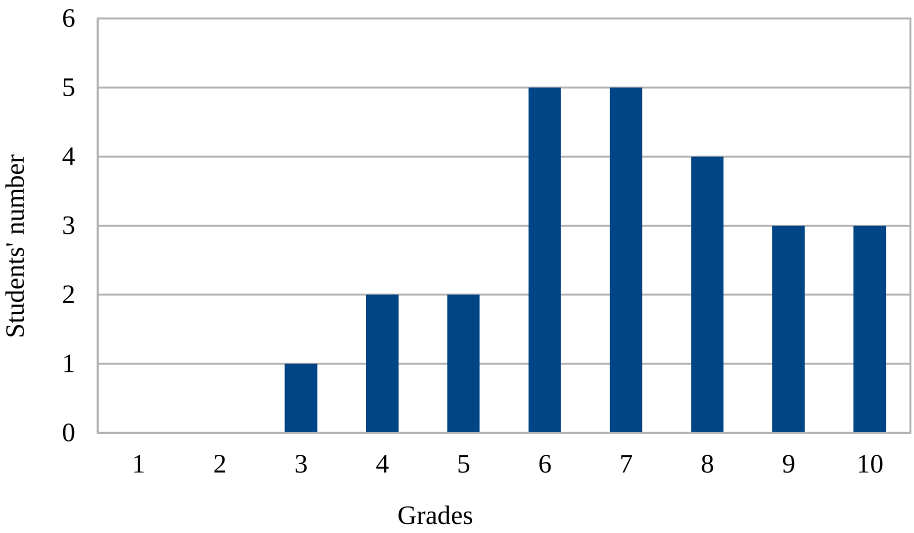

Figure 6. Students' grades frequency in the assessment test following the interdisciplinary teaching approach

RESULTS AND DISCUSSIONS

Analyzing indicators which compare the results of the two teaching approaches on the issue of stratospheric ozone, the mono-, and the interdisciplinary method, respectively, we have recorded their variation in *Table 16*.

Table 16. Variation of indicators reflecting the level of students' acquisitions following the inderdisciplinary teaching approach

Analyzed indicator		**Monodisciplinary lesson**	**Interdisciplinary lesson**	**Variation of analyzed indicator**
Class average		5.88	7.04	1.16 points increase
Grade frequency	3-4	36.00%	12% students	24.00% decrease
	5-6	24.00%	28.00%	4.00% increase
	7-8	24.00%	36.00%	12.00% increase
	9-10	16.00%	24.00%	8.00% increase
% item types solving	“Knowledge” type items	87.00%	93.00%	6% increase
	“Understanding” type items	71.10%	83.70%	12.6% increase
	“Aplication” type items	54.60%	69.40%	14.8% increase
	“Analysis” type items	22.92%	40.30%	17.38% increase
Number of not approached/ not solved (0 points)		61	22	63.93% decrease
% not solved items (0 points)		7/12 (58.33%0	5/12 (41.66%)	16.67% decrease

Number of integral solutions	130	163	25.38% increase
% of item solving	1220 points/max.2250 = 54.22%	1539 points/ max. 2250 = 68.4%	14.18% increase

Analysis of the results obtained by students in the assessment for the interdisciplinary lesson and their comparison with those obtained in the monodisciplinary teaching approach lesson reveals:

- the more detailed presentation of issues poorly assimilated in the monodisciplinary lesson brought about an increase in the item solving percentage. Thus, the percentage of solving items aimed at understanding the mechanism of ozone decomposition by freons, knowledge application in explaining and analyzing issues that imply working with constructs from Geography, Physics and Biology related to the influence of climate, latitude and altitude on the production or thinning of the ozone layer, related to the relationship between plants and the variation of stratospheric ozone concentration, increased significantly;
- class average rose by 1.16 points,
- the frequency of small grades decreased in favour of good and very good grades;
- the percentage of all items solved increased (by 14.18%), especially the cognitive “application” level (by 14.8%) and the “analysis” ones (by 17.38%);
- there was a decrease in insuccessful approaches of items (with 0 score) or in the disinterest of approaching certain items, with 63.93%, which leads to the conclusion that the students’ degree of satisfaction in perceiving this issue in an interdisciplinary manner increased significantly. At the same time, the percentage of items not solved at all decreased by 16.67%;
- the number of completely solved items increased by 25.38

CONCLUSIONS

The interdisciplinary approach has added value to the lesson in terms of information (adequate to systemic understanding, appropriate to the lesson sequences, rigorously presented by each specialized teacher, from methodical and scientific points of view) valorized and learned, and of the motivation for studying this topic, due to to the novelty of team work, both for students and for teachers.

The teaching research presented in this paper is a plea for the interdisciplinary approach to the issue of ozone, in particular, but also other polyvalent issues in terms of methodological and scientific approaches. These approaches provide an ascendant in the knowledge, comprehension, application and systematic analysis of knowledge in related areas, stimulating the students’ motivation and enthusiasm for the study of sciences.

REFERENCES

[1] Drăgan, N., Meiroşu, E., Tomescu, N., (2003), Chimia Mediului și a Calității Vieții, Editura LVS Crepuscul, Ploiești, pp. 27-41.
[2] Florescu. N., Popescu, V., Popescu, A., (2006) Fizică, Manual pentru clasa a XI-a, Editura Gymnasium, Dâmbovița, pp. 171-172.
[3] Hădărean, M., Lupuți, G., (2003), Chimie pentru grupele de performanță, Editura Dacia Educațional, Baia-Mare, pp. 101.
[4] Mândruț, O., (2004), Geografie fizică. Pământul-Planeta Oamenilor, Editura Corint, București, pp. 58-59.
[5] Mândruț, O., (2006), Geografie. Probleme fundamentale ale lumii contemporane, Editura Corint, București, pp. 40-41.
[6] Mihail, A., Ariniş, I., (2000), Biologie, Manual pentru clasa a IX-a, Editura All 2000, București, pp. 101-104.
[7] Nenițescu. C., D., (1985), Chimie Generală, Editura Didactică și Pedagogică, București, pp. 617-619.
[8] Țurlea, S., (1989), S.O.S., Natura în pericol, Editura Politică, București, pp. 149-165.
[9] Vlădescu, L., Badea, I. A., Doicin, L. I., (2008), Chimie C1, Manual pentru clasa a XI-a, Editura Art, București, pp. 37-38, 65.
[10] Ministerul Educaţiei, Cercetării şi Tineretului, Consiliul Naţional pentru Curriculum, (2004), Programă Școlară pentru Clasa a IX-a, Ciclul Inferior al Liceului, Biologie, București, pp. 4-14.
[11] Ministerul Educaţiei şi Cercetării, Consiliul Naţional pentru Curriculum, (2006), Programe

Şcolare pentru Ciclul Superior al Liceului, Fizică, clasa a XI-a, Bucureşti, pp. 10-13.
[12] Ministerul Educaţiei şi Cercetării, Consiliul Naţional pentru Curriculum, Programe Şcolare pentru Ciclul Superior al Liceului, (2006), Geografie, Probleme Fundamentale ale Lumii Contemporane, clasa a XI-a, Bucureşti, pp. 6-9.
[13] Ministerul Educaţiei, Cercetării şi Inovării, Consiliul Naţional pentru Curriculum, (2009), Programe Şcolare pentru Ciclul Superior al Liceului, Chimie, Clasa a XI-a, Bucureşti, pp. 5-9.
[14]http://corinaanghel.ro/2012/11/19/despre-obiective-de-invatare-taxonomia-lui-bloom/25P1D_G%5E1280X720.MMERRA_LSH.mp4
[15] http://climate.ncsu.edu/edu/k12/.ozonelayer
[16]http://www.shutterstock.com/s/ozone+layer/search.html
[17] http://www.theozonehole.com
[18]http://www.slideshare.net/reshma889/ozone-depletion-and-global-warming
[19]http://www.weatherquestions.com/What_is_the_ozone_layer.htm -climate ozon
[20]http://ozonewatch.gsfc.nasa.gov/ozone_maps/movies/OZONE_D2013-07-01%

Analele Universităţii din Oradea-Fascicula Chimie, Vol. XXIII, 2016

EXTRACTION AND STABILITY OF ANTHOCYANINS FROM FOREST FRUITS

Sanda PĂLĂCEAN
Compania de Apă Someş SA; sandapalacean@gmail.com

Abstract: *The overall objective of this paper work is to study the influence of the solvent on the extraction of anthocyanins from forest fruits and to track the stability of these natural pigments from the obtained extract.*

Key words: anthocyanins, forest fruits, natural pigments, extraction, stability, experimental activities.

INTRODUCTION

Anthocyanins are the most important pigments of superior plants; these are non-toxic and are easily incorporated into water based compounds and could be used as natural water-soluble dyes. Anthocyanins are obtained from grapes, forest fruits, red cabbages, apples, radishes, tulips, roses, orchids and so on. Fruits are the most important source of anthocyanins from nature. These can be found mainly in the fruit peel, like apples and grapes for instance but can also be found in the fruit pulp of cherries and cranberries. Because of their color, which varies from orange and red to blue, anthocyanins could be the ideal replacement for synthetic red dyes, however the usage of these natural pigments is not convenient because of their low stability caused by the pH, the storing temperature, presence of enzymes, light, oxygen, etc. Another important property of anthocyanins is being antioxidant, which plays a vital role in preventing neuronal and cardiovascular diseases, cancer and diabetes. Anthocyanins can improve the nutritional value of processed food, preventing the oxidation of lipids and proteins found in food products.

.

THE CONCENTRATION OF ANTHOCYANINS IN FOREST FRUITS

In forest fruits, the anthocyanins concentration is correlated with the dark color of the fruit, the darker the color, the highest concentration of anthocyanins. From all forest fruits, the highest concentration of anthocyanins can be found in cranberries (300-600 mg/100g fresh fruit) and black currant (80-810 mg/ 100 g).The table 1 shows the concentration of anthocyanins that can be found in different forest fruits[28].

Depending on the species, forest fruits have different quantities of individual anthocyanins. Strawberries and mountain lingonberries have a simple anthocyanins profile with a single major pigment. The main anthocyanin from strawberries is 3-glucosylpelargonidin[33], and for mountain lingonberries is 3-galactosyl cyanidin.The black currant contains 4 important anthocyanins: 3-glucosyl cyanidin, 3-galactosyl cyanidin, 3-glucosyl delphinidin and 3-galactosyl delphinidin[27]. For lingonberries, the two aglycones are cyanidin and peonidin, which together with the three remains of monosaccharides: 3-galactoside, 3-glucoside and 3-arabinosid give a total of six main anthocyanins. Other forrest fruits like cranberries and crowberries have a more complex anthocyanin profile. Both types contain five main aglicons: delphinidin, cyanidin, petunidin, malvidinand peonidin. There were fifteen different anthocyanins identified in cranberries, formed by combining the five aglicons with 3-glucoside, 3-galactoside, 3-arabinosid[27]. The distribution of anthocyanins varies between different types of forrest fruits but also between different species of the same type

Tab.1. Anthocyanins concentration found in different forest fruits[28]

Type of fruit		**Anthocyanins (mg / 100 g fruit)**
Black currant *(Ribes nigrum, L.)*		80-810
Cranberries (Vaccinium myrtillus, L.)		300-600
Lingonberries *(Vaccinium oxycoccus, L.)*		20-360
Mountain lingonberries(Vaccinium vitis-idaea, L.)		35-170
Cowberry *(Empetrum nigrum, L.)*		300-560
Rasberry (Rubus ideaeus, L.)		20-220
Strawberry *(Fragaria ananassa L.)*		10-80

METHODS OF ANALYSIS: EXTRACTING AND OBTAINING ANTHOCYANINS

The solvent extraction is the most common method used for extracting diferent compounds that are found in fruits. Phenolic compounds were extracted by soaking fresh fruits into extraction solvents or by grinding, drying or freeze-drying the fruits folowed by solvent treatment. Anthocyanins are polar molecules, so the most common solvents used for extraction are lower alchohols (ethanol, methanol) and acetone or mixing them with water. The use of these solvents results in the coextraction of nonphenolic compounds, such as saccharides, organic acids and proteins, for obtaining anthocyanins further purification processes (for example, solid phase extraction) are necessary. Choosing the extraction method is done as such so that the extraction coefficient of pigments is the highest and the one of the other compounds is the lowest and also the degradation of compounds during the extraction process should be prevented.

Amongst the most common methods of extraction are the ones that use methanol or acidified ethanol as extractors. From these two, the methanol extraction is the most efficient one; it has been determined that in the case of anthocyanins extraction from grapes, the methanol extraction is 20% more efficient than the ethanol one, and 73% more efficient that the one using plain water[24], however in the food industry, ethanol is preffered because of the methanol's toxicity.

As mentioned, the raw material submitted for extraction contains other classes of compounds that can interfere with anthocyanins, masking or changing their properties.

The process of obtaining the anthocyanins extract requires in most of the cases a pre-processing of the raw material to eliminate the undesired influence of certain factor, the pre-processing includes using mecanical, phisico-chemical and chemical methods.

Industrial installations for modern extractions allow us to adapt the grinding and mixing of raw material, temperature, pH, time of extraction, ratio between the mass of raw material and the solvent volume, which enables to forecast the quality and quantity of the resulted extract.

Anthocyanins extraction

A. Room temperature

Weigh 2 grams of dried berries and mix by shredding, then put them in a Berzelius beaker. Add 50 ml of solvent (water, ethanol) and leave at room temperature for 10 minutes. After this time, the mix is filtered under vacuum. The extract is introduced in a volumetric flask of 50 ml and calibrated using solvent. The obtained solution is used to determine the anthocyanins from forest fruits. The process is reiterated at 20, 30, 40, 50 and 60 minutes. In order to investigate the effect of stiring for the extraction process, the same experiment is done, but the mix is stirred for 10 minutes.

B. High temperature

In this case, we used water at boiling point (100^0C), in which we added 2 grams of dried forest fruits. After 10 minutes, the mix was filtered, cooled then the procedure described above (A) was applied.

Using the pH differential method to determine the level of monomeric anthocyanins

A.Preparing the buffer solutions

- *Buffer solution of KCl, 0*.025 M with pH 1.0: 1,96 grams KCl is stirred with 980 ml distilled water in an Erlenmeyer beaker. Measure the pH of the solution and adjust to 1 using concentrated HCl. Transfer in a volumetric flask of 1 liter and calibrate using distilled water.
- Buffer solution of sodium acetate 0.4 M with pH 4.5: Stir 54,43 grams of sodium acetate trihydrated with 960 ml distilled water. Measure the pH and adjust to value 4.5 using concentrated HCl. Transfer in a volumetric flask of 1 liter and calibrate using distilled water.

B. Determine the level of anthocyanins

- Prepare 2 diluated solutions 1:1 with buffer solution, one with buffer solution with pH=1, the other with pH = 4.5, then leave for 15 minutes to balance.
- Bring the spectophotometer to zero (using distilled water) for every wave length used.
- Measure the absorbance of the two diluated solutions at different wave lengths: at $\lambda_{vis\text{-}max}$ (515 nm)and 700 nm (for the turbidity correction) using distilled water as blank sample.
- Calculate the absorbance of the solutions using the formula:

  ○ $A = (A_{pH\ 1.0} - A_{pH\ 4.5})_{525\ nm} - (A_{pH\ 1.0} - A_{pH\ 4.5})_{700\ nm}$

♦ Calculate the level of anthocyanins, in cyanidin-3-glucoside equivalents, in mg/l extract. The molecular weight and the extinction coefficient used in the formula correspond to cyanidin, having M=449.2 and ε= 24600.

RESULTS AND DISCUSSIONS

Anthocyanins reversibly change color once the pH is modified which limits anthocyanins from being used eficiently as food colorants for many applications, but offer an easy and convenient method for measuring total pigment concentration. The colored oxonium form predominates at 1.0 pH and the colorless hemiketal form at 4.5 pH (Fig. 1). The difference of absorbance between the solutions with different pH values is due to the monomeric anthocyanin pigments. The pH-differential method is based on this reaction and permits accurate and rapid measurement of the total anthocyanins from different matrices, even in the presence of other interfering compounds[18]. The reversible transformations in the anthocyanins structure, caused by pH modification, show different spectra of absorbance. (Fig. 2)

To determine the total monomeric anthocyanins from the sample that contains also other phenolic compounds, the absorbance of the solution is measured for the two values of the pH, at two different wave lenghts: λ_{max} and 700 nm. This is possible because anthocyanins have the same absorbance wavelength between 490-550 nm.

.

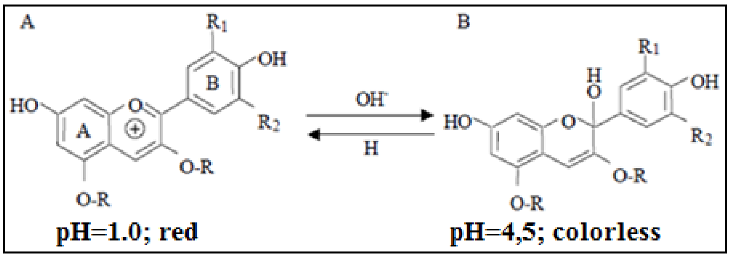

Fig.1. Structures of flavynium cation (A) and the hemiketal form of anthocyanins R=H or glycosidic substituent

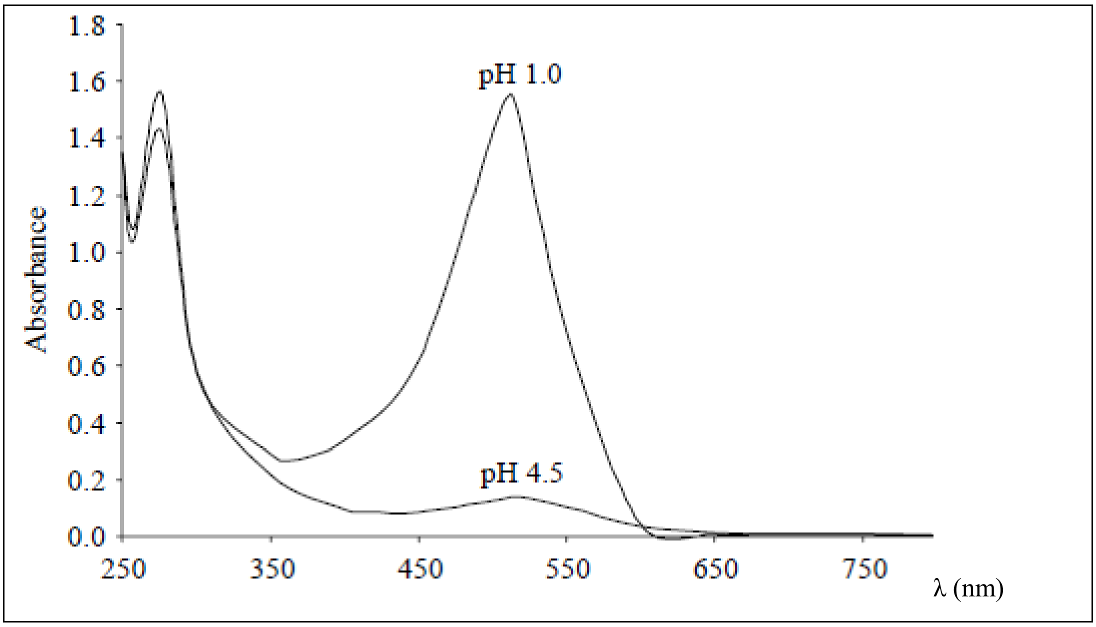

Fig.2 UV-Visible spectra of anthocyanins in at pH=1.0 and pH=4.5 buffers

The total concentration of anthocyanins is calculated based on molecular weight and molar extinction coefficient of the anthocyanin compound that can be found in the highest proportion in the sample. The molar absorbancy coefficients are the absorbance of a solution of 1% concentration measured in a pathlength of 1 cm, at the wavelength characteristic to the maximum absorbancy from the visible domain. The absorbance depends on the chemical structure of the anthocyanin pigment, but also on the solvent used to determine it (table 2), (table 3). When using this procedure, extinction coefficients determined in aqueous solutions should be used rather than those determined in ethanol or methanol because of solvent effects. The number of anthocyanins for which the molar extinction coefficients was calculated is however limited.

Tab.2. Molar absorbance of anthocyanins

Pigment	Solvent	Molar absorbance (ε)
Cy	1% HCl in ethanol	24600
Cy-3-Glu	Aqueous buffer pH=1	26900
Dp-3-Glu	1% HCl in methanol 10% ethanol;pH = 1,5	29000 23700
Mv	0,1% HCl in ethanol	37200
Mv-3,5-diGlu	0,1% HCl in ethanol HCl 0,1 N	10700 37700
Mv-3-Glu	0,1% HCl in methanol 0,1 N HCl	29500 28000
Pg	0,1% HCl in methanol	19780
Pg-3-Glu	1% HCl in ethanol	31620

The total concentration of monomeric anthocyanin pigments is calculated using the formula:

$$TA = \frac{A \cdot M \cdot F \cdot 1000}{\varepsilon \cdot l}$$

where: TA= Total Anthocyanins (mg/L)

A = absorbance, calculated using the formula:

$A = (A_{\lambda vis\text{-}max} - A_{700})_{pH=1} - (A_{\lambda vis\text{-}max} - A_{700})_{pH=4,5}$

M = molecular weight

F = dilution factor

ε = molar extinction coefficient ($l.mol^{-1}.cm^{-1}$)

l =pathlength (=1c)

Tab.3. Molecular weight of main anthocyanins

Compound	Pg	Cy	Pn	Dp	Pt	Mv
	271	287	301	303	317	331
+ hexose	433,2	449,2	463,2	365,2	479,2	493,2
+ 2 hexose	595,4	611,4	625,4	627,4	641,4	655,4

In order to determine the content of monomeric anthocyanin pigments extracted from forrest fruits, the pH differencial method was applied.

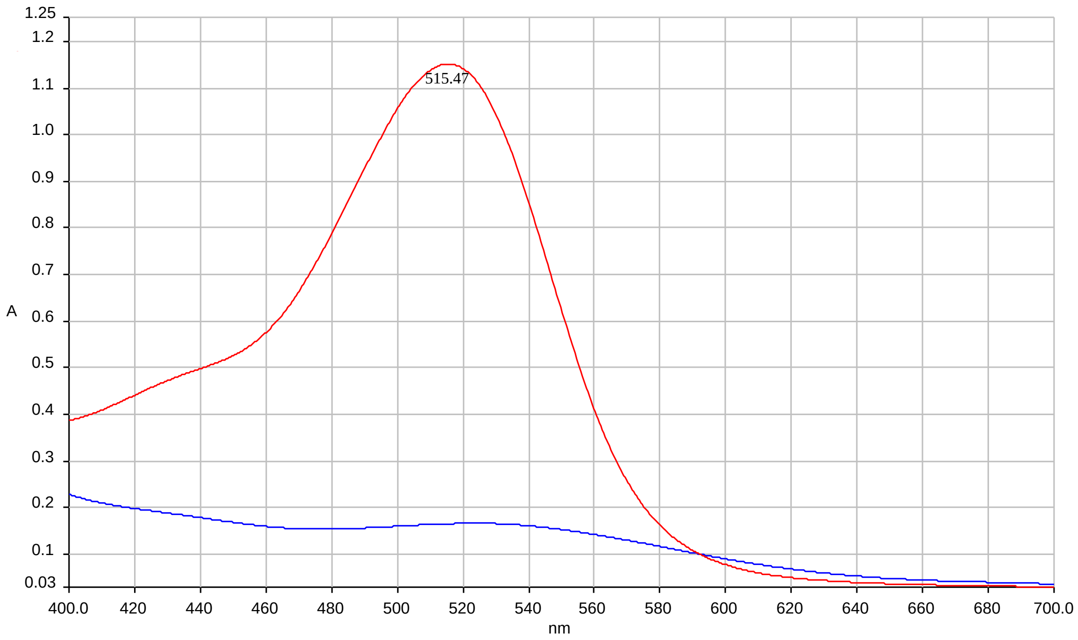

Fig.3. UV-VISIBLE spectra of forrest fruits extract in solutions having pH 1.0 and pH 4.5

The bandwidth of maximum intensity can be observed, this is a characteristic of anthocyanin pigments at the wavelength $\lambda_{vis\ max}$ = 515 nm, pH=1. The total content of anthocyanins was determined from the absorbance values measured in the obtained solutions after the process of extraction, done every 10 minutes, using water and ethanol as solvents. The anthocyanins concentration extracted using different solvents (water and ethanol at room temperature) at intervals of 10 minutes is shown in tab.4 and tab.5.

Tab.4. Anthocyanins from forest fruits in aqueous extract

Time of extraction	Absorbance	Anthocyanins extracted (cyanidin equivalent) mg/L
10 min	0.159	21.24098
20 min	0.2276	30.40533
30 min	0.3459	46.20915
40 min	0.3625	48.42677
50 min	0.3668	49.00121
60 min	0.4113	54.94601
10 min stiring	0.2948	30.38265

Tab.5. Anthocyanins from forest fruits in alcohol extract

Time of extraction	Absorbance	Anthocyanins extracted (cyanidin equivalent) mg/L
10 min	0.503667	67.28537
20 min	0.523367	69.91712
30 min	0.554767	74.11188
40 min	0.639467	85.42704
50 min	0.657867	87.88512
60 min	0.65840	87.95637
10 min stiring	0.608967	81.35251

There a notable difference between anthocyanin concentrations obtained using the two solvents (Fig. 4). In this case, the most efficient extraction of anthocyanin pigments from forrest fruits was done in ethanol.

The influence of stiring over the efficiency of the extraction was investigated. Results show that stiring is actually quite essential in the extraction process. At the same time of extraction (10 minutes) the total monomeric anthocyanins extracted in ethanol was with 21% higher than the extraction done when stiring, whereas the influence of stiring is more visible when water was used as the extraction solvent, the number of anthocyanins extracted in this case was 43% higher

.

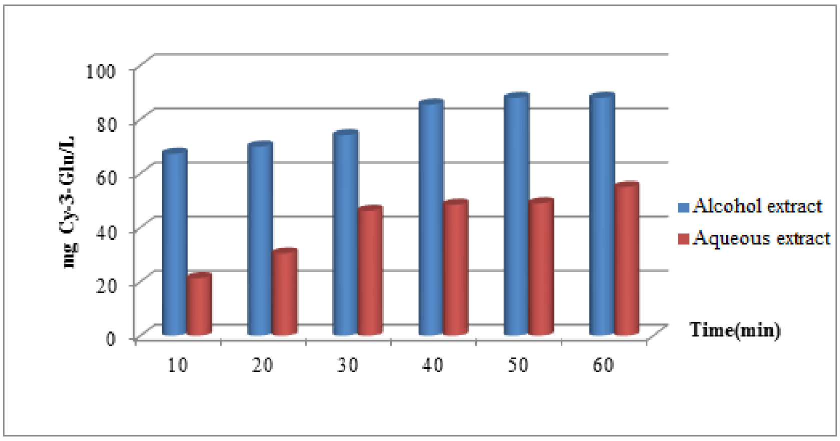

Fig.4. How solvent influences the anthocyanin efficient extraction from forest fruits

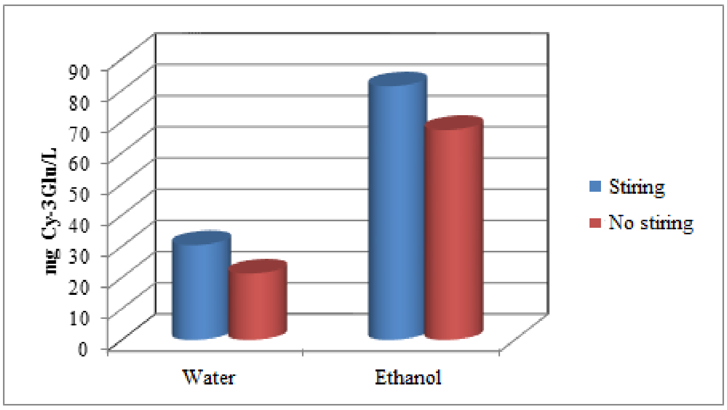

Fig.5. Influence of stirring over efficiency extraction of anthocyanins from forest fruits

Figure 6 shows the impact of extraction time over the anthocyanin pigments recovery grade from the forrest fruits mixture used. Independent of the solvent used, the longer the time extraction was, the more anthocyanins were extracted. Time influenced even more the extraction process when wáter was used as extraction solvent, the quantity of anthocyanins extracted was 2.6 times bigger than in the case of the extraction done in 10 minutes. Similarly, for the same intervals of time but using ethanol, the quantity was 1.3 bigger.

The combined effect of extraction time and solvent over the efficiency of the extraction process is also reinforced by the fact that at shorter intervals of extraction the solvent influence is more visible than at longer extraction intervals. At 10 minutes, the total anthocyanins extracted in ethanol is 3.2 times bigger than the one extracted in wáter, while at 60 minutes, this ratio is only 1.6 times bigger.The effect of the extraction time was also investigated for infusions obtained from a mixture of forest fruits. The results (tab.6) confirm that increasing the extraction time results in more anthocyanin pigments in the obtained solution (regardless of the temperature)

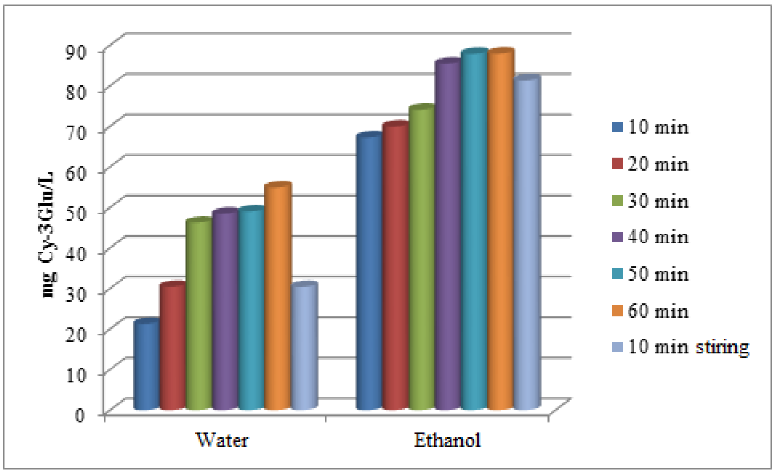

Fig.6. How time influences the efficient extraction of anthocyanins from forest fruits

Tab.6. Anthocyanins from forest fruits in aqueous infusion

Time	Absorbance	Extracted anthocyanins (cyanidin equivalent) mg/L
5 min	0.46	21.26
10 min	0.59	54.33
15 min	0.65	59.78

Figure 7 ilustrates the total of anthocyanins extracted under different conditions (room temperature, water boiling point, ethanol at room temperature) at the same time of extraction (10 mins). Based on the obtained values, it is clear that for a short extraction time, at high temperature the efficiency of natural pigments extraction increases considerably. Several studies show that for a long extraction time, the process is less efficient because the pigments degrade in hot solution.[15, 6]. It can be concluded that the ethanol extraction at room temperature is more efficient than the water extraction at boiling point

Because the color stability of anthocyanins is influenced by several phisico-chemical factors, the degradation rate of pigments increases during their storage[6, 14].The anthocyanins stability for forest fruits tea was analysed at room temperatura, the results are noted in Tab.7

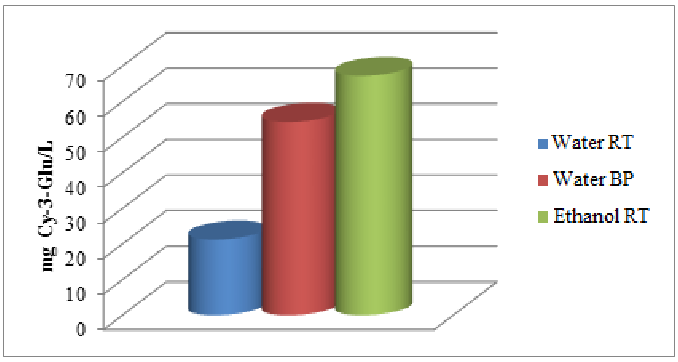

Fig.7. How temperature influences efficiency of anthocyanins extraction from forest fruits

Tab.7. Anthocyanins degradation over time

Time (hours)	0	24	48	72	96	120
Anthocyanins (mg/L)	598.86	547.80	501.60	452.98	415.63	397.15

Resulted data confirm that anthocyanins pigments suffer degradation when stored at room temperature. The level of anthocyanins dropped by approx. 32% after five days (fig.8).

To determine the cinetic parameters of degradation from the investigated extract, the variation ln(C/C_0) in time is represented in the following graphic(Fig.9).

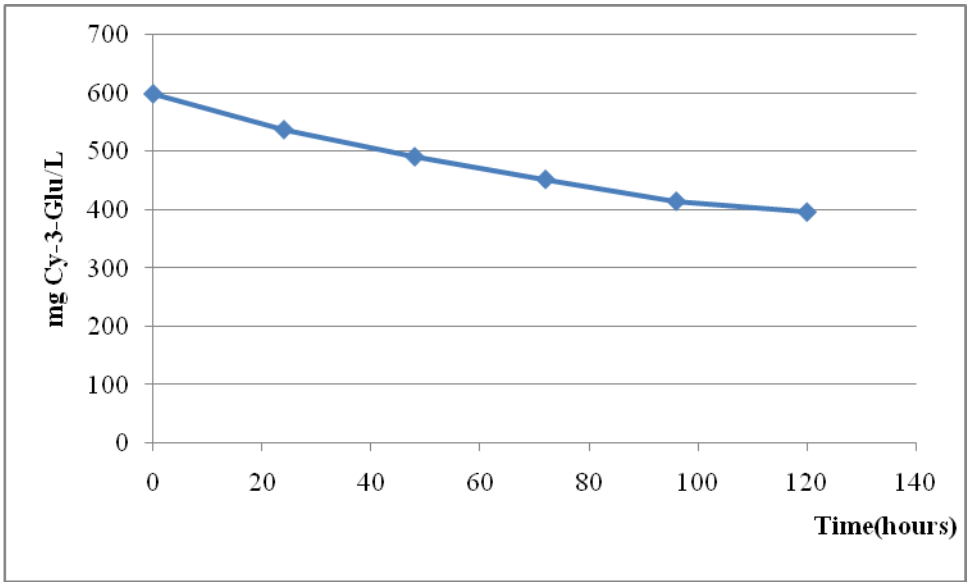

Fig.8. Variation of anthocyanins in time

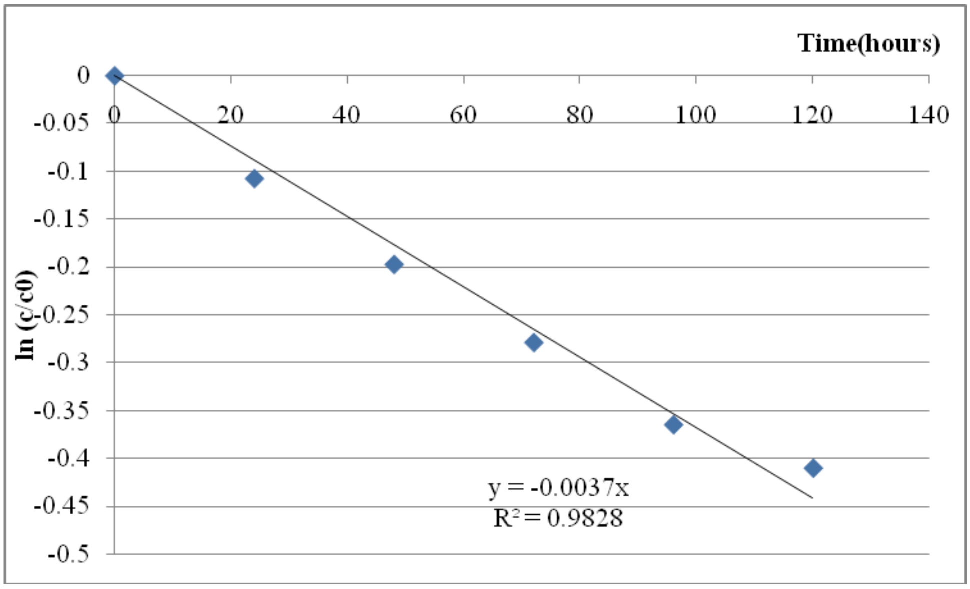

Fig.9. Graphical representation of the ln(C/C_0) variation in time

The linear variation ln(C/C0) confirms that the anthocyanins from forest fruits degrade following a cinetic of first order, characterized by a speed law of type:

$$\ln[TA] = \ln[TA_0] - kt$$

where:[TA] = total monomeric anthocyanins at specific time t (mg/L)

[TA_0] = initial monomeric anthocyanins total (at specific time t_0) (mg/L)

k = speed constant (days^{-1})

t = time of reaction (days)

The half time of the reaction can be calculated using the following formula:

$$t_{1/2} = (\ln 0.5)/k$$

The value of the speed constant (determined from the graphical representation in Fig. 9) is 0.0037 hours and the corresponding half-time value is 187.3 ore (7.8 days). These results are in-line with the rest of the studies done on the stability of anthocyanins from forest fruits.

CONCLUSIONS

1. Because they are beneficial for health, the usage of anthocyanin molecules as natural pigments for several food products is expected to increase in the next years.
2. The pH differential method was successfully used to determine the level of anthocyanins in forest fruit extracts.
3. It was confirmed that the solvent influences the efficiency of the extraction of anthocyanin pigments from forest fruits.
4. Extraction time has a major influence on the efficiency of the extraction of anthocyanins from forest fruits.
5. The stability of anthocyanins from forest fruits tea changes during storage time.

REFERENCES

[1] B. de Ancos, E. Ibanez, G. Reglero, M. P. Cano, *J. Agric. Food Chem*., **2000**, *48*, 873-879
[2] O. M. Anderson, G. V. Francis, *Annual Plant Reviews – Plant Pigments and Their Manipulation*, **2004**, *14*, 293-341.
[3] E. L. Attoe, J. H. Elbe, *J. Food Sci*., **1981**, *46*, 1934-1937
[4] A. Bakowska-Baraczak, *Pol. J. Food Nutr. Sci*., **2005**, *14*, 107-116
[5] D. Baqchi, C. K. Sen, M. Bagqchi, M. Atalay, *Biochem. (Mosc.),***2004**, *69*, 75-80
[6] T. Boranbayeva, F. Karadeniz, E.Yilmaz, *Food Bioprocess Technol*., **2014**, *7*, 1894-1902
[7] R. Brouillard. Chemical structure of anthocyanins. In: *Anthocyanins as Food Colors.* Pericles Markakis (ed.), Academic Press Inc., New York, **1982**, p.1-38.
[8] A. Castaneda-Ovando, M. L. Pacheco-Hernandez, M. E. Paez-Hernandez, J. A. Rodriguez, C. A. Galan-Vidal, *Food Chem*., **2009**, 859-871.
[9] R. N. Cavalcanti, D. T. Santos, M. A. A. Meireles, *Food Res. Int.,***2011**, *44*, 499-509
[10] P. H. Choo, S. Matsui, K. Misaki, T. Matsuda, *Environ. Sc. Tech.*, **2007**, *41*, 652-657.
[11] M. Dyrby, N. Westergaard, H. Stapelfeldt, *Food Chem*., **2001**, *72*, 431-437
[12] J. H. von Elbe, S. J. Schwartz Colorants. In: *Food Chemistry*. Fennema OR (ed.) 3rd ed., Marcel Dekker Inc., New York, **1996**, p.651-723.
[13] Z. Fang, M. Zhang, Y. Sun, J. Sun, *Food Chem*., **2007**, *103*, 268-273
[14] D. Farcassetti, C. DelBo, P. Simonetti, et al., *J. Agric. Food Chem*., **2013**, *61*, 2999-3005
[15] U. A. Fischer, R. Carle, D. R. Kammerer, *Food Chem*., **2013**, *138*, 1800-1809
[16] T. Fossen, R. Slimestad, O. M. Andersen, *Phytochem.*, **2003**, *64*, 1367-1374.
[17] A. Garcia-Palazon, W. Suthanthangjai, P. Kajda, I. Zabetakis, *Food Chem*., **2004**, *88*, 7-10
[18] M. M. Giusti, R. E. Wrolstad, *Curr. Prot. Food Anal. Chem*., **2001**, F.1.2.1-1.2.13
[19] J. Jenshiroobha, M. Saravanakumar, K. M. Aravindhan, P. Suganyadevi, *Res. Plant. Biol.*, **2011**, *1*, 5-12
[20] S. Kara, E. A. Ercelebi, *J.Food Eng*., **2013**, 116, 541-547
[21] I. Konczak, W. Zhang, *J. Biomed. Biotechnol*., **2004**, *5*, 239-240.
[22] J. M. Kong, L. S. Chia, T. F. Chia, R. Brouillard, *Phytochem*., **2003**, *64*, 923-933.
[23] A. Z. Mercadante, F. O. Bobbio, *Anthocyanins in foods: occurrence and physicochemical properties; Food Colorants. Chemical and Functional Properties*, Ed. C.Socaciu, CRC Press, New-York, **2008**, 195-299.
[24] R. P. Metivier, F. J. Francis, F. M. Clydesdale, *J. Food Sci.,***1980**, *45*, 1099-1100
[25] E. Nikkhah, M. Khayamy, R. Heidari, R. Jamee, *J. Biol. Sci.,***2007**, *7*, 1412-1417
[26] L. A. Pacheco-Palencia, P. Hawken, S. T. Talcott, *Food Res. Int*., **2007**, *40*, 620-628
[27] A. Patras, N. P. Brunton, C. O'Donnell, B. K. Tiwari, *Trends Food Sci. Technol.*, **2010**, *21*, 3-11
[28] M. Rein, Copigmentation reactions and colour stability of berry anthocyanins. Doctoral disertation, Univ. Helsinki, Finland, **2005**, p. 15
[29] E. Sadilova, R. Carle, F. C. Stintzing, *Molec. Nutr. Food Res*., **2007**, *51*, 1461-1471
[30] C. F. Stintzing, A. S. Stintzing, R. Carle, B. Frei, R. E. Wrolstad, *J. Agric. Food Chem.*, **2002**, *50*, 6172-6181.
[31] K. Takeda, *Proc.Jpn. Acad Ser. B*, **2006**, *82*,142-154
[32] K. Torskangerpoll, O. M. Andersen, *Food Chem*., **2005**, *89*, 427-440
[33] P. J. Tsai, L. Delva, T. Y. Yu, Y. T. Huang, L. Dufosse, *Food Res. Int*., **2005**, *38*, 1059-1065
[34] N. C. Veitch, R. J. Grayer, *Nat. Prod. Rep*., **2011**, *28*, 1626-1695
[35] T. C. Wallace, *Adv. Nutr*., **2011**, *2*, 1-7.

Analele Universităţii din Oradea-Fascicula Chimie, Vol. XXIII, 2016

SEPARATION AND ANALYSIS OF VOLATILE OIL FROM ORANGE PEEL

Mioara Sebeşan*, Radu Sebeşan, Sorin Hodişan***

[*] University of Oradea, Faculty of Sciences, Department of Chemistry, Oradea, Universităţii, 1, Romania
[0.**] University of Oradea, Faculty of Electrical Engineering and Information Technology,Street
Universităţii, Nr.1, 410087, Oradea
Phone: (040)0259-408 640 , E-Mail: msebesan@uoradea.ro.

Abstract: *In this paper we studied the essential oil, which was separated of orange peel.*
Orange oil mainly consists of monoterpene hydrocarbons (α- and β-pinene, myrcene, camphene, limonene, ocimen, α-felandren, p-cymene), oxygenates terpenes (linalool, α-terpineol, nerol, citronellol, citronellal, citral, acetates of linalyl, geranyl and neril, β-phenoxyethanol, etc.
Obtaining the oil from orange peel was made, by extraction with Soxhlet extractor. For the essential oil obtained was determined, the physico-chemical properties. Essential oil from orange peel is used in perfumery and flavoring for sweets.

Keywords : essential oil from orange peel, monoterpene hydrocarbons, physico-chemical analysis

1. INTRODUCTION

The first mention about oranges appears in Arabic script, but the period and first ways of cultures in Europe remain uncertain. Orange blossom is the symbol of State Florida and it is associated with good luck. In the past, bridal bouquets containing the orange blossom. The essential oil of orange looks like a greenish liquid, with aromatic odor and taste, characteristic. It is obtained from pericarp the orange fruit, that is grown in the US, Brazil, Mexico, Guinea, Italy, Greece, Israel. The essential oil consists of a mixture of terpenes. The main chemical substances that have been identified in the chemical composition of the essential oil of orange (Citrus sinensis L.) are terpenes: α- and β-pinene, myrcene, camphene, and (+) - limonene which representing about 90-96% of oil volatile orange.

A). Myrcene

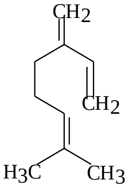

Myrcene has a pleasant aroma, sweet, balsamic, fresh, it is also found in the other oils. One can get synthetic by β-pinene pyrolysis and by linalool dehydration.

B). Limonene

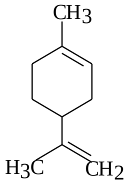

Limonene has a smells fresh, citrate of lemon, it is found in citrus (+) in the conifers and other volatile oils. He be can obtained by sintetic, by isomerization of β-pinene and α-pinene.

C). α-Pinene

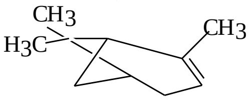

α-pinene has a smell of fir, is found in coniferous turpentine, turpentine and the other volatile oils.

D). β –Pinene

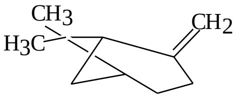

β -Pinene smells of fir, is found in coniferous, turpentine, and other volatile oils.

E). Camphene

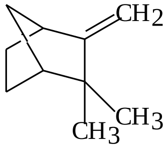

Camphene has a smell of camphor is found and in conifers. He be can obtained synthetically from pinene by addition of the HCl and dehydrochlorination.

The essential oil of orange peel (Citrus sinensis L.) also contains other oxygenates compounds, linalool, α-terpineol, nerol, citronellol, citronellal, citral, acetates of linalyl, geranyl and neril, β-phenoxyethanol, etc. Compositions of essential oils being influenced by species and the climatic environment of development of the plant. Gas chromatographic analysis of the concrete orange, help to establish its chemical composition. For the gas chromatography analysis be use the following conditions:

- Polar capillary column: DB WAX or similar, sized 50 m x 0.32 mm x 1 mm;
- Program temperature: 50ºC (5 min.), 50 - 200 ° C (5°C / min ..) 200 - 250ºC (10° C / min.), 250ºC (10 min.) ;
- Injector temperature 250ºC -
- Detector temperature 250ºC.

We obtain a gas chromatogram, from which be can determine the mass concentrations of each component odorant - flavoring.

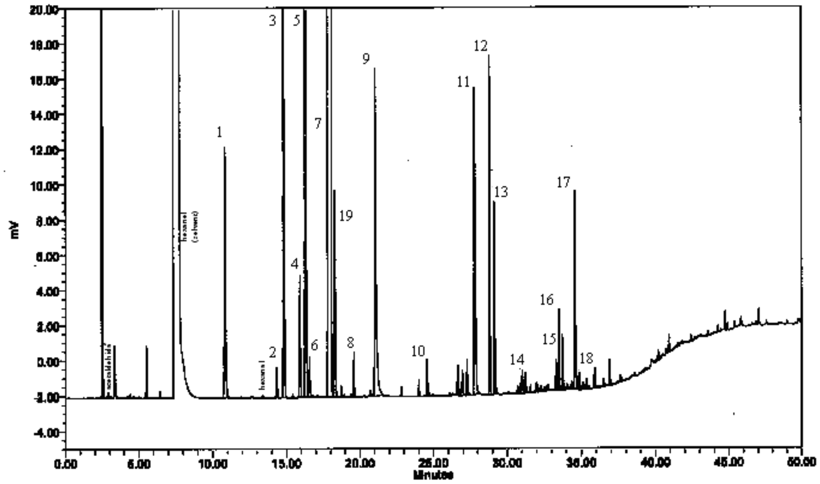

Figure 1. Gas chromatogram for essential oil of orange peel.
1-α-pinene, 2- β-pinene, 3- sabinene, 4-Δ-caren 5-myrcene, 6-α-felandren, 7- limonene,
8- γ-terpinene, 9- camphene, 10-octane, 11- nonanal,12-linalool,13- octane-ol, 14-terpinene-4-ol, 15-neral,
16-α- terpineol, 17-citronellol, 18- carvone, 19- β-felandrene.

In this paper we will present the results for several physico-chemical analysis of essential oil separated from orange peel.

2. EXPERIMENTAL DATA

Obtaining the volatile oil of orange peel was done by steam entrainment of water, followed by drying of the essential oil obtained on anhydrous sodium sulfate and by redistillation. After that, orange essential oil was subjected to the following physical and chemical analysis.

1. *Identification of limonene and pinene of the volatile oil from orange peel*

In volatile oil of orange is found, both α-pinene, as β-pinene, besides major limonene and other terpenes and sesquiterpenes. Their identification is based on their transformation in nitroso chloride and analysis of the crystals obtained, according to the reaction:

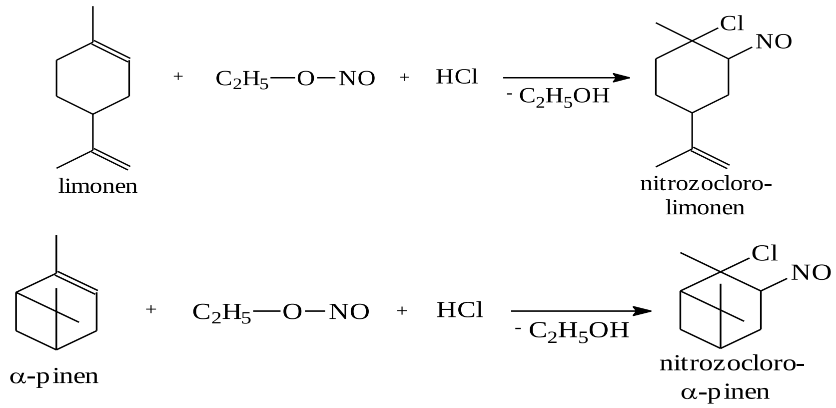

Nitrosochloropinene be crystallized under irregular pyramidal shapes and nitrosochlorolimonene under shape needle-like. After analyzing the obtained crystals is found, that limonene is the major component.

2. Determination of acidity to the essential oil of orange peel (Citrus sinensis L.)

Determination of acidity for essential oil was made by titration with 0.1N KOH in the presence of 1% alcoholic solution of phenolphthalein. The acidity index is calculated using the formula:

$$IA = \frac{5.61 \cdot V_{0.1N}}{m} \quad \text{(mg KOH/g)}$$

where: $V_{0.1N}$ – volume of 0.1N potassium hydroxide solution used for the titration (ml); m - the mass of volatile oil taken it (g).

2. Determination of phenols in essential oil of orange peel

10 ml of essential oil were introduced into a 100-ml flask, above which 1N KOH solution was added, the flask was closed and stirred for a few minutes. After stirring, we leave to stand for 1 hour. The undissolved oil from orange is forced to ascend into the neck of the balloon,in the portion graduated, by addition of a 1N KOH solution.

The content of phenols, expressed as a percent volume,, is calculated using the formula:

$$Fenoli\ (\%) = 10 \cdot \left(10 - V_{ulei\_nedizolvat}\right)$$

where: $V_{ulei\ nedizolvat}$ – the volume of undissolved oil, read on the portion graduated neck flask (ml).

3. Determination of iodine index to the essential oil of orange peel

Weigh 0.25 g of sample oil which was dissolved in 10 ml of chloroform; Add 20 ml of iodine bromide measured using a burette, closed tightly the glass and allowed to stand for 30 minutes in the dark. Was added 30 ml of 1N potassium iodide and 100 ml of distilled water and the liberated iodine is titrated with a 0.1N sodium thiosulfate solution, stirring after each drop. When the solution is pale, place 1 ml aqueous 1% soluble starch indicator and continue the titration with thiosulfate until the blue coloration of the solution is disappeared. Perform a blank test in parallel under the same conditions and with the same quantity of chloroform and bromide solution iod. Index of iodine is calculated using the formula:

$$I.I. = \frac{1.269 \cdot (V^0 - V)}{m} \quad \text{(g } I_2\text{/g sample)}$$

where: V^0 -the volume of sodium thiosulphate solution used in the titration of the blank (ml); V – the volume of sodium thiosulphate solution used in the titration of the sample oil (ml); m – mass of oil taken for analysis (g).

4. Determination of the refractive index of the essential oil of orange peel

To determine the refractive index was used the Abbé refractometer. Power is done by opening the two prisms (thermostated at 20°C) and putting a few drops of sample on the prism, or by feeding prisms slightly parted with a few drops of a suitable pipette.

The prisms is then closed and the device is allowed to stand for a few minutes before the determination, so as to equalize the temperature of the sample to that of the refractometer, after which reading is performed. Between readings, to clean the prisms by means of an absorbent textile material, and then using a piece of cotton soaked in suitable solvent (e.g., ethanol, trichlorethylene, toluene, diethyl ether, petroleum ether) and allowed to evaporate the solvent.

Calibration of the apparatus can be made using distilled water (n_D^{20} = 1.3330).

3.RESULTS AND DISCUSSION

Determination of acidity index for essential oil of orange peel was made by titration with 0.1N KOH in the presence of 1% alcoholic solution of phenolphthalein. The acidity index calculated is:

$$\mathrm{IA} = \frac{5.61 \cdot \mathrm{V}_{0.1\mathrm{N}}}{\mathrm{m}} \cong \frac{5{,}61 \cdot 4{,}8}{6} = 4{,}48(\mathrm{mg\,KOH/g})$$

where: $V_{0.1N}$ – volume of 0.1N potassium hydroxide solution used for the titration (ml); m - the mass of volatile oil taken it (g).

Determination of phenols in essential oil of orange peel. The content of phenols, expressed as a percent volume, calculated is:

$$Fenoli\,(\%) = 10 \cdot \left(10 - V_{ulei\_nedizolvat}\right) = 10 \cdot (10 - 5{,}34) = 46{,}6\%$$

where: $V_{ulei\ nedizolvat}$ – the volume of undissolved oil, read on the portion graduated neck flask (ml). Separation and phenolic content examination may be performed after determining the total content of phenols.

Determination of iodine index to the essential oil of orange peel Index of iodine calculated is:

$$\mathbf{I.I.} = \frac{\mathbf{1.269 \cdot (V^0 - V)}}{\mathbf{m}} = \left(\frac{\mathbf{1{,}269(10{,}2 - 2{,}6)}}{\mathbf{5}}\right) = \mathbf{1{,}92}$$

(g I2/g sample)

where:

V^0 -the volume of sodium thiosulphate solution used in the titration of the blank (ml);

V – the volume of sodium thiosulphate solution used in the titration of the sample oil (ml);

m – mass of oil taken for analysis (g).

Determination of the refractive index of the essential oil of orange peel. For orange peel essential oil, refractive index measured by us is: n_D^{20} =**1,4715,** measurement was done at a wavelength λ=589,3 nm, and at temperature of 20°C.

.

4.CONCLUSIONS

Essential oils are volatile aromatic substances produced by plants and can be extracted by different methods. In terms of chemical compounds volatile oils are not unitary, but are mixtures of dozens or even hundreds of most organic substances having polyisoprene skeleton known as terpenes and terpenoids. It has been observed that the volatile oil has more compounds of which one is the characteristic, the basic compound, which gives the flavor of oil. Identification of organic compounds in plants is important because separation and knowledge of their chemical structure is the essential step in explaining their therapeutic action characteristic. Currently plants are increasingly being studied for their therapeutic actions. Separation and knowledge of the chemical structure is the essential step in explaining their therapeutic action that characterizes them. For this reason, methods of extraction, separation, and identification of compounds are the most important steps in analyzing the chemical composition of plants. Qualitative and quantitative determination of volatile compounds present in the oils is a subject of modern research. For essential oil of orange peel we determinate, following chemical analyzes, several parameters, which can help us in determining the quality of extract of orange peel. After examining the values determined for the acidity index, iodine, phenol content, is found that the values determined for parameters of essential oil of orange peel, are within normal limits, the separated oil entering the category of essential oils the good quality.

REFERENCES

[1] D. Hădărugă, N.Hădărugă, (2002).Compuşi odoranţi şi aromatizanţi, Editura Politehnica Timişoara, Timişoara.

[2] Hădărugă, D.I., (2003). Relaţii structură – proprietăţi în clasa substanţelor odorante, *PhD Thesis*, Universitatea de Vest Timişoara**.**

[3] *** (1989). Thermal Generation of Aromas, vol. 409, Parliment, T.H.; McGorrin, R.J.; Ho, C.-T. (eds), *Americal Chemical Society*, Washington DC**.**

[4] *** (1982). Chemistry of Heterocyclic Compounds in Flavours and Aromas, Vernin, G. *(ed.), Ellis Horwood Ltd.,* Chichester**.**

[5] Yaylayan, V.A., (1997). “Classification of the Maillard Reaction: A Conceptual Approach”, *Trends Food Sci. & Technol., 8*, 13-18.

[6] Fors, S., (1983). "Sensory Properties of Volatile Maillard Reaction Products and Related Compounds"; In: Maillard Reactions, *American Chemical Society*, Washington**.**
[7] Mottram, D.S., (1998). "Flavour Formation in Meat and Meat Products: A Review", *Food Chemistry* , *62*(4), 415-424.
[8] * * * (1992). Les Arômes Alimentaires, *Tec & Doc – Lavoisier,* Apria, Paris**.**
[9] P.J. Teisseire, (1994). Chemistry of Fragrant Substances, *VCH Publ., Inc.*, New York**.**
[10] I. Ciulei, E. Grigorescu, U. Stănescu, (1993). Plante medicinale. Fitochimie şi fitoterapie, vol. 2, *Ed. Medicală*, Bucureşti**.**
[11] I. Ciulei, E. Grigorescu, U. Stănescu, (1993). Plante medicinale. Fitochimie şi fitoterapie, vol. 1, *Ed. Medicală*, Bucureşti.
[12] M. Sebeşan, G. Badea, R.Sebeşan, S. Hodişan (2013)."*Physico-chemical study of volatile oil extracted from coriander"* Analele Universității din Oradea Fascicula Chimie.

STUDIES REGARDING THE OPTIMAL CONDITIONS FOR THE SYNTHESIS OF COPPER AND IRON AMMONIUM PHOSPHATE

Claudia MORGOVAN[1], Anda PETREHELE[1], Alexandrina FODOR[1]

[1]University of Oradea, 1 Universitatii Str., 410087, Faculty of Sciences, Department of Chemistry, Oradea, Romania, E-Mail: cmorgovan@yahoo.com

Abstract: *This paper presents the optimal conditions of separation of copper and ferrous ions resulted from residual solutions, and their revaluation as microelements fertilizers, as metal-ammonium phosphates.*

In order to precipitate this ions, we used diammonia phosphate and ammonia solution 25%. We studied the influence of certain factors (solution concentrations, temperature, process duration) about separation degree of copper and ferous ions.

We determined the optimal conditions of the synthesis of copper and iron-ammonium phosphate, who determined a maximum separation degree of copper and iron from solution.

Key words*: copper and iron-ammonium phosphates, separation degree, microelement fertilizer.*

INTRODUCTION

All around the world, a special attention is being payed to the development and modernization of the mineral fertilizer industry. The agricultural sector especially needs concentrated and complex, solid and liquid fertilizer assortments and fertilizers with microelements[1].

Today, in the world, there is the tendency of improving of existing technologies and to promote new technologies, so called „clean technologies”, without production of wastes or with possibility of waste recycling.

In this paperwork, we studied the optimal conditions of separation of copper and ferrous ions from residual solutions resulted from galvanic industry, and their revaluation as metal-ammonium phosphates.

METHODS, TECHNIQUES, MATERIALS

To a previously established volume of waste solution, wich contents chloride copper and ferrous chloride of a certain concentration, with permanent stirring up, we added the diammonia phosphate saturated solution, in order to achieve a molar report of $(NH_4)_2HPO4:(Cu^{2+}+Fe^{2+})$ = 1,02:1. The reaction mass was neutralized with ammonia (25% solution) [2].

The pH of the reaction mass to different reports $NH_3:(Cu^{2+}+Fe^{2+})$, taking into account the ammonia added. In order to determine the pH of the reaction mass, the analyser PH/ion Mettler Toledo Switzerland was used. The precipitate product, separated by filtration, was dried in the drying oven, at 70º.

In the filtrate, the content of residual copper and iron was determined, and the solid products were subject to chemical analysis.

The content of copper and iron from the filtrate and the final product was determined through spectrophotometry of atomic absorption, using the spectrophotometer of atomic absorption VARIAN SPECTR AA 110.

STUDY AREA

The lab research intended to establish the optimal conditions of the process of obtaining the copper-ammonium phosphate and ferrous-ammonium phosphate by processing with diammonia phosphate and ammonia of the solutions of copper and ferrous chloride, in order to achieve a maximum degree of separation of the copper and iron from the solution [2,3].

pH of the reaction mass

The waste solution, which contains copper chloride (76 g/l) and ferrous chloride (195 g/l), was treated with diammonia phosphate saturated solution, in order to achieve a molar report of $(NH_4)_2HPO4:(Cu^{2+}+Fe^{2+})$ = 1,02:1.

The reaction mass was neutralized with ammonia (25% solution).

Because the pH of the reaction mass represents the control parameter of the process of neutralization with ammonia, the dependence of the pH from the molar report and the mass report NH_3:(Cu^{2+}+Fe^{2+}) was determined. The experimental data obtained are presented in figure I.

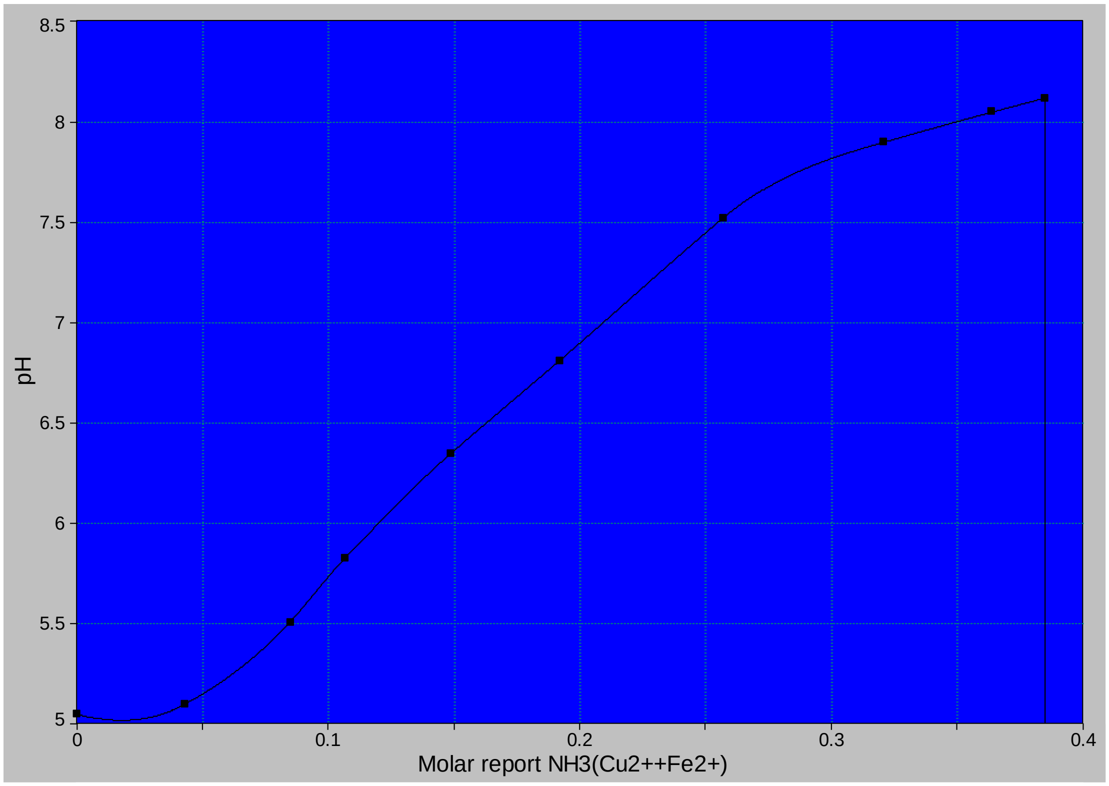

Figure I. The dependence of the reaction mass's pH from the report NH_3:(Cu^{2+}+Fe^{2+}) (molar), for a solution with a content of 76 g/l $Cu^{2+}$and 195 g/l Fe^{2+}, at a molar report $(NH_4)_2HPO4$:(Cu^{2+}+Fe^{2+}) = 1,02:1, at 25º.

After adding the diammonium phosphate, the reaction mass has the pH = 5,05, which represents the starting point of the neutralization process with ammonia of the reaction mass.

The experimental data proves that between the reaction mass's pH and the report NH_3:(Cu^{2+}+Fe^{2+}), there is a well defined difference. The curve traced indicates three fields: the first field, corresponds to a slow increase of the pH (pH = 5,05-5,51); the second field, determines a sudden increase of the pH (pH = 5,51 – 7,90); the last field, when the pH slowly increases to a constant value. In this field, the partial pressure of the ammonia over the system increases, leading to ammonium loss [4,5].

RESULTS AND DISCUSSIONS

Separation degree of the copper and iron in the solution

In order to establish the best conditions of the process of obtaining the copper and ferrous-ammonium phosphates from copper and iron chloride solutions, by processing with diammonia phosphate and ammonia, the influence of certain parameters was analyzed (the final pH of the reaction mass, temperature, concentration of the chloride, duration of the process) over the separation degree of copper and iron.

The experimental data regarding the influence of the reaction mass's pH over the separation degree of the copper and iron from the solution are presented in figure II.

The separation degree of the iron from the solution, after adding the diammonia phosphate (saturated solution) is α = 97,65%.

The separation degree of the copper from the solution, after adding the diammonia phosphate (saturated solution) is α = 99,91%.

The maximum separation degree of both copper and iron corresponds of the optimum pH mass of 6,53.

Temperature

The experimental data regarding the influence of temperature over the degree of separation of copper and iron from the solution are detailed in figure III.

According to the experimental data, it results that, at an optimum pH, the separation degree of the copper and iron is maximum and does not depend of the temperature (within the limits studied). The optimum temperature is considered of 55º, because at this temperature a crystalline precipitate is obtained, precipitate that is easily decanted and filtered [2,4,5].

Duration of the process

The experimental research proved that, in pH optimum conditions, in order to obtain a crystalline, easy to filter precipitate, it is necessary for the duration of the process to be about 55-60 minutes.

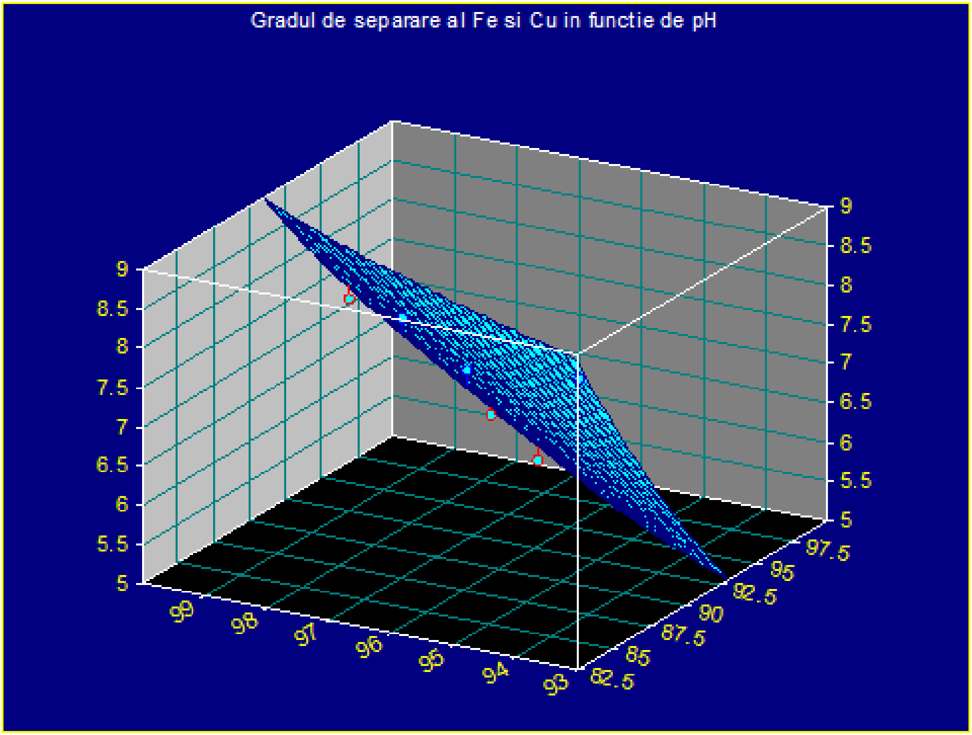

Figure II. The dependence of the separation degree (α) of the iron and copper from the solution from the pH of the reaction mass, for a solution with a content of 195 g/l Fe^{2+} and 76 g/l Cu^{2+}, at a molar report $(NH_4)_2HPO_4:(Fe^{2+}+Cu^{2+})$ = 1,02:1, at 25ºC.

CONCLUSIONS

The experimental research regarding the influence of various parameters over the separation degree of copper and iron from the chlorine solutions allowed the establishment of optimum conditions of the process of obtaining the copper- and ferrous-ammonium phosphates.

The optimum conditions of the processing time of the copper and iron chlorine solutions with diammonia phosphate and ammonia, determining a maximum separation degree of the copper and iron, respectively the shaping of a crystalline precipitate that is easily decanted and filtered are: molar report NH_3:(Fe^{2+}+Cu^{2+}) = 1,02:1, reaction mass's pH ~ 6,5, temperature 55º, duration of process is 55-60 minutes [2,4].

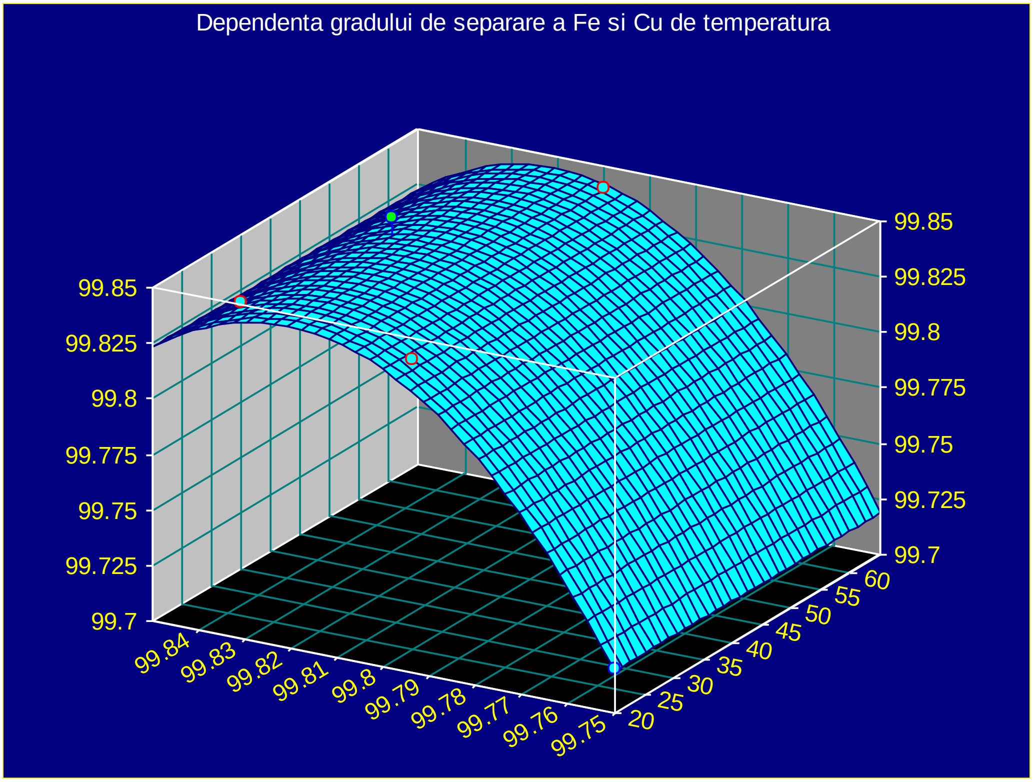

Figure III. The dependence of the separation degree (α) of the copper and iron from the solution from the temperature, for a solution with a content of 195 g/l Fe^{2+} and 76 g/l Cu^{2+}, at a molar report $(NH_4)_2HPO_4$:(Fe^{2+}+Cu^{2+}) = 1,02:1= 1,02:1, at an optimum pH.

REFERENCES

[1.] Iovi, A., Iovi, C., Negrea, P., (2000), *Tehnologii ecologice. Chimia şi tehnologia îngrăşămintelor cu microelement*e, Ed. Politehnica, Timişoara, pp. 195-202;

[2.] Morgovan, C.,(2009), *Contribuţii la studiul proceselor de valorificare a ionilor metalici proveniţi din deşeuri ale industriei galvanice sub formă de îngrăşăminte cu microelemente*, Ed. Politehnica, Timişoara, pp.82-90;

[3.] Morgovan C., Marian E., Iovi A., Bratu I., Borodi G., (2010), *Rev. Chim*, Bucuresti, 61 (3), pp. 259-262;

[4.] Morgovan C., (2007), *Analele Universităţii din Oradea*, Fascicola Chimie, pp. 65-69;

[5.] Morgovan C., Marian E., Iovi A., Bratu I., Borodi G., (2009), *Rev. Chim*, Bucuresti, 60 (12), pp. 1282-1284;

Analele Universităţii din Oradea-Fascicula Chimie, Vol.XXIII, 2016

ELECTROCHEMICAL AND MORPHOLOGICAL CHARACTERIZATION OF ANODIZED TIO$_2$ USED FOR BATTERY ANODES

Mariana Prodana[1], Marius Enachescu[2], Daniela Ionita[1]
[1] Faculty of Applied Chemistry and Materials Science, University Politehnica Bucharest;
prodana_mariana@yahoo.com
[2] Center for Surface Science and Nanotechnology, University Politehnica Bucharest

Abstract.*In the last decade, low-dimensional nanostructural materials have attracted increasing scientific and technological attention due to their physical properties and their potential applications. Dimensionality has a crucial role in determining the properties and performance of nanomaterials. Therefore, the control of size and shape of nanomaterials it is of great importance. Titania nanotubes have improved properties compared to any other form of titania for applications in water and air purification photocatalysis, sensing, water photoelectrolysis for hydrogen generation, photovoltaics, photoelectrochemical solar cells, electronics and optics.*

In the present study, the electrochemical characteristic and morphology of anodized oxide film on cp-Ti in etilen glycol + 2%v/v H_2O + 0.5wt%NH_4F are investigated using potentiodynamic polarization, ac-impedance, complemented with SEM and EDX analysis examinations to predicate the suitable conditions for preparing the anodized oxide films on Ti to be good for batteries anodes. Different anodization voltages were applied to investigate the most suitable voltage required for anodization.

Key words*: nanostructure, battery, potentiodynamic polarization.*

1. Introduction

Ordered TiO$_2$ nanostructures have garnered much research for their use in solar energy applications [1]. TiO$_2$ can be formed by the anodization method leads to an aligned array with an adjustable morphology that can be optimized for its various applications. The morphology parameters, e.g., nanotube length, diameter, smoothness, depend on the anodization conditions, such as voltage, electrolyte composition, temperature and anodization time.

Various organic electrolytes containing fluoride ions have been used to synthesize TiO$_2$ nanotube arrays of extended lengths [2]. In this study, TiO$_2$ nanotube arrays were fabricated by the anodization of titanium foils in ethylene glycol solution containing hydrofluoric acid. The microstructure of the TiO$_2$ nanotubes was studied by scanning electron microscopy (SEM) with an EDS detector.

The objective of this study is to investigate the effect of anodization time and the post-treatment (ultrasonication) on the nanotube characteristics. The charge transfer resistances were investigated by electrochemical impedance spectroscopy (EIS). With this technique it is possible to identify the phenomena proceeding within the different elements (electrolytic solution, electrodes, etc.) at the interfaces between these materials. Several parameters regarding the electrons transport can be determined and give an indication about the specific surface of the TiO$_2$ nanotubes.

2. Experimental part

2.1. *Preparation of TiO$_2$ nanotube arrays*

The amorphous TiO$_2$ nanotube arrays were fabricated by the anodization of titanium foils (25 x 25 mm, 0.5 mm thick, 99.6% purity).

The Ti foils were ultrasonically degreased successively in acetone, ethanol and then cleaned in deionized water for 10 min. The foils were then dried prior to anodization. A two-electrode configuration was used for the anodic oxidation, with platinum foil as the cathode.

The anodization was carried out at constant potential. The anodization bath is made of ethylene glycol containing 0.2 M HF and 2% H_2O (in volume).

The bath temperature was maintained at 22^0 C. The distance between the two electrodes was fixed at 2.5 cm. A DC power source was used to drive the reaction and the anodizing voltage was set at various voltages (10V, 20V, 30 V and 40 V) for obtaining nanotube arrays. The anodization voltage is a crucial parameter, in particular to control the diameter of the nanotubes [3].

It is demonstrated that at low anodizing voltage, the morphology of the porous film is similar to that of porous (sponge-like) alumina [4].

Excessively high voltages may cause high local currents and can affect the homogeneity of the surface. After anodization, the samples were washed with deionized water.

2.2. *Samples characterization*

The morphologies of the titania nanotubes were studied using a field emission scanning electron microscope (QUANTA INSPECT F SEM) with a 1.2 nm field emission gun.

The length of the nanotubes was measured from cross-section images, obtained from mechanically cracked samples.

Tafel plots. The polarization curves were registered between ±200mV and free potential at a scan rate of 2mV/s and corrosion parameters such as jcorr – current density, Ecorr – corrosion potential, Rp – polarization resistance and v_{corr} – corrosion rate were evaluated.

The electrochemical impedance spectra (EIS) were measured by using an Autolab (PGSTAT N301) potentiostatic assembly of three electrodes in a single compartment using the sample as working electrode, platinum as a counter electrode and Ag/AgCl (KCl saturated solution) as a reference electrode.

Measurements were carried out at the open circuit potential (without applying electrical current) and recorded over a frequency range of 105 Hz to 10–2 Hz with an amplitude of the alternating current potential of 5 mV.

The active areas of all the samples was 1 cm^2. All experiments were carried out in 1.5M LiOH + 4.0M KOH electrolyte.

3. Results and discussion

It has been reported that a certain anodization potential is necessary to yield ordered TiO_2 nanotube arrays and 10 V was suggested as the lowest required potential [5]. In this study, we applied much higher anodization potential expecting to control the nanotube size. The anodization voltage is one of the most important parameters pertaining to the surface morphology of TiO_2 nanotube arrays [6].

We will refer at three samples: sample1—TiO_2 nanotubes obtained by anodizing on titanium at 10 V, sample 2—TiO_2 nanotubes obtained by anodizing on titanium at 20 V, and sample 3— TiO_2 nanotubes obtained by anodizing on titanium at 30 V, sample 4— TiO_2 nanotubes obtained by anodizing on titanium at 40 V.

3.1. *Morphology analysis*

In Fig. 1 we can see the morphology of samples S2, S3, S4, the diameter of the TiO_2 nanotubes and also the length measured from SEM. All the parameters obtained from SEM were summarized in Table 1.

For all the samples the morphology is specified for TiO_2 nanotubes. The structure is uniform and tubular distributed on the surface of titanium samples.

Table 1. The length and the diameter of the samples 1-4

Sample	Diameter (nm)	Length (nm)
Ti anodized at 10V	50	320
Ti anodized at 20V	65	496
Ti anodized at 30V	78	556
Ti anodized at 40 V	98	1393

The smallest diameter and the smallest length were obtain for sample 1 while the higher diameter of the nanotubes and the bigger length were obtained for sample 4. By increasing the anodization potential we obtain an increasing in the nanotubes diameter and also in length. Our results are consistent with those in the literature [7]

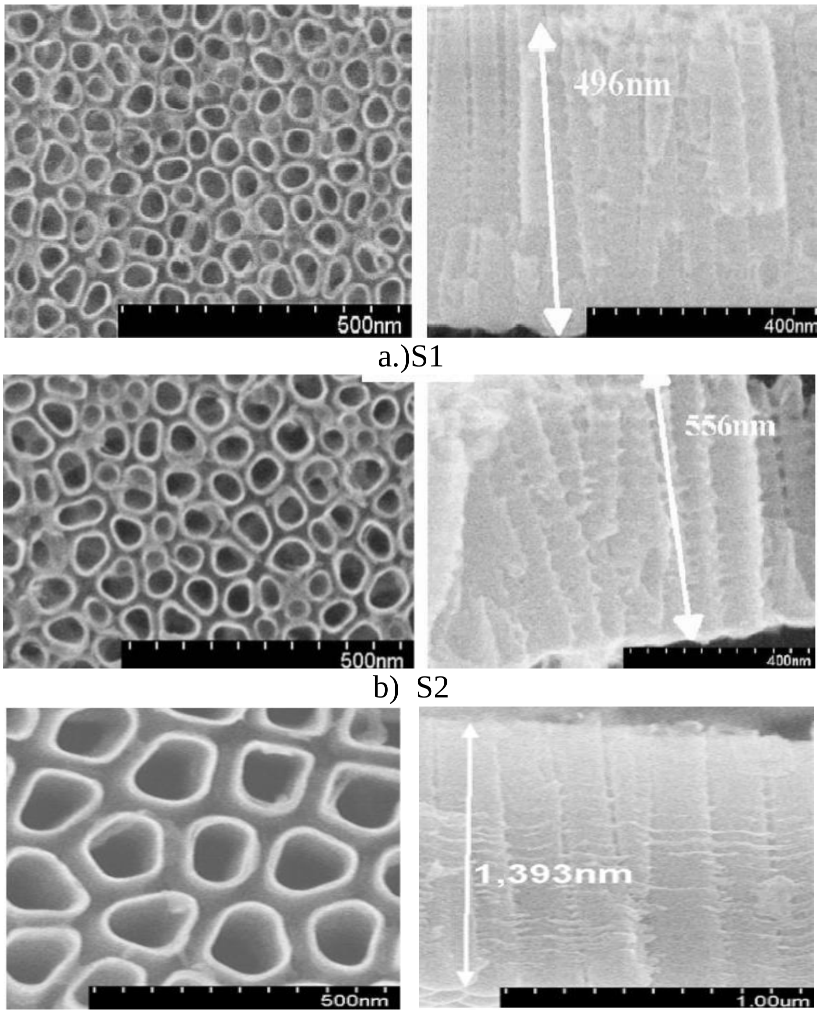

a.)S1

b) S2

c) S3

Figure 1. SEM micrographies for samples 1-4

3.2. *Electrochemical analyses of TiO_2 nanotube arrays*

Electrochemical determinations have been performed at 298 K temperature. Tafel plots - potentiodynamic curves (logarithm of the measured current versus potential) obtained at initial immersion time for samples 1 to 4 are presented in Fig.2.

The corresponding computed electrochemical stability data are presented in Table 2.

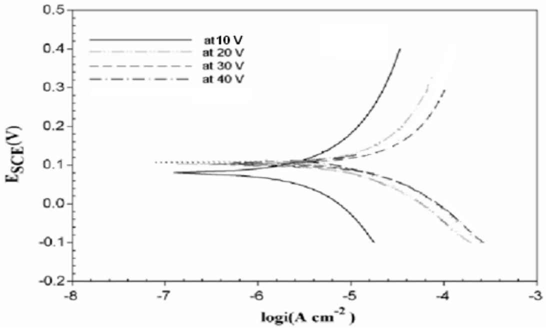

Figure 2. Tafel plots for samples 1-4

Table 2. The electrochemical parameters obtained from Tafel plots for samples 1-4

Anodization potential	jcorr(µA/cm^2)	Ecorr (mV)	Rp (ohm)	Vcorr (mm/an)
10V	0.25	56	725	8. 6 $*10^{-4}$
20V	0.18	95	952	6.5 $*10^{-4}$
30V	0.47	102	668	1.4 $*10^{-3}$
40V	0.51	110	560	1.8$*$ 10^{-3}

As we can see from Tafel plots and from Table 2 the smallest corrosion rate is obtained for sample 2, the higher corrosion rate is for sample 4. This results are consistent to pre-researched results of some titanium alloys [8].

3.3. *EIS measurements*

The results of EIS tests are presented through Bode and Nyquist diagrams.

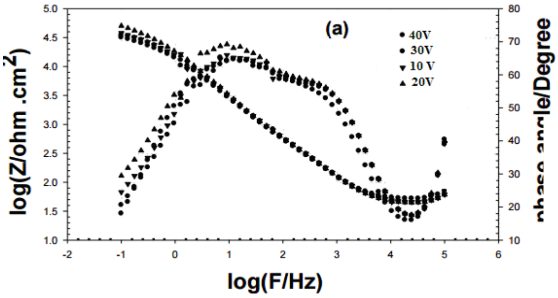

a). Nyquist plots

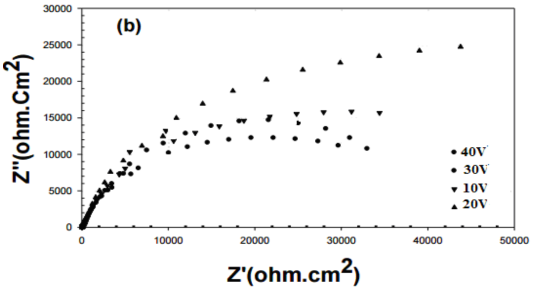

b). Bode plots

Fig. 3. EIS plots for samples 1-4

The EIS spectra exhibit a typical behavior for a metallic material covered by a porous film that is exposed to an electrolytic environment [9].

In the EIS diagrams, two relaxation time constants were clearly indicated by two peaks on phase angle plot (Fig. 3a) the first in the high-frequency part that arises from the ohmi electrolyte resistance and the impedance resulting from the penetration of the electrolyte through a porous film, and the second in the low-frequency part accounting for the process at the substrat/electrolyte interface. It is clear that the impedance depends of the anodization potential from the Nyquist plot (Fig. 3a).

It can be noted that the phase angle drops to zero degrees at high frequencies, indicating that the impedance is dominated by solution resistance. Moreover, in the low-frequency region, the phase angle drops slightly toward lower values thus indicating the contribution of surface film resistance to the impedance. The maximum value of phase shift angle in a wide range of frequency shown in Bode diagrams are similar and average of ~70°

From Bode and Nyquist plots, equivalent circuits that fit the experimental data were proposed. (Fig. 4)

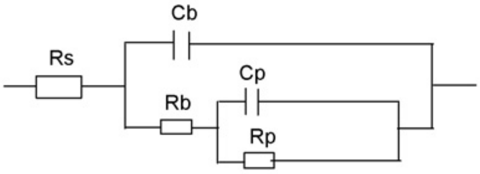

Fig.4. Equivalent circuit used to model impedance spectra of the samples .

Constant phase element, CPE, was introduced instead of pure capacitors in the fitting procedure to obtain good agreement between the simulated and experimental data. The impedance of CPE is defined as Z CPE $= 1/(Q(J\omega)n)$, where $Q(\omega^{-1} s^{n} cm^{-2})$ is the combination of properties related to both the surface and the electro active species independent on frequency, "n" is related to a slope of the log *Z* vs. log*f* and ω is the angular frequency.

This circuit can be regarded as an electrical representation of a two layer model of the oxide film consists of a barrier compact inner film and a porous outer layer [10]. This model consists of a resistor, R_s, representing the solution resistance in series to two parallel combinations, *R*b and *C*b representing the resistance and capacitance of the inner barrier film and then *R*p and C_p, representing the outer porous film resistance and capacitance, respectively.

The electrochemical parameters by fitting the circuits are presented in Table 3

Table 3. Electrochemical parameters fitting the circuits.

samples	R_s [$\Omega\cdot cm^2$]	$R_b\times 10^3$ [$\Omega\cdot cm^2$]	C_b [$\mu F/cm^2$]	n_1	$R_p\times 10^3$ [$\Omega\cdot cm^2$]	C_p [$\mu F/cm^2$]	n_2
S1	102.5	88.5	186.2	0.96	283.2	75.8	0.89
S2	101.8	54.8	2.85	0.95	986.5	1.89	0.90
S3	105.1	28.6	302.8	0.96	186.4	198.5	0.91
S4	104.6	14.5	421.7	0.94	85.8	254.4	0.85

The larger pore diameter in the samples S4 array introduces a larger effective exposed area in close proximity with the electrolyte thus enabling diffusion of corrosive ions in the electrolyte [11].

The larger nanotubes provide more channels for the electrolyte to reach the barrier layer consequently increasing the chance of the reaction between corrosive ions and titanium oxide [12].

4. Conclusion

We obtained with good results TiO_2 nanotubes on Ti samples by an anodic procedure in ethylene glycol containing 0.2 M HF and 2% H_2O. The Tafel curves and EIS results indicate that the electrochemical stability of the nanotubular surface depends on the diameter of the TiO2 nanotube. A diameter that is large leads to decreased corrosion resistance.

Acknowledgments

This work was supported by Romanian Ministry of Education and by Executive Agency for Higher Education, Research, Development and Innovation Funding, under projects PCCA 2- nr. 66/2014.

5. References

1. Park, J.T.; Patel, R.; Jeon, H.; Kim, D.J.; Shin, J.-S.; Kim, J.H.. J. Mater. Chem. 22 (2012) 6131.
2. S. Yoriya , W. Kittimeteeworakul and N. Punprasert, J. Chem. Chem. Eng. 6, (2012) 686.
3. J Zhao, Xi Wang, R Chen, L Li, Solid State Communications, 134 (2005) 705
4. Y Lin,Q Lin,X Liu,Y. Gao,J He,W Wang,Z Fan, Nanoscale Res Lett. 10 (2015) 495.
5. D. Gong, C.A. Grimes, O.K. Varghese, W. Hu, R.S. Singh, Z. Chen, E.J. Dickey, J. Mater.Res.16 (2001) 3331.
6. S. Bauer, S. Kleber, P. Schmuki, Electrochem. Commum 8 (2006) 1321–1325.
7. Lai, C.W.; Sreekantan, S. J. Nanomater. 2011 (2011) 1
8. A Mazare, M Dilea, D Ionita, I. Demetrescu, Surface and Interface (2014) 46.
9. I Thompson, D Campbell Corros. Sci 369 (1994) 187.
10. V.S. Saji, H.C. Choe, Corros. Sci. 51 (2009) 1658.
11. D.S. Kong, Langmuir 24 (2008) 5324
12. A. Balamurugan, S. Rajeswari, G. Balossier, Mater. Corros. 59 (2008) 855

KINETIC STUDY ON CR(VI) ELECTROCHEMICAL REDUCTION IN AQUEOUS ACID SOLUTION

Gabriela Elena BADEA[1], Anca COJOCARU[2], Ioana MAIOR[2]
[1]University of Oradea, Faculty of Science, Armata Română 1, 410087 Oradea, ROMANIA,
gbadea@uoradea.ro
[2]Politehnica University of Bucharest, Calea Griviţei 132, 060032, Bucureşti, ROMANIA

Abstract. *Hexavalent chromium Cr(VI) is a major pollutant present in industrial wastewaters common to the metal and mineral processing, as well as plating industries.This study presents results at the reduction of Cr(VI) at Pt electrode in 1 N H2SO4 deaerated solutions as a function of chromate concentration, using potentiostatic polarisation method. Tafel slope and limiting current density, the kinetic parameters, are significantly modified passing from 0.01 N to 0.1 N Cr(VI) concentration, because of the change of the equilibrium between the different chemical species, in aqueous acid solution.*

Key words: *Hexavalent chromium, electrochemical reduction, Pt electrode*

INTRODUCTION

Chromium is found in group-six of the periodic table and has the ability to form stable complexes in a range of oxidation states from –2 to 6. Of these Cr(III) and Cr(VI) are the most common. Hexavalent chromium Cr(VI) is a major pollutant present in industrial wastewaters common to the metal and mineral processing, as well as plating industries. Cr(VI) is considered carcinogenic and mutagenic, and is capable of displaying considerable diffusion rates through soils and aquatic environments, as well as being a strong oxidizing agent readily absorbed through the skin, even in small quantities it irritates plant and animal tissues [1, 2].

The most probable Cr(VI) species in aqueous solution are , and , the relative distribution of which as chemical species, depends on the solution pH and on Cr(VI) concentration [3]. However, none of them form insoluble species of the pollutant, such that its separation is not feasible from the wastewater through a direct precipitation method [4].. Consequently, there is an increasing interest in developing procedures for the removal of toxic hexavalent chromium from environment. Many of these procedures rely on the reduction of Cr(VI) to the trivalent state, which is much less toxic and can be easy adsorbed at a variety of inorganic and organic materials at neutral pH.
−272OCr−24CrO−4HCrO

Among the electrochemical processes, the direct electroreduction of Cr(VI) was attempted using polyaniline film [5] or polypirrole films[6].

In this work the reduction reaction of Cr(VI) on platinum electrode in 1 N H2SO4 deaerated solutions as function of chromate concentration was studied by the potentiostatic polarisation method.

EXPERIMENTAL

The measurements were performed in a conventional three-compartment electrochemical cell separated by fretted glass disk, with a PS 2 potentiostat, using the stepwise technique of 20 and 40-mV/ 1 minute. The working electrodes, having the geometrical area of 0.06 cm2, were made of polycrystalline platinum. Before to the measurements, the electrode was treated as following: boiled in the 50% nitric acid solution, washed with double distilled water. A platinum sheet with an area of 1 cm2 was used as counter electrode and a saturated calomel electrode (SCE) as reference electrode.

The solutions were prepared from the chemically pure reagents and doubly distilled water. The Cr(VI) ion was added as K2CrO4. Before the measurement the solutions were deaerated with purified nitrogen for 45 minutes. All measurements were carried out at the room temperature (23±1oC).

RESULTS AND DISSCUSION

The Figure 1 shows the potentiostatic polarisation curves as function of concentration obtained at Cr(VI) reduction on platinum electrode in deaerated 1 N H2SO4 solutions. The electrochemical kinetics parameters are presented in Table I.

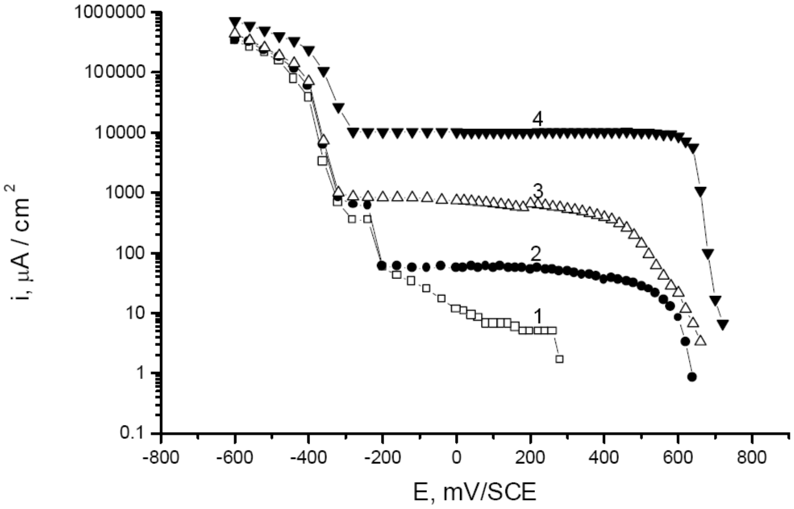

Fig. 1. Chatodic potentiostatic polarization curves (20 mV/ 1minute) for Cr(VI) reduction on Pt electrode in 1 N H_2SO_4 deaerated solutions as function of K_2CrO_4 concentration (N): 1 – 1x10^{-4}; 2 – 1x10^{-3}; 3 – 1x10^{-2}; 4 – 0.1.

The reaction kinetics of Cr(VI) reduction depends on chromate concentration. The Tafel slope decreases significantly with chromate concentration increase (Fig. 2 and Table I). Up to the concentration of 0.01 N K2CrO4 inclusive, the (n) parameters has the average value α approximate of 0.5, what shows that there are not surface processes. Contrary, at 0.1 chromate concentration the (n) parameters becomes more than 2, indicating a process controlled by the surface reaction. α

Table I. Electrochemical parameters of the Cr(VI) reduction on Pt electrode in 1N H_2SO_4 solutions as function of K_2CrO_4 concentration.

K_2CrO_4 conc., N	b, mV/decade	αn	I_L, mA/cm²
1x10^{-4}			
1x10^{-3}	133	0.44	0.053
0.01	92	0.64	0.516
0.1	23	2.56	10.166

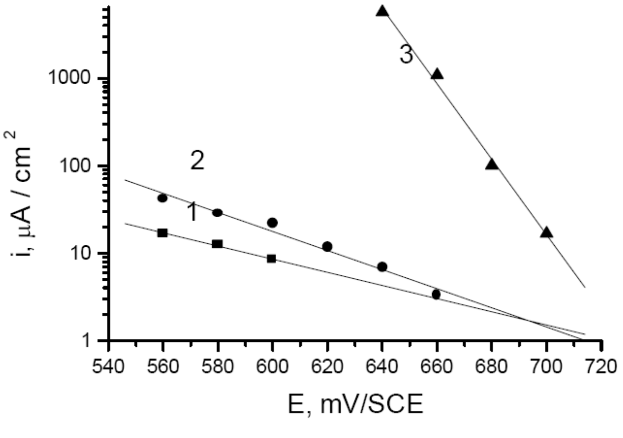

Fig. 2. Tafel lines for Cr(VI) reduction as function of K_2CrO_4 concentration (N): 1 – 1x10^{-3}; 2 – 1x10^{-2}; 3 – 0.1.

All polarization curves are characterized by the limiting current density, of which variation with chromate concentration is direct proportional with this . up to 0.01 N K2CrO4 (Table I and Fig. 3a), indicating a mass transfer control of the reaction rate

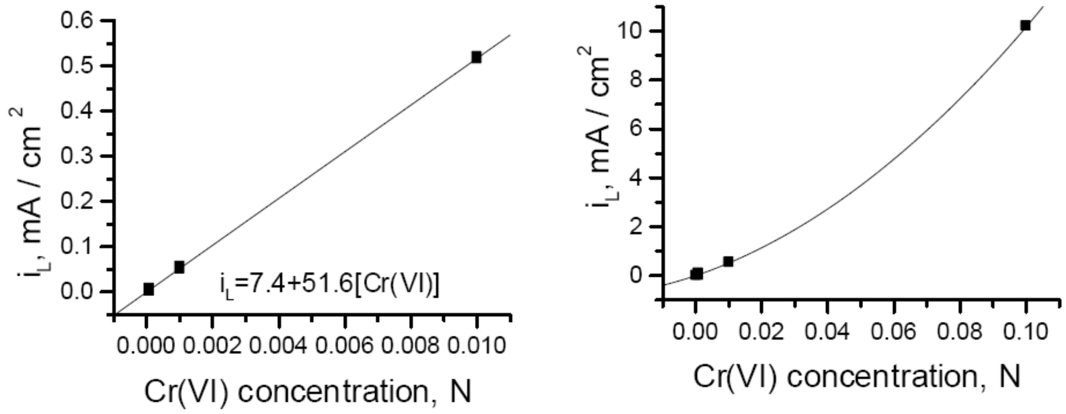

a b

Fig. 3. The dependence of the limiting current density of Cr(VI) concentration:
a – Concentration range of 1x10-4÷1x10-2; b) – All studied concentration range.

Figure 3b, corresponding to whole concentration domain, shows a polynomial dependence of the limiting current density of Cr(VI) concentration. This different behaviour in function of Cr(VI) concentration may be due to the different chemical species of Cr(VI) existent in acid solutions.

The theoretical distribution of the predominant chemical species Cr(VI) depends on pH and chromium concentration, conform to the scheme [3] presented in Figure 4.

In studied solutions the Cr(VI) or −log [Cr(VI)] has values 4, 3, 2 and 1 for Cr(VI) concentrations of 1x10-4, 1x10-3, 1x10-2 and 0.1 N, respectively. The pH value is approximate 1. Thus in solutions containing ≤ 0.01 N Cr(VI) is the predominant specie, which reduces after electrochemical reaction.

At 0.1 N Cr(VI) the predominant specie is and the electrochemical reduction reaction is give by equation:

$$Cr_2O_7^{2-} + 14H^+ + 6e \rightarrow 2Cr^{3+}(aq) + 7H_2O$$

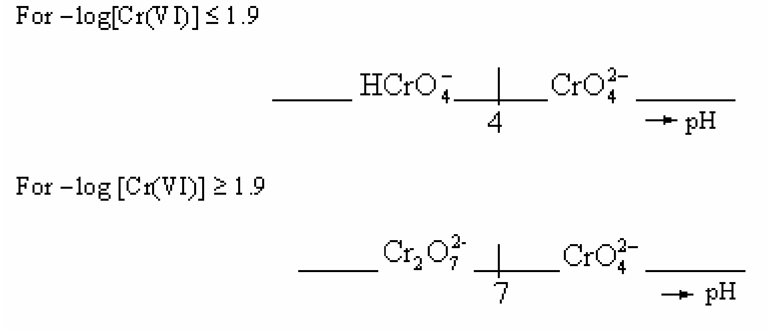

Fig. 4. Scheme of the theoretical distribution of the predominant chemical species Cr(VI)

Therefore, for the same Cr(VI) concentration, the reactant concentration is twice more in case of reaction (2), what explains the increase of the limiting current density of 20 times, at 0.1 N comparative with 0.01 N Cr(VI) (Table I).

$$\mathrm{HCrO_4^- + 7H^+ + 6e \rightarrow Cr^{3+}}(aq) + \mathrm{4H_2O}$$

CONCLUSIONS

The kinetics of the Cr(VI) reduction on Pt electrode in 1N H_2SO_4 depends on its concentration. The Tafel slope significantly decreases and the limiting current density increases of 20 times when it passes from 0.01 N to 0.1 N Cr(VI) concentration, due to the modification of the equilibrium between the different chemical species in solution.

REFERENCES

1. J. Gaulhofer and V. Biabchi, “Chromium, Metals and their compounds in the environment”, VCH Wheinheim, 1991, p. 30.

2. M. Stoepler, “Hazardous Metals in the Environment. Techniques and Instrumentation in Analytical Chemistry”, Elsevier, New York, 1992, p. 373.

3. C. Barrera-Diaz, M. Palomar-Pardave, M. Romero-Romo and S. Martinez, “Chemical and electrochemical considerations on the removal process of hexavalent chromium from aqueous media” J. Appl. Electrochem., 2003, 33, 61.

4. Nriagu and E. Nieboer, “Chromium in the Natural and Human Environments”, Wiley Series, New York 1988, p. 82.

5. L.A.M. Ruotolo and J.C. Gubulin, “Reduction of Cr(VI) using polyaniline films”, J. Appl. Electrochem., 2003, 33, 1217.

6. R. Senthurchevan, Y. Wang, S. Basak and K. Rajeshwar, “ Reduction of Cr(VI) in aqueous solutions by polypirrole”, J. Electrochem. Soc., 1996, 143, 44.

7. Barrera-Díaz C, Lugo-Lugo V, Roa-Morales G, Natividad R, Martínez-Delgadillo SA., Enhancing the electrochemical Cr(VI) reduction in aqueous solution, J Hazard Mater. 2011 Jan 30;185(2-3):1362-8. doi: 10.1016/j.jhazmat.2010.10.056.

8. Wei Jin, , Hao Du, Shili Zheng, Yi Zhang, Electrochemical processes for the environmental remediation of toxic Cr(VI) A review, Electrochimica Acta, Volume 194, 10 March 2016, Page 489, doi:10.1016/j.electacta.2016.01.130.

INFLUENCE OF WATER CHEMICAL PROPERTIES ON CORROSION OF URBAN COLD WATER GRID

Petru CREŢ[1], Gheorghe C. IONESCU[2]

[1]University of Oradea, Department of IT&Communications, Romania, pcret@uoradea.ro
[2]University of Oradea, Faculty of Constructions, Cadaster and Architecture, Romania,
gheionescu@gmail.com

Abstract. *In the new perspective of the sustainable development, the increasing of the energy efficiency is a result of interdisciplinary studies, taking in account not only the scientific knowledge, but also concepts of economic and environmental protection. This paper presents a case study, made in Oradea and include a case study on the monitoring of water chemical properties and discussions on possible influence on the corrosion and of the steel pipes of water distribution grid.*

Key words: *water parameters, water pipes corrosion*

INTRODUCTION

The complex system of heat transport in Oradea include: highways and district heating connections and the distribution grid is almost overlaped on cold water distribution grid. By the year 2009, there were made pipe replacement with new, pre-insulated pipes, only up to 8%, the rest being classic isolated. It is estimated that heating transportation losses are 26% compared to 5% as would be recommended.

Main heating network has a length of about 426 km of pipelines and a secondary network of 142 km. Their state of wear is relatively advanced. Losses in the year 2013 as the networks are about 13% above the normal 8%, perform the partial rehabilitation[1-5].

.

Even if the main concern is increasing the energy efficiency of transport and distribution of heat, hot water, water that is treated in addition to the cold water and hot water, can not be a question relevant about corrosion resistance apart from the chemical composition of cold water. Basically this study supports the idea that the problem of corrosion of pipelines (Figure 1) for carrying water should be treated in a uniform manner, whether it is hot or cold water taking into account the full complexity of the phenomenon: the chemical composition of water and and soil, microbiological composition, atmospheric conditions, temperature, pressure, flow variations, turbulence, stray, material issues where there are welds or the bimetallic corrosion

Figure 1. Cold water pipes presenting internal and external corrosion and scaling.

Transport and distribution system of drinking water company belongs to SC Compania de Apa Oradea SA., which in addition has as objects not only the transport, but also the collection, adduction and water treatment, pumping water, rainwater harvesting, wastewater treatment and discharge them into the environment [5].

EXPERIMENTAL

The experimental determinations were performed in a central laboratory of the SC Compania de Apa Oradea SA, for physical and chemical analysis, microbiological and organoleptic characteristics. Analysis standardized methods are presented in Table1.

Table 1. Analytical methods for chemical parameters and limits for drinking water [5]

Parameter	Units	Value	Method
pH	pH unit	6.5-9.5	SR ISO 10523/97
Dissolved Oxygen	mgO_2/l	5	SR EN ISO 8467
Total Hardness	German grade.	min.5	SR ISO 6059/84
Chlorides	mg/l	250	SR ISO 9297 /01

The main objectives are monitoring the quality of drinking water and the waste that is discharged into municipal sewage, to discharge into the environment [5].The laboratory has been checked at the raw water and chlorinated water being pumped into the distribution grid and supply areas. This is done in a monitoring program audit treatment plants and supply areas [5], as required by law: Law no.458/2002 on drinking water quality, as amended by Law 311/2004 and Decision 974/2004.

RESULTS AND DISCUSSIONS

From the information extracted from the database BAPFCB - physico-chemical and biological characteristics of water from urban [1] can plot the evolution over time of the measured parameters during 01.06.2013-30.06.2013(station 1).

.

It has made clear that the permissible limit refers to potable water and not the potentially aggressive (corrosive) water, which is discussed in each particular case. The water in thermal power plants and / or cooling system is a complex environmental corrosion.

The major environmental factors which influence the corrosion of metallic materials, in particular carbon steel, widely used in the construction of these facilities are: the presence and concentration of dissolved oxygen and chlorides (Figure 2), pH (Figure 3), the content of CO_2 dissolved, the nature and concentration of dissolved salts, water hardness (Figure 4), the temperature and the speed of movement of water [1,6].

Experimental determination of the chemical properties of water are shown in Figures 2-4 and correspond to one month, June 2013. Graphics were made using Origin Lab Software.

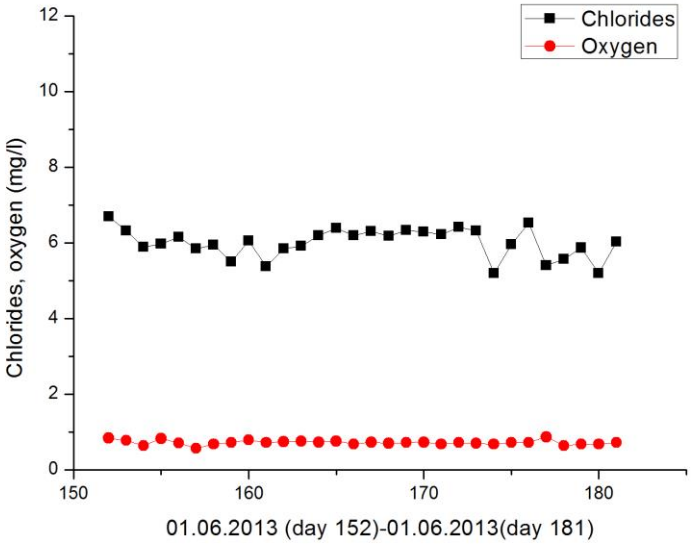

Figure 2. Variation of oxigen and chloride concentrations from cold water- june 2013.

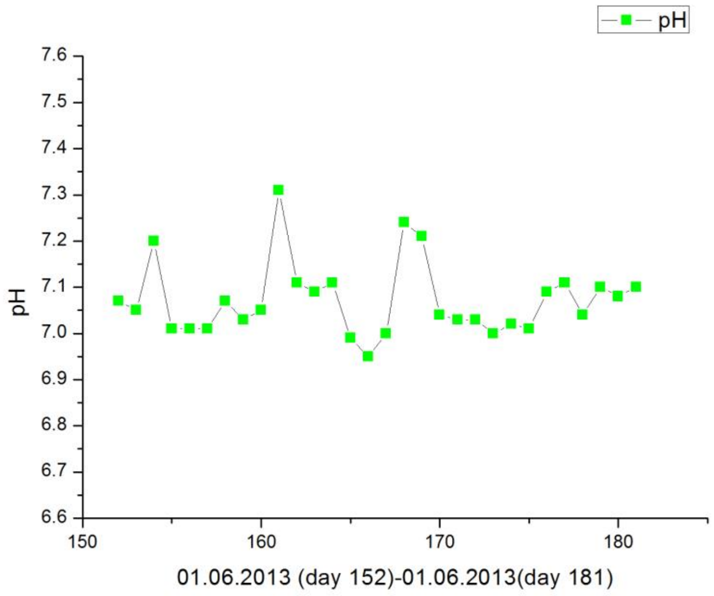

Figure 3.Variation of pH in cold water- june 2013

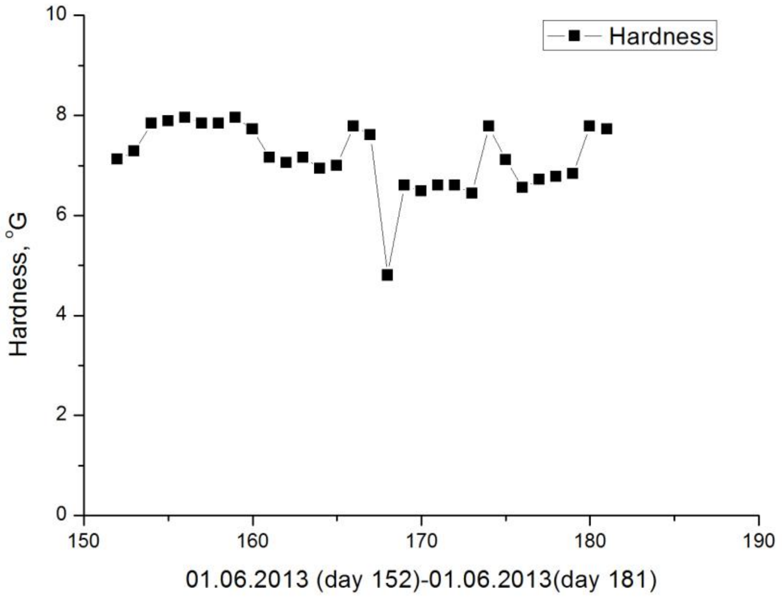

Figure 4. Variation of cold water hardness-june 2013.

The mechanism of corrosion process in natural waters (6 <pH <8) is the overall reaction of corrosion of iron, steel main element, given by the equation:

$$Fe + H_2O + ½ O_2 \rightarrow Fe(OH)_2$$

In the presence of dissolved oxygen outer surface of the iron hydroxide is oxidized to the ferric hydroxide According to the reaction:

$$Fe(OH)_2 + ½ H_2O + ½ O_2 \rightarrow Fe(OH)_3$$

A high concentration of germs automatically attract a larger amount of chlorine used in water chlorination and finally, taking into account the balance:

$$Cl_2 + H_2O = H^+Cl^- + H^+ClO^-$$

a greater amount of chlorine ions, Cl^-, resulting in the dissociation of the hydrochloric acid, the chemical species responsible for the initiation and propagation of the most dangerous forms of localized corrosion, pitting corrosion.

The film of rust forms on the surface of iron is normally from three layers of hydrated iron oxides with different oxidation states; a ferro-ferric oxide layer, Fe_3O_4 is often an intermediate layer between FeO black interior and exterior Fe_2O_3 [6].

Water hardness is one of the factors that determine the formation of the protective film.

Fresh natural waters containing dissolved calcium and magnesium salts in varying concentrations, depending on the water source. If the concentration of such salts is low, the water is called soft. A soft water is more corrosive than a tough one. The mechanism of protection afforded by hard water is natural deposition of a thin film formed mostly of $CaCO_3$ that prevents diffusion of oxygen from the surface. As shown in Figure 4, only a single day in June 2013, the total hardness fell below the limit of 5.

.

CONCLUSIONS

Worn-out installations, the lack of accurate information to databases related causes corrosion factors of physical and chemical present at a time, location dropped to the transport and distribution grids of cold water leads indirectly to many problems related to efficiency centralized heating system at the level of Oradea, with heat losses well above the permissible values. A not very long-term solution is currently conducting a rehabilitation process by replacing old pipes with new ones, with better technologies.

Acknowledgments

The authors are grateful to the specialists from S.C. Compania de apa Oradea, S.A., for the cooperation and help for chemical data aquisition

REFERENCES

1.P.Creţ- Ph.D.Thesis, „Contributions to energy efficiency improvement of hot water transport and distribution urban networks”, University of Oradea, 2015.
2.http://cdn3.bihon.ro/2013/07/Masterplan-Oradea-2030.pdf
3.http://www.isoplus.de/rohttp://www.panoramio.com/photo/54883288
4.http://oradea.ro/fisiere/module_subpagini_fisiere/640/complet.pct.41.pdf
5.www.apaoradea.ro
6 T. Badea, M. Popa, M. Nicola, *Ştiinţa şi ingineria coroziunii*, Ed. Academiei Române, Bucureşti, 2002.

Analele Universităţii din Oradea-Fascicula Chimie, Vol. XXIII, 2016

GEOCHEMISTRY OF LOW-TEMPERATURE GEOTHERMAL FLUIDS AND WELL SCALES

Oana STĂNĂŞEL[1], Hrefna KRISTMANNSDOTTIR[2], Ludovic GILĂU[1]
[1]University of Oradea, Romania, [2] Efla Engineering Company, Iceland
ostanasel@uoradea.ro

Abstract: *Direct geothermal uses have been reported both in Romania and Iceland. As a result of a research cooperation between the authors from the mentioned institutions, a geochemical assessment of Romanian geothermal field is presented based on analytical data of fluids sampled at the wellhead of low-temperature well. Analyses of the water samples include major and minor elements. According to different diagrams, geothermal waters have been classified. With the aid of speciation programs, the analytical data were used to model individual species activities in the initial aquifer fluids that feed the well. The modelled aquifer fluid compositions were used to assess how closely equilibrium is approached between solution and various minerals. Then the deposits which have been formed by geothermal water utilization were structurally analysed.*

Key words: *ternary equilibrium diagrams, scale*

1. INTRODUCTION

Renewable energy is becoming an increasingly important part of international development. Geothermal energy plays the main role as a renewable source of energy. In the north-westerm part of Romania there is a large geothermal area, an important one being Oradea geothermal reservoir. It has been exploited by 12 geothermal wells. It was selected in the present study well 1717 from Iosia area. The well was drilled at 3200 m depth. At the beginning of production the wellhead temperature was around 90°C, later becoming around 70°C. The flowrate is about 8 l/s.

2.SAMPLING AND ANALYTICAL METHODS

Water sampling and treatment was according to inhouse practice at University of Akureyri from Iceland[7], based on internationally acknowledged methodology for sampling[1,3,4,5,8].

Temperature, oxygen and hydrogen sulfide were measured on site. Oxygen was measured by the use of Chemetrix ampules. Hydrogen sulfide was measured in an alkaline solution by titration with mercury acetate with dithizone as indicator. pH was measured electrometric. Total carbonate was measured by alkalinity titration by 0.1 M HCl and back titration by 0.1 M NaOH after flushing the CO_2 out ot the acidified sample by nitrogen gas.

Chloride, calcium and magnesium were measured in the laboratory of University of Akureyri with a 794 Basic Titrino títrator from Metrohm. Chloride was measured by potentiometer Mohr titration and Ca and Mg by EDTA titration.

All main elements: sodium, potassium, calcium, magnesium, strontium, iron, silica, boron and sulfur were analysed by ICP-AES methods in Iceland. Trace elements were also measured in Iceland by ICP-MS techniques. Chloride, sulfate, bromide and fluoride were analysed by ion chromatography.

The sample of scale was finely ground in an agate mortar and packed by pressing and smoothing the powder into the depression by a glass plate. The prepared sample was run in a diffractometer. The sample was radiated by Cu radiation (Kα 1) and rotated from 2Θ of 5° to 70°.

3. RESULTS AND DISCUSSIONS

3.1. Results of water analysis

In table 1 are shown the results of analysis of main elements in the water samples, in mg/L. There are also shown the concentrations of trace elements and nutrient components. The data from Table 1 indicate that waters can be classified as calcium-sulphate, with a basic pH. The main cations concentrations in sample are relatively low. The strontium concentration is high compared to other geothermal waters. Silica is suspiciously low in the sample. The value of total dissolved solids is low, being less than 0.5g/L.

Table 1. Chemical composition of water samples

Sample Location	Oradea-1717
Temp.°C	71.9
pH/°C	8.19/23
SiO_2 mg/L	2.4
B mg/L	0.223
Na mg/L	45
K mg/L	17.4
Ca mg/L	58.1
Mg mg/L	15.8
Sr mg/L	3.2
Fe mg/L	0.038
Al mg/L	1.86
CO_2 mg/L	27.1
H_2S mg/L	0.156
O_2 mg/L	0
SO_4 mg/L	232
Cl mg/L	32.9
F mg/L	0.93
Diss.sol. mg/L	459
NH_3 mg/L	0.104
Br μg/L	102
Li μg/L	91.6
Mn μg/L	45.1
Mo μg/L	2.72

In figures 1 and 2 the results are plotted in different classification diagrams[9]. The Schoeller diagram (Figure 1) utilizes the equivalent concentration of sulfate, carbonate, chloride, magnesium, calcium and the sum of the alkali ions, sodium and potassium on the y-axis and these elements are lined up on the x-axis in this order. The Durov diagram (Figure 2) utilizes two triangular diagrams, one for plotting the proportions (in equivalent concentrations) of the main cations and the other for the equivalent concentrations of the main anions connected into a square, adding total dissolved solids and pH of the water samples in connecting rectangles.

Concentration of chloride is rather low, about 33 mg/L. Calcium and sodium are the main cations and potassium and magnesium are in about the same concentration. Hydrogen sulfide is rather low, 0.156 mg/L, but high enough to give some inbuilt corrosion defense. No oxygen was measured at wellhead.

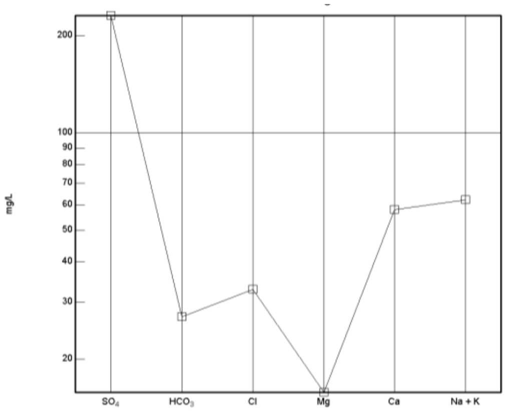

Figure 1. Waters classification according to Schoeller diagram.

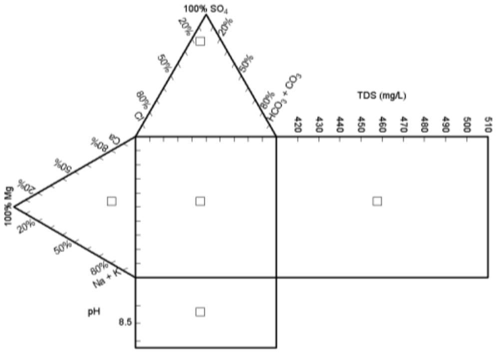

Figure 2. Waters classification according to Durov diagram.

For a classification in terms of the major anions Cl^-, SO_4^{2-} and bicarbonate, the triangular diagram[1] was used, where the position of a data point in this diagram is obtained by evaluating the percentage of Cl^-, SO_4^{2-} and HCO_3^- relative to the sum of the concentrations (in mg/L) of all three constituents. The data points for the geothermal waters from Iosia, well 1717 plot (Figure 3) in the field of steam heated waters, within the field of more than 80% sulphate and about 15% bicarbonate.

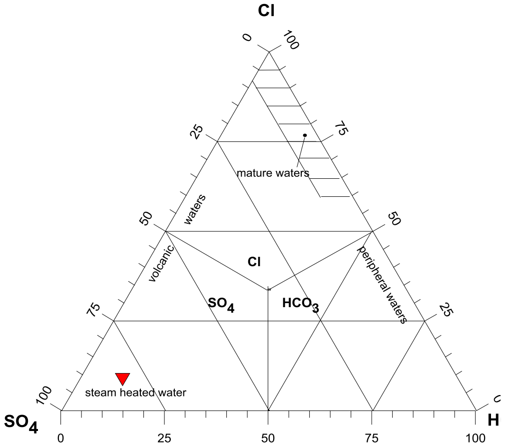

Figure 3. Major anions ternary diagram

The Na-K-Mg ternary diagram of Giggenbach[6] and Arnorsson for well 1717 (Figure 4) indicates that these waters do not reach the fully equilibrated water curve, they plot in the immature region. Waters from the studied well have a high percentage of Mg. This could be a reason that these waters have not attained equilibrium with the reservoir rocks.

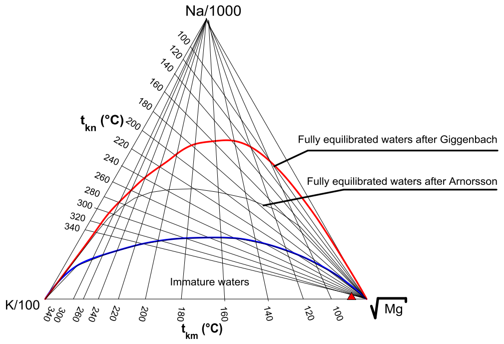

Figure 4. Na-K-Mg equilibrium diagram

3.2. Monitoring of scales

By studying the fluid-mineral equilibrium, you can get a useful assessment of equilibrium/disequilibrium conditions for geothermal fluids, the results giving a good prediction on scaling and corrosion tendencies in a particular geothermal system. A computer simulation program WATCH[2] has been used to calculate the saturation indexes for particular mineral phases believed to occur in the reservoir. They were plot against temperatures which can be reached during geothermal water utilization (Figure 5).

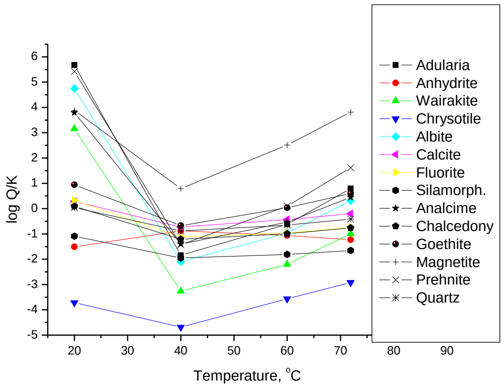

Figure 5. Mineral-equilibrium diagram

The sample is slightly supersaturated with respect to calcite, but if the water is cooled under pressure and not deaerated and pH kept constant, the water will become in equilibrium with calcite at 30°C. There is recorded a supersaturation with magnetite both at the wellhead temperature and at all lower temperatures. Prehnite is supersaturated at well production temperature. Most of the minerals are undersaturated at wellhead temperature.

A sample of scale taken from the wall of distribution pipe was analysed by X-ray diffraction. There were identified siderite and calcite (Figure 6). Mineral deposition with iron content and calcium were expected after simulation.

4. CONCLUSIONS

Aquifer fluid composition has been assessed from analytical data on water samples collected at the wellhead of an important production well from Oradea. The type of water was calcium-sulphate. The studied geothermal water appears to be a steam heated water, which may suggest boiling in the reservoir when has occurred transformation of hydrogen sulphide into sulphate.

Changes which occur in temperature water generally lead to changes to mineral saturation. The state of mineral saturation of the aquifer water with respect to the following minerals was studied: adularia, anhydrite, albite, analcime, calcite, chrysotile, chalcedony, quartz, goethite, magnetite, prehnite, fluorite, amorphous silica. The results for all ferrous bearing minerals indicate supersaturation. Calcite scaling tendency for the selected well water is expected. The oversaturation in respect with these minerals was confirmed at structural analysis of the solid deposition sample.

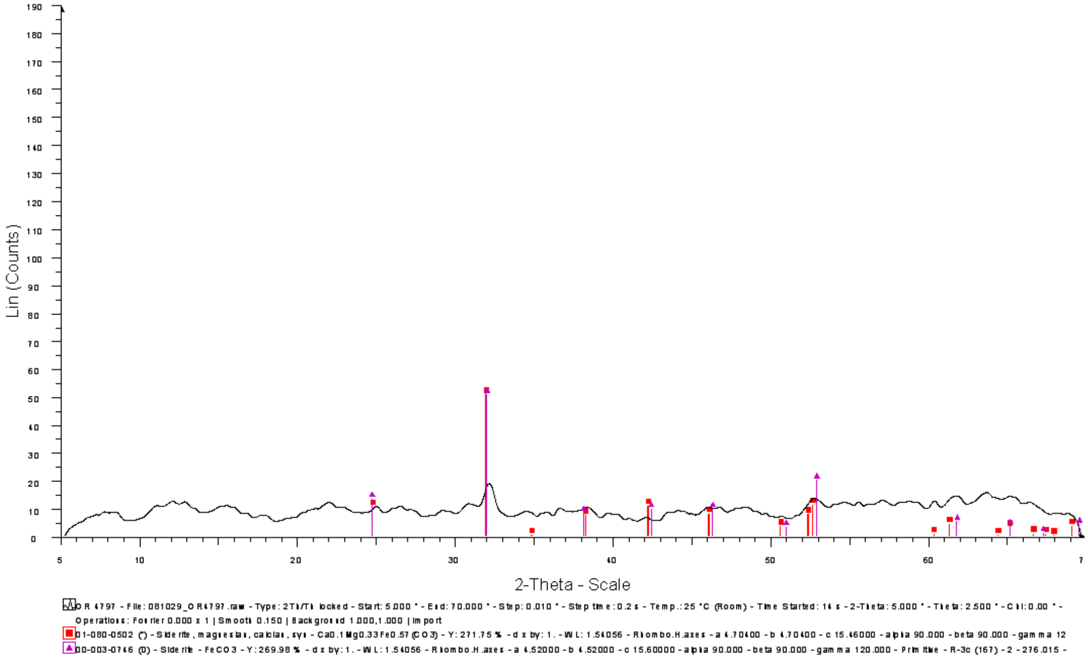

Figure 6. The XRD analysis of scale

REFERENCES

[1]. Arnórsson, S. (ed.): Isotopic and Chemical techniques in Geothermal Exploration, Development and Use. International Energy Agency Vienna, (2000), 351 p.

[2]. Arnorsson, S., Bjarnason, J.O., The speciation program WATCH, version 2.3. Orkustofnun, Reykjavik, (2004).

[3]. Counce, D., Grigsby, C.O., Goff, F. and Shevenell, L.: Chemical Analysis and sampling Techniques for Geothermal Fluids and Gases at the Fenton Hill Laboratory, Los Alamos National Laboratory LA-11006-MS, (1987), 84 p.

[4]. Drever, J.I.: The geochemistry of natural waters, Surface and groundwater environments, Prentice Hall, Upper Saddle River, (2002), 436 p.

[5]. Franson, M.H. (ed.): Standard Methods for the Examination of Water and Waste-water, 15th Edition, American Public Health Association, Washington DC, (1980), 1134 p.

[6]. Giggenbach, W.F. In: Application of geochemistry in geothermal reservoir development. F. D'Amore, UNITAR/UNDP publication, Rome, (1991).

[7]. Kristmannsdóttir, H.: Sampling of hot and cold water for geochemical measurements Instructions for practicals in the course VAG1103 Háskólinn á Akureyri, Auðlindadeild, Skýrsla HK- 04/10, (2004), 11 p.

[8]. Kristmannsdóttir, H.: Chemical characteristics of potable water and water used in district heating systems in Iceland. Proceedings13th Scandinavian Corrosion, (2004).

[9]. The Spreadsheet for water analyses, Rock Ware, AqQa, (2006).

(12pt)

INSTRUCTIONS FOR AUTHORS (TIMES 14 PT BOLD, CAPITAL LETTERS, CENTRED)

(10pt)

First name SURNAME[1], First name SURNAME[2] (10 pt bold)
[1]Affiliations and addresses (10 pt)Affiliations and addresses (10 pt)

(10pt)
(10pt)

Abstract: *Abstract of 50-120 words (10 pt italic). It contains concise information about: objectives of the work, the results obtained, conclusions*

Key words: List 2-6 keywords. (l0 pt, italic).

(10pt)
(10pt)

INTRODUCTION (l2PT. CAPITAL, BOLD)

The paper has to be written in English. Each paper should be concise including text, figures and tables. Authors are kindly requested to submit a paper a hard copy or in electronic format in Microsoft Word file form. Acceptable versions are MS-Word 2003, 2007, 2010. The suggested structure of the main text: Introduction; Methods, techniques, materials, Study area; Results and Discussions; Conclusions; References. (10pt)
(10pt)

INFORMATION (12 PT CAPITAL, BOLD)

Page layout (10 pt, bold)

- Use A4 format (210 x 297 mm),
- Margins: Top–2,5cm, Bottom-3cm, Left-4 cm and Right - 3 cm
- Paragraphs: alignment - justified, line spacing – 1,
- Font style: Times New Roman.
- Text: l0pt.: regular, text in tables: 10 pt, 1 line space and centred, 2 columns,
- equations: Equation editor, 10 pt, centred,
- *caption of tables and figures: 10 pt, italic*

All tables and figures follow the References or could be inserted within the text. Tables, together with figures should be placed in their order of appearance in the text. Tables should be numbered consecutively. Table captions containing the number of the tables, followed by the caption, and should be placed above the table. Tables should be clearly captioned and all symbols should be properly explained in either the table or its caption.

Figures (min. 300 dpi) can be in colour, but must also be clear enough for black and white reproduction. They should be centred and numbered consecutively and so referred to in the text. Each must be clearly captioned (after the Figure number) below the figure.

Equations will be centred and numbered consecutively (right aligned).

All references would be cited within the text as superscripts after the punctuation's marks.[1]

(10pt)

All papers cited should be listed under the **REFERENCES** (1 column), in alphabetical order according to the author's last name. The list of references should follow the format given below:

(Journal Article)

[1] Abbott, M. B., Petersen, M. M., and Skovgaard, O. (1978). On the numerical modelling of short waves in shallow water, Jnl Hydraulic Res; Vol 16 (3), pp. 23-44.

(Report)

[2] Carter, B., and Connell, C. (1980). Moa Point Wastewater Treatment Plant and Outfall Study, Report for the Wellington City Council, Wellington, pp. 31.

(Book)

[3] Grady, C.P.L., and Lim, H.(1980). Biological Wastewater Treatment Theory and Application, Marcel Dekker, New York, pp. 375.